Downloaded from orbit.dtu.dk on: May 04, 2023

DTU Library

Synthesis and Investigation of the Bio-polymerization of Cutin Monomers and Derivatives

Scavée, Gauthíer Mike L

Publication date:
2018

Document Version
Publisher's PDF, also known as Version of record

Link back to DTU Orbit

Citation (APA):
Scavée, G. M. L. (2018). *Synthesis and Investigation of the Bio-polymerization of Cutin Monomers and Derivatives*. Technical University of Denmark.

General rights
Copyright and moral rights for the publications made accessible in the public portal are retained by the authors and/or other copyright owners and it is a condition of accessing publications that users recognise and abide by the legal requirements associated with these rights.

- Users may download and print one copy of any publication from the public portal for the purpose of private study or research.
- You may not further distribute the material or use it for any profit-making activity or commercial gain
- You may freely distribute the URL identifying the publication in the public portal

If you believe that this document breaches copyright please contact us providing details, and we will remove access to the work immediately and investigate your claim.

Synthesis and Investigation of the Bio-polymerization of Cutin Monomers and Derivatives

PhD Thesis 2018

Gauthier Mike L. Scavée

Department of Chemistry
Technical University of Denmark

There is only one corner of the universe
you can be certain of improving,
and that's your own self.

Aldous Huxley

Preface

The work presented in this manuscript is the results of a 3 years research project carried out by the author at the Technical University of Denmark (DTU) from December 2014 to February 2018, under the supervision of Professor Mads H. Clausen as part of the Danish program to obtain a Ph.D. A four-month external stay was carried out under the supervision of Professor Jocelyn K. C. Rose at the Plant Biology Section at Cornell University (CU) as part of the Ph.D. studies.

This dissertation covers six projects described in four chapters, illustrating a multidisciplinary Ph.D. program. Chapter one is a brief introduction of the two plant polyesters, cutin and suberin along with an overview of the developed chemistry for the synthesis of cutin monomer. Chapter two is divided into four section and describes the synthesis of a cutin monomer and six monomer derivatives and their use as molecular tool in enzymatic polymerization assays. Chapter 3 contains experimental protocols and compound data for the chemical approach. Finally, chapter 4 gives an overview of the work that was performed on the identification of suberin synthase and the investigation of cutin synthase 1 hydrophobic tunnels as part of my external stay at CU.

Acknowledgment

First and foremost, I would like to express my gratitude to my supervisor, Mads H. Clausen for giving me the great opportunity to conduct my Ph.D. in his group. Thank you very much for your continuous support and guidance throughout this challenging and interesting project. Thank you for keeping your door open at all time and for the frequent discussion about the project and for your open-mindedness.

I would also like to thank all the past and present members of the Clausen group for creating such a great work environment, for the scientific discussions and for the nice and enjoyable events and group dinners. Many thanks goes to my labmates: Thomas Flagstad, Carlos Azevedo, Rico Petersen and Viola Previtali, for the great lab atmosphere as well as for our daily conversation and chemistry talk. Jorge Peiró Cadahia is also thanked for our frequent relaxing coffee breaks where we discussed various topics, work related or not. Mike would like to thanks Kim Mortensen for the great chemistry advice and for our frequent runs together. I would like to give a special thanks to Christine Kinnaert, who have been a great colleague but also a great friend, for being a good listener in good and bad times. I would also like to thanks Geanna Min for the fun times in the lab and outside of the lab, we will always remember the great wall of 122. In particular, I would like to thanks Ignacio "Nacho" Martínez San Segundo, with whom I have shared labs, project, chemistry and also a ton of amazing moments in and outside of the labs, these past three years would have never been as enjoyable without a great friend like you.

Thank you to Professor Jocelyn K. C. Rose for inviting me in his group for my external stay. This external stay allowed me to learn about a field that I had very little knowledge in prior to my external stay, molecular biology. The entire Rose group is thanked and in particular Ph.D. student Nicholas Segerson who had the patience to teach me everything I know about molecular biology. A huge thanks goes to Stephen "THE shit" Snyder for his technical help and the frequent random conversations. Many thanks goes to Eric Fich and Trevor Yeats for sharing their knowledge about cutin and suberin. Thanks to Michelle Laterrade for our occasional late evening talks in the lab. I would also like to thanks Yoshihito Shinozaki and Paco Romero for the time spent together outside of the lab.

Many thanks goes to the NMR team, Associate Professor Charlotte H. Gotfredsen, Professor Jens Ø. Duus, Kasper Enemark-Rasmussen and Anne Hector for their hard work maintaining the NMR at all time. A huge thanks goes to the technical staff at DTU who manage to keep the entropy in the department to a minimum. In partic-

ular, I would like to thanks Philip Charlie Johansen whose professionalism is truly admirable and who helped me out at more than one occasion during the weekends and holidays.

The Novo Nordisk Foundation and the Technical University of Denmark are gratefully acknowledged for financial support.

My friends and family are acknowledge for their unconditional support. A special thanks goes to all my friend from the University of Namur who are still supporting me after all that time spent together and in particular Orian and Jean who are always there in times of need or thirst. I would also like to thanks the Naninnois who I grew up with and are still very important to me up to this date.
Thanks also goes to my cousin John Meersman who took me under his wings when I was 15 and taught me a lot. Your work ethic and honesty still inspires me to this date and the time spent working with you was really life changing and means a lot to me.
I would also like to thanks all of my siblings and in particular, Steve who has always supported throughout my entire education. Your support has really helped me get to where I am now and I can't be thankful enough for everything you did for me.

My deepest gratitude goes to my love and wife Anastasia without whom I would have never been able to finish this thesis. Your undying love and supports means the world to me. Thank you Honey for leaving everything just to take care of me and maintaining me alive throughout the end of my Ph.D.

I want to express my gratitude to my parents, to whom I owe everything. Without your eternal support and love, I would have never been able to be where I stand today. Thank you for taking care of me and raising me the way you did.

Finally, this thesis is dedicated to my late grandmother, Denise Dave, a wise and strong woman without whom I would have never started this Ph.D. You talked me into starting the Ph.D. and I am very thankful for that. This experience helped me grow as a scientist but also as a person and I owe it to you. Merci de tout mon cœur Mamy et repose en paix.

Abstract

Cutin and suberin are two plant polyesters whose formation is tightly linked to plants ability to thrive in areal medium due to their ability to restrict gas and water loss and movement. Additionally, these two polymers present properties which make them suitable for the polymer industry. Hence, understanding the bio-formation of these polymers is important for both, fundamental biology as well as for industrial applications. In this context, the identification of cutin synthase 1 (CUS1) in tomato fruit, made possible through a collaborative effort between the group of Professor Jocelyn K. C. Rose at Cornell University and the group of Professor Mads H. Clausen at the Technical University of Denmark, represents an important milestone towards this goal. This enzyme, which is part of the GDSL esterase/lipase superfamily, was proven to catalyze the *in vitro* oligomerization of 2-mono(10,16-dihydroxyhexadecanoyl)glycerol (2-MHG), the main precursor of tomato cutin. However, up to date, very little is known about CUS enzymes, their selectivity, their tertiary structure and their mechanism of action.

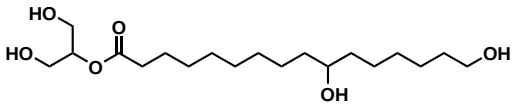

2-mono(10,16-dihydroxyhexadecanoyl)glycerol

2-MHG

This thesis presents the synthesis of another cutin monomer, a deuterated derivative of this monomer as well as five other 2-MHG derivatives. All these compounds have been synthesized to be used in CUS1-mediated polymerization to gain more information on CUS1 selectivity and mechanism of action. Additionally, the use of one of these compound as a CUS1 ligand in co-crystallization experiments has been initiated. Obtaining CUS1-ligand crystals would be an essential tool towards the discovery of CUS1 tertiary structure through X-ray diffraction (XRD) analysis.

The second part of this dissertation discloses a biological approach towards the understanding of CUS1 mechanism of action. In particular, the interaction between CUS1 and its substrates through the formation of hydrophobic tunnels was investigated through the formation of CUS1 mutants through site-directed mutagenesis.

Additionally, the investigation of several Arabidopsis GDSL mutants as potential suberin synthase was initiated through the production and characterization of knockdown mutants via RNA silencing.

List of Abbreviation

1-MHG	1-mono-(10,16-dihydroxyhexadecanoyl)glycerol
2-MHG	2-mono-(10,16-dihydroxyhexadecanoyl)glycerol
ABC	ATP-binding casette
Ac	acetyl
aq.	aqueous
ATP	adenosine triphosphate
bdg	bodyguard
Bn	benzyl
br.	broad
CDI	1,1'-carbonyldiimidazole
cDNA	complementary DNA
CoA	coenzyme A
COSY	correlation spectroscopy
d	doublet
DCA	dicarboxylic acid
DCC	*N*,*N*'-dicyclohexylcarbodiimide
DCR	DEFECTIVE IN CUTICULAR RIDGES
DCVC	dry column vacuum chromatography
DDQ	dichloro-5,6-dicyano-1,4-benzoquinone
DEPC	diethyl pyrocarbonate
DMAP	4-dimethylaminopyridine
DMF	*N*,*N*-dimethylformamide
DMP	Dess-Martin periodane
DMSO	dimethyl sulfoxide
DNA	deoxyribonucleic acid
DPA	day post-anthesis
DTU	Technical University of Denmark
EDTA	ethylenediaminetetraacetic acid
equiv.	equivalent
ER	endoplasmic reticulum
ESI	electrospray ionization
FA	fatty acid
FAE	fatty acid elongase
FAR	fatty acyl reductase
FT	fourier transform
GC-MS	gas chromatography mass spectrometry

continued on next page

GPAT	glycerol-3-phosphate acyltransferase
h	hour(s)
HDPE	high density polyethylene
HMBC	heteronuclear multiple bond correlation
HMDS	hexamethyldisilazane
HPLC	high-performance liquid chromatography
HRMS	high resolution mass spectrometry
HSQC	heteronuclear single quantum coherence
Hz	hertz
*i*Pr	isopropyl
IR	infrared spectroscopy
KCS	β-ketoacyl-CoA synthase
LACS	long-chain acyl-CoA synthetase
LDPE	low density polyethylene
LTP	lipid transfer protein
m	multiplet
MAG	monoacyglyceryl ester
MALDI	Matrix-Assisted Laser Desorption/Ionization
Me	methyl
MES	2-(*N*-morpholino)ethanesulfonic acid
mp.	melting point
Ms	mesyl
MS	Mass Spectrometry
NAP	2-Naphthylmethyl
NBR	acrylonitrile-butadiene rubber
NMR	nuclear magnetic resonance
OD_{600}	optical density at 600 nm
p	pentet
PCR	polymerase chain reaction
PET	polyethylene terephthalate
PG	protecting group
Ph	phenyl
PMMMA	polymethyl methacrylate
PP	polypropylene
ppm	parts per million
PPTS	pyridinium *p*-toluenesulfonate

continued on next page

PS	Polystyrene
q	quartet
qPCR	quantitative polymerase chain reaction
quant.	quantitative
RH	relative humidity
RNA	ribonucleic acid
RNAi	ribonucleic acid interference
rt	room temperature
s	singlet
sat.	saturated
SDM	site-directed mutagenesis
SEM	scanning electron microscopy
sept	septet
sqPCR	semi quantitative polymerase chain reaction
UPLC-MS	ultra performance liquid chromatograph mass spectrometer
t	triplet
T-DNA	transfer DNA
TBAF	tetra-*n*-butylammonium fluoride
TBS	*tert*-butyldimethylsilyl
*t*Bu	*tert*-butyl
THF	tetrahydrofuran
Ti Plasmid	tumor inducing plasmid
TLC	thin layer chromatography
TMS	trimethylsilyl
UV	ultra violet
WT	Wild Type
XRD	X-ray diffraction
δ	chemical shift

Contents

Chapter 1

Introduction

1.1 The Plant Cell Wall

In order to maintain their rigidity and support their body, vertebrates rely on a rigid skeleton made of bones while insects and crustacean develop an exoskeleton based on the polysaccharide chitin. Conversely, plants achieve rigidity through the presence of an organelle which helps maintaining an internal hydrostatic pressure within cells and through the formation of a rigid extracellular structure, namely, the plant cell wall.[1] The latter also plays a role in cells differentiation, cellular adhesion, intracellular signaling and defense against pathogens.[2]

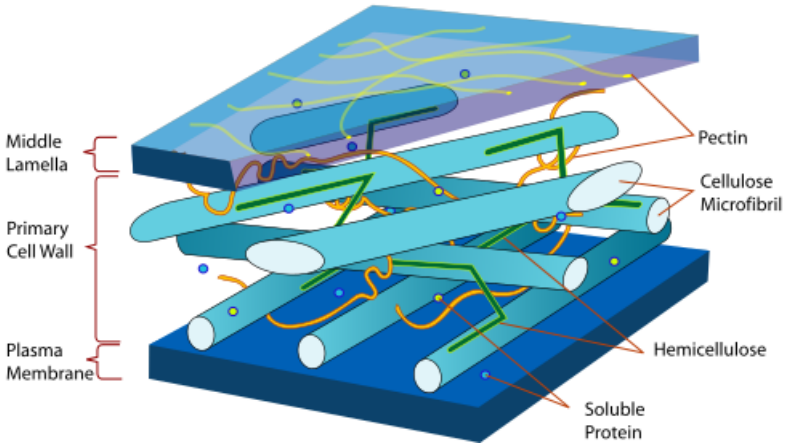

Figure 1.1: Representation of the primary cell wall[3]

A simplified model divides the plant cell wall into two different types, the primary and the secondary cell wall. The primary cell wall is produced when the cell is growing. Therefore, it is rather thin and flexible. In contrast, the secondary cell wall is thicker and sturdier and is deposited on certain type of cells when these have ceased to grow. The primary cell wall, represented on Figure 1.1, is mainly composed of polymeric cellulose, tied together via hydrogen-bonds to form microfibrils. These microfibrils are held together, through non-covalent interaction, by a family of branched polysaccharides called hemicellulose which comprise mainly xyloglucan, xylan, mannan and arabinogalactan.[4] This cellulose-hemicellulose framework is embedded in pectin, a polysaccharide which is considered as the most complex polysaccharide

known to man.[5]

In the secondary cell wall, the amounts of cellulose is typically higher, but the rigidity of the secondary cell walls is mainly due to the presence of another biobolymer called lignin. Lignin is a very complex and not well-defined polymer made of different phenolic monomers.

Apart from their cell wall, land plants also present another feature that is extremely essential to the development, structure and protection of the plants, namely, the cuticle.

1.2 The Plant Cuticle

The world as we know it today would be remarkably different without the terrestrial colonization of plants that happened roughly 450 millions years ago.[6] This event drastically shaped both the biosphere and the atmosphere of Earth.[7] At that point, many challenges had to be overcome by plants in order to survive in this new environment. One those challenges was the regulation of water intake and output. In this context, plants evolution led to the formation of a protective layer allowing plants to thrive in this new aerial medium, the cuticle.[8] The cuticle covers all land plants aerial epidermis and is considered by some as an extension of the cell wall of epidermal cells, a cutinized cell wall. The cuticle acts as a skin for the plant and plays various roles including acting as a primary barrier against biotic and abiotic stresses such as mechanical stresses, pests, microorganism and UV light. The cuticle is also accounted for the regulation of gas exchange and act as a protection against desiccation.[6,9–12] It is also believed to be a key component in establishing organ boundaries. In this context, a common phenotype of defective cuticle mutants of *Arabidopsis thaliana* is organ fusion.[13–16]

The cuticle is a lipophilic composite material made of organic soluble compounds referred to as cuticular waxes, embedded in a polymeric scaffold named cutin (discussed in more details in section 1.3). The cuticle is generally descrived as having two distincts layers as depicted in Figure 1.3. The first of those layers, called the cuticular layer, is located adjacent to the polysaccharidic cell wall. The name cuticular layer was first employed by von Mohl in 1847, who defined this layer as a cuticularised cell wall layer.[17] This layer is mainly composed of cutin as well as polysaccharides from the cell wall.[6,17,18] Overlying the cuticular layer, is the cuticle proper. This layer contains less polysaccharide and is mainly composed of cutin and waxes. The waxes contained

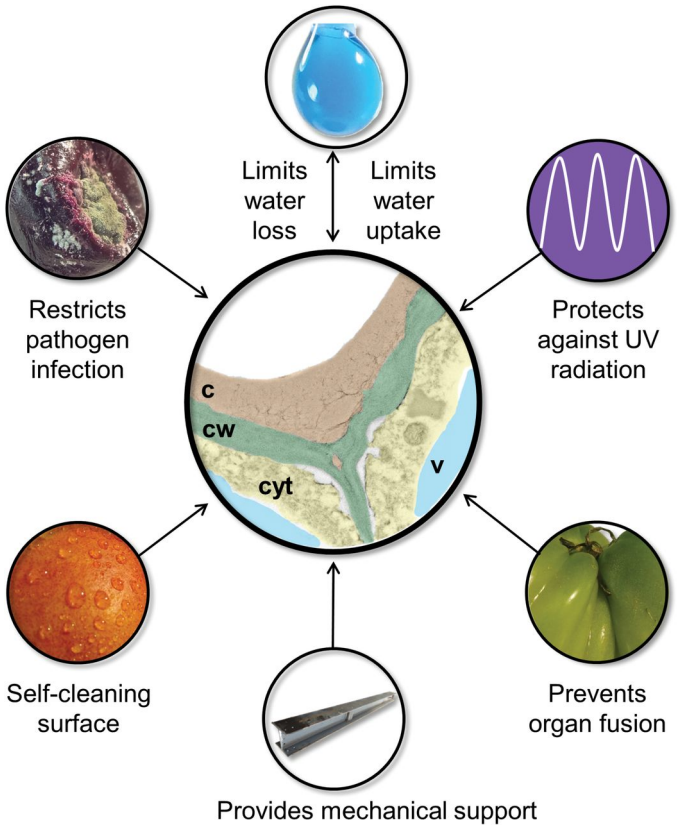

Figure 1.2: Representation of the different role and function of a fruit cuticle. The central image is a colourized transmission electron microscopy image of a small green tomato fruit; c, cuticle; cw; cell wall; cyt; cytoplasm; v, vacuole.[11]

within the cutin matrix are commonly named intracuticular waxes. Additionally, a set of waxes, called the epicuticular waxes, are also deposited on the outermost layer of the cuticle. The epicuticular waxes can be found either in the form of a film, which will give a glossy aspect commonly displayed by many fruits and leaves, or as epicuticular crystals which are responsible for the glaucous aspect of Arabidopsis stems as well as *Brassica oleracea* (broccoli) leaves.[6]

Cuticular waxes are mainly composed of a set of linear unsaturated compounds such as very long-chain fatty acids (VLCFA) and their corresponding aldehydes and primary alcohols, as well as some *n*-alkanes. These various compounds are typically found with chain length of 20 to 40 carbon atoms.[6,19–21] Furthermore, the presence of a series of esters comprised of C16-C34 fatty acids and C20-C36 primary alcohols have also been described.[6,22,23] In some species, other metabolites such as triterpenoids and flavonoids can also be detected in various amounts.[6,20,21,24]

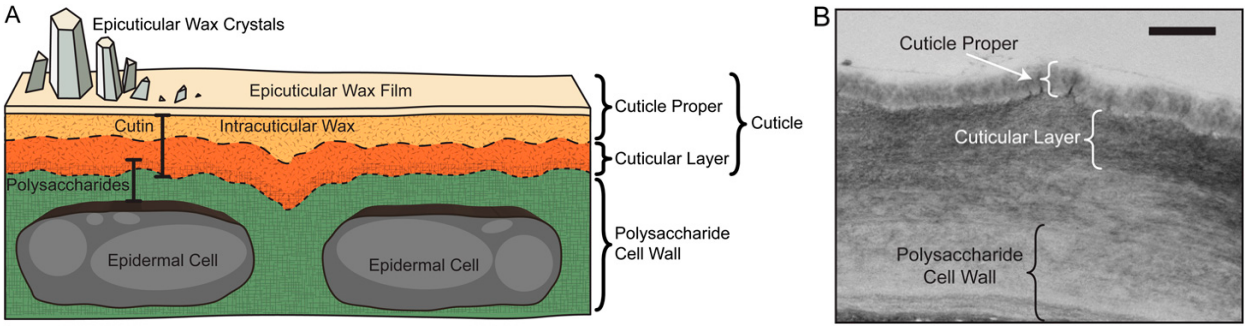

Figure 1.3: A, Schematic representation of the epidermal cell layer and the cuticle. B, Cell wall and cuticle of an Arabidopsis stem epidermal cell observed by transmision electron microscopy; scale bar = 5 µm.[6]

The cuticular waxes are involved in several important process. As an example, waxes are crucial for the water permeability of the cuticle. A study showed that the fruit of a tomato (*Solanum lycopersicum*) mutant (*LeCER6*) possessing an altered cuticular wax profile, showed a drastic increase in cuticle water permeance (approximately 4 fold higher) compared to *wild type* (wt) fruits. To study the contribution of the whole wax fraction, the permeance of fruits that were dewaxed through an immersion in $CHCl_3$ was also studied and showed an increased water permeance by a factor of 10 when compared to the wild type tomato fruit.[25,26]

In some cases, epicuticular waxes and crystals have been associated with the photoprotective properties of the cuticle, potentially through scattering of the UV radiation.[11,12] In this context, flavonoids and other cuticular phenolic compounds have also been shown to absorb a significant fraction of UV radiation.[12]

Additionally, epicuticular waxes and crystals have been suggested to play a role in the plant-insect interaction. As an example, it is thought that the epicuticular crystals present on the carnivorous plants *Nepenthes alata* would be responsible for its slippery surface, necessary for the plants to trap the insects it needs to get fed.[27] The self-cleaning properties, or lotus effect, of plant leaves is also believed to be dependent on the wax crystals through the formation of hydrophobic nanostructures which creates a superhydrophobic surface.[28–30] The presence of this surface is important as it allows the plant to avoid the accumulation of harmful pathogens as well as dust who could prevent lights from going through the plants and therefore hinder the photosynthesis.[6]

However, in order to maintain all those components in place and well distributed, the presence of cutin, which serves both as a scaffold and a support for intra and epicuticular waxes, is necessary.

1.3 Cutin

1.3.1 The composition of cutin

Cutin is a polyester of which the monomeric composition have been previously analyzed through the depolymerization of isolated cuticles. Various depolymerization methods such as alkaline hydrolysis, transesterification, either using sodium methoxide or methanol in acidic conditions and through the use of reductive cleavage with $LiAlH_4$, have been used in order to study cutin monomeric profile.[8]
Cutin is chiefly composed of ω-hydroxy fatty acid dominated by C16 and C18 linear compounds. Examples of typical monomers can be seen in Figure 1.4. Interestingly, the monomeric composition of cutin varies greatly depending on the species, tissue and ontogeny. As an example, angiosperm cutins contains a substantial amount of C18 monomers, however, this class of monomer is only present in trace amount if present at all in gymnosperms.[31] Additionally, the presence of a small amount of C22 ω-hydroxy fatty acid derived from behenic acid was found in some species of berries[32] and the presence of longer chain monomers (C20 to C28) was also confirmed in arabidopsis leaves.[33] This suggests that some species might display a monomeric profile dominated by longer carbon chains similarly to the other main plants polyester called suberin (disclosed more in details in section 1.4).

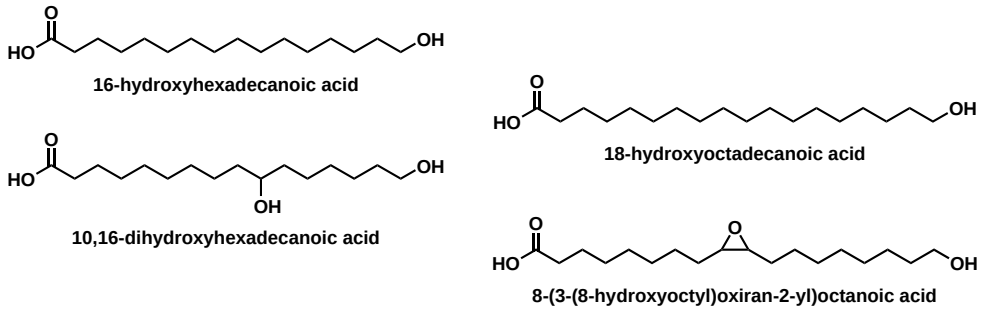

Figure 1.4: Examples of typical cutin monomers obtained through the depolymerization of cutin.[6,18]

It is important to note that *Arabidopsis thaliana*, a plant that is widely used as a model organism in biology, presents a very atypical monomeric composition. Indeed, arabidopsis leaf cutin posseses a substantial amount of α,ω-di carboxylic acid (DCA), with chain length of 16 and mostly 18 carbons, along with 2-hydroxy fatty acids.[33,39] Both of those monomer classes account for 50% of the monomer mixture obtained by acid catalyzed methylation.[33] Interestingly, despite the atypical composition of Arabidopsis stem and leaves, Arabidopsis flowers still diplay a more classical cutin composition dominated by C16 ω-hydroxy acids.[34,40] This very unusual monomeric com-

Table 1.1: Comparison of the monomeric composition of cutin arabidopsis leaves,[33] Arabidopsis flowers (extracted from reference[34,35] and raw data obtained by Nicholas Segerson[36]) and tomato fruits.[21,37,38] Major components are highlighted in bold.

Compound class	Features	Arabidopsis Leaf % (w/w)	Arabidopsis Flower % (w/w)	Tomato Fruit % (w/w)
Fatty acids 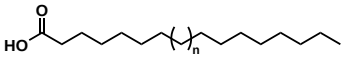	C16	1.32		0 - 0.5
	C18	0.71		0 - 0.2
	C20	0.51		
	C22	1.71		
	C24	2.56		
	C18:1	0.45		
	C18:2	0.82		
n-alcohols 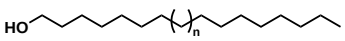	C16	0.06		
	C18	0.42		
	C26	0.37		
	C28	0.73		
ω-hydroxyacids 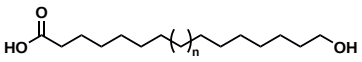	C16	1.59	4 - 5	3 - 5
	C18	0.42		0 - 8
	C18:1	0.20	2 - 3	
	C18:2	2.36	2 - 4	
	C18:3	1.83	~5	
	C20:1	0.60		
α,ω-diacid 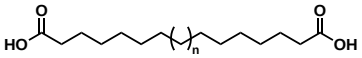	C16	**10.63**	3 - 8	1 - 2
	C18	2.74	1 - 5	
	C18:1	6.58	7 - 8	
	C18:2	**20.97**	4 - 12	
2-OH acids 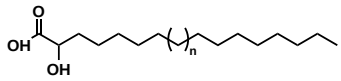	C16	0.23		
	C18	0.33		
	C20	1.43		
	C22	1.50		
	C23	0.48		
	C24	4.52		
	C25	0.42		
	C26	2.30		
	C28	1.47		
	C24:1	1.26		
Mid chain oxygenated acids 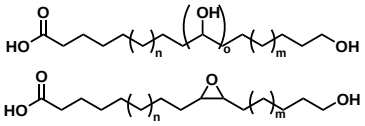	9(10)-hydroxy C16	1.43		
	9(10),16-dihydroxy C16	1.17	**30 - 60**	**72 - 82**
	9(10),18 dixydroxy C18			0.8 - 1.0
	9-oxo-16-hydroxy C16			~2
	9,10,18-trihydroxy C18			0.4 - 1.2
	9,10,18-trihydroxy C18:1			~0.7
	9,10-epoxy-18-OH C18			~0.8

position along with the difficulty to handle Arabidopsis cuticle due to its thin and fragile nature, led scientists to focus their interests on other plants as model organism for analyzing cutin composition.[15]

In recent years, *Solanum lycopersicum* has been growing in popularity as a model organism for cuticle experiments owing to its thick and astomatous cuticle, the ease to isolate a large amount of cuticle for test studies and its more classical monomeric composition. Tomato fruits presents a cuticle density in the order of 1 $mg.cm^{-2}$ compared to Arabidopsis stems that range between 0.5 to 10 $\mu g.cm^{-2}$, hence making it easier to obtain samples from tomato fruit for biomechanical studies.[15,33,41] In this section, we will focus primarily on the cutin composition of tomato fruits and will compare it to the composition of Arabidopsis leaves cutin for reference. This comparison can be found in Table 1.1.

It is important to note that table Table 1.1 does not represent an exhaustive list and that other types and classes of compounds have been found during the depolymerization experiments. For example, the presence of glycerol has been observed in amount that ranges from 1 to 14% (w/w) in several plant species.[37] However, this presence is not so surprising as it was proven that glycerol-3-phosphate acyl transferase (GPAT) enzymes are involved in the deposition of cutin.[34,42,43] these enzymes are responsible for the formation of glyceryl esters, which are believed to be the true precursor of cutin.[44] *Arabidopsis thaliana* cutin has been proven to contain a large amount of glycerol (as observed on the monomer profile obtained through NaOMe catalyzed transmethylation). This high glycerol content can be explained by the DCA-rich cutin composition of Arabidopsis as glycerol can act as a bridge between two or three dicarboxylic acids.[45] The presence of aromatic acids such as ferulic and coumaric acid was also detected in small amount in a variety of species.[24,29,32,36,37,46]

1.3.2 The structure of cutin

Despite the fact that the monomeric composition of cutin has been thoroughly studied in the past, not much is known about the three-dimensional structure of cutin. X-ray diffraction studies were performed on *Solanum lycopersicum* cutin and showed that cutin is an amorphous polymer with low degree of crystallinity and posseses two different basal spacing of approximately 0.45 and 1 nm respectively.[47] On the other hand, analysis of the cuticle through transmission electron microscopy shows that the

cuticle displays three different ultrastructures, amorphous, reticulate and lamellate[31] (The reticulate and lamellate ultrastructures can be observed on Figure 1.5[48]). However, it is not clear yet if those observed ultrastructures arise from a specific spatial arrangement of cutin which could be composition dependents, from other cuticular components such as the waxes and/or the carbohydrate fraction of the plant cell wall or from the interaction between cutin and other cuticular components.[31]

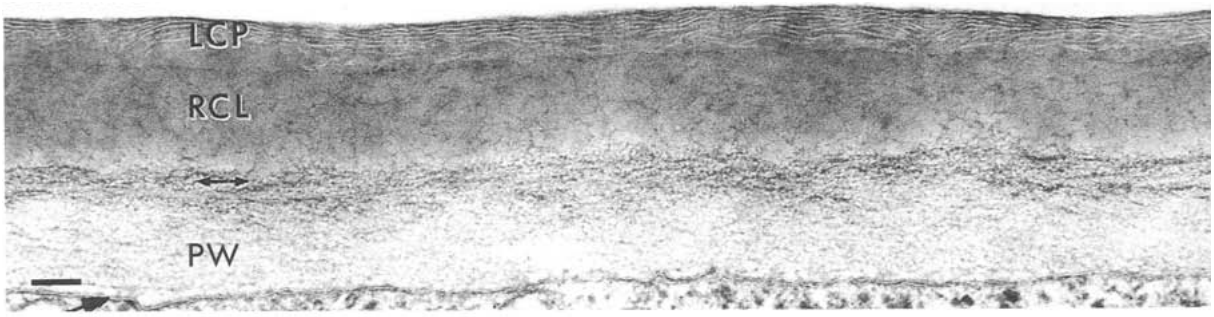

Figure 1.5: Transmission electron micrograph of a bladder of *Utricularia lateriflora*. LCP, lamellate cuticle proper; RCL, reticulate cuticular layer; PW, primary cell wall; Double-ended arrow, supposed pectin layer, bar = 0.1 µm.[48]

The monomeric profile of cutin is typically dominated by compounds possesing one, two or three free hydroxyl groups for one single carboxylic acid. This composition suggests that cutin posseses a larger amounts of free hydroxyl groups with respect to carboxylic groups. This hypothesis was confirmed by the reductive depolymerization of cutin using $LiBH_4$, a reagent that allows for the selective reduction of esters in the presence of carboxylic acid.[49] With the presence of a high amounts of free hydroxyl groups and of both secondary and primary alcohols within the monomers, one could wonder about the presence of branching within the structure of cutin. In order to answer this question, it is possible to derivatize the free hydroxyl groups prior to performing the depolymerization.[31,50] Several species were subjected to such experiments and studies demonstrated that in most cases, a majority of the terminal hydroxyl are esterified. In a similar fashion, monomers possessing a mid-chain hydroxy groups shows a high degree of mid-chain esterification. These findings suggests that cutin tends to possess a highly branched dendrimeric structure, as depicted in Figure 1.6. The presence of diacids and glycerol in the cutin of several species also open the opportunity for cross-links between different dendrimeric units. However, to our knowledge, no proof of the existence of such cross-linkages have been discovered yet. For this reason, cross-linkages were omitted in the model depicted in Figure 1.6.
The interaction between cutin and other cuticular components is also a question that is tightly related to cutin structure. For example, in the cuticular layer, cutin interacts

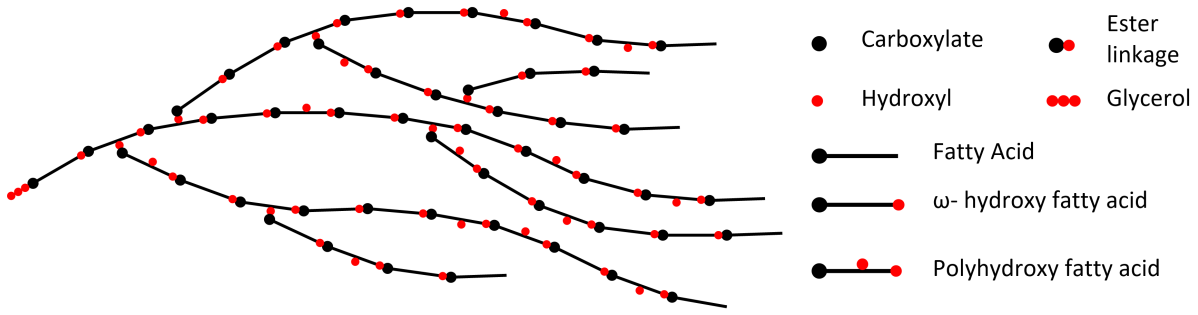

Figure 1.6: Schematic representation of the proposed cutin structural assembly inspired from Pollard *et al.* 2008.[18]

with the cell wall polysaccharides. However, the nature of the polysaccharide that is linked to cutin as well as the type of interaction involved is still an open question. Due to the structure and nature of cutin, different covalent interaction can be envisaged as depicted in Figure 1.7. On one hand, cutin can interact with the carbohydrate fraction through the formation of ester linkage between polysaccharide free hydroxyl groups and a cutin free carboxylic acid. Additionally, ester bonds could also be formed through the condensation of a cutin free hydroxyl groups and a carboxylic acid from the pectin or hemicellulose backbone such as galacturonic acid. On the other hand, cutin could interact with the cell wall polysaccharides through ether bond between carbohydrate free hydroxyls and cutin free alcohols. This hypothesis is supported by the presence of covalently linked carbohydrates with cutin oligomer obtained by the mild depolymerization of lime fruit cutin.[51] In particular, HMBC coupling suggest that the carbohydrate and the polyester moiety are linked by an ether bond.[52] However, this results does not exclude the existence of ester linkages as both type of linkages could coexist within the same cuticular matrix.

As discussed previously, cutin posseses basal spacings of approximately 0.45 and 1 nm, meaning that cutin is not airtight.[47,53] A common assumption is that the space between cutin chains is generally occupied by other cuticular components such as the intracuticular waxes. This spacing and the overall structure of cutin can in some cases be influenced by various conditions such as the pH and the presence and nature of some ions within the cutin matrix.[47]

Studying the structure of cutin is of high importance as the properties of a polymer is tightly linked to its structure. Additionally, furthering our understanding on the association of cutin with other cuticular components might be crucial in order to better delineate the importance and impact of this association on the overall structure and properties of the cuticle. However, the high variety of monomers and waxes as well

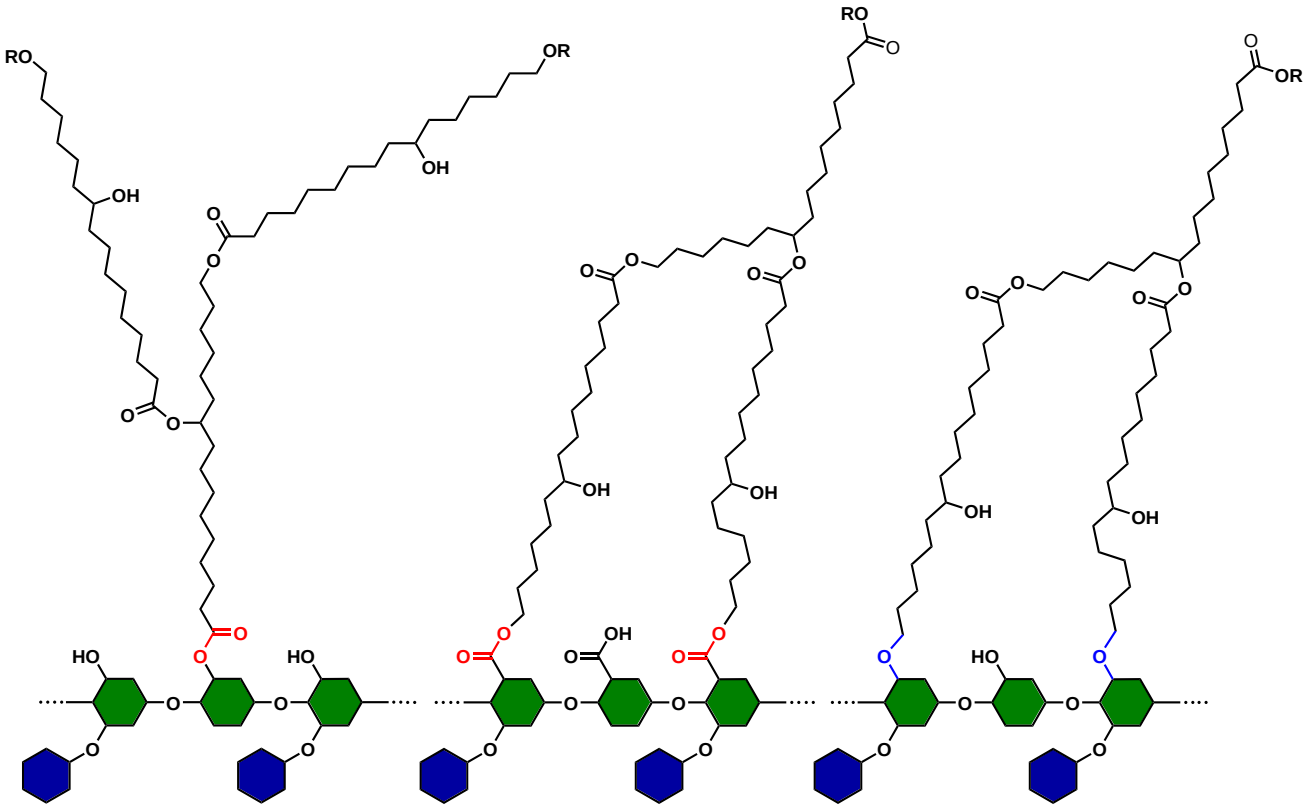

Figure 1.7: Simplified representation of possible linkages between cutin and the cell wall polysacharride. Inspired from Fich *et al.* 2016 and Kinnaert *et al.* 2017.[2,31] Green ring, Galacturonic acid; Blue ring, Xylose.

as the variety in monomeric profile among different species and tissues proved to be a major challenges as those parameters could have a huge impacts on the overall structure of cutin.

1.3.3 The role and properties of cutin

1.3.3.1 Barrier against desiccation

As described earlier, cutin serves as a scaffold for the various cuticular components. As such, cutin might not always have a direct impact on some of the cuticular properties such as the protection against desiccation. And indeed, a series of tomato mutants displaying a drastic decrease (> 95%) in fruit cutin deposition only showed minor increases in water loss.[54] A similar result was observed in a study focusing on RNA interference (RNAi) lines, presenting as well a moderate to high cutin deficiency.[21] In this case, the water permeability of the cuticle was determined through the use of toluidine blue, a hydrophilic dye that can only stain plants if the cuticle is permeable to water, as depicted in Figure 1.8. In this last studies, only one of the lines

(L17) showed a drastic water permeability decrease which was caused by a general organizational defects as observed by atomic force microscopy (AFM).[21] Despite the fact that the waxes were proven to be responsible for the protection against desiccation,[55] there is no direct correlation between the amount of cuticular waxes and the water permeance of the cuticle.[56] These observations suggest that neither the thickness of cutin nor the amount of waxes influence the permeance, but that the integrity of the cutin and the interactions between cutin and the cuticular waxes are important to create an efficient transpiration barrier. This hypothesis is further supported by the presence of hydrophobic interaction between cutin and the cuticular waxes as observed by solid state nuclear magnetic resonance (NMR). This supports that the strong interaction between the polymer matrix and the waxes are necessary to create a tight barrier against desiccation.[53]

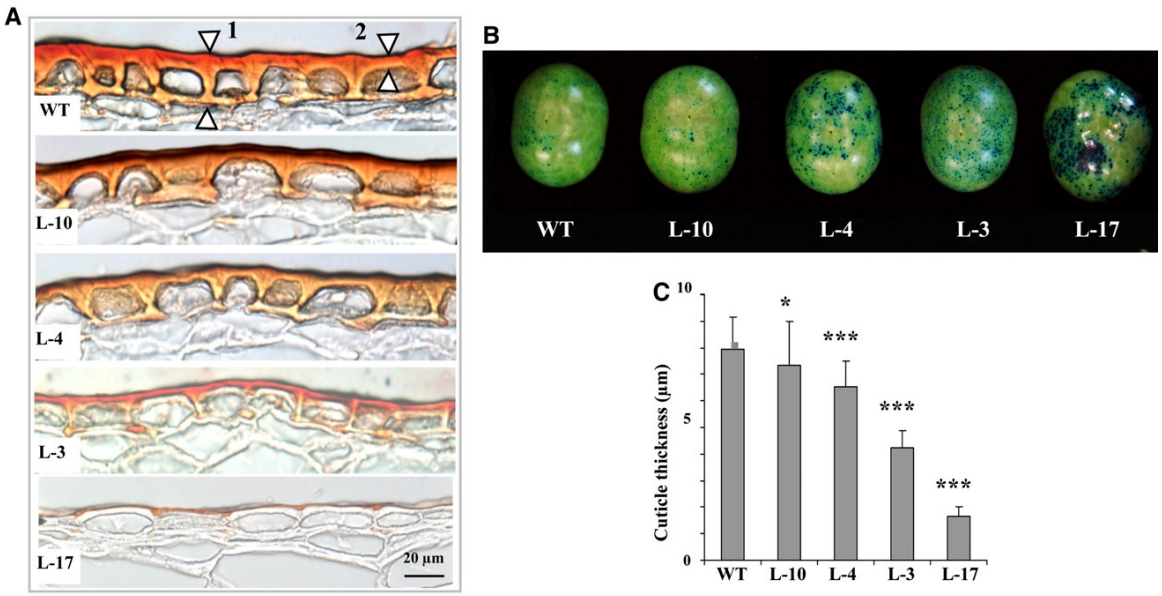

Figure 1.8: A, Tomato exocarp of wild type and transgenic lines stained with Sudan Red to highlight the cuticle. B Tomato fruits of wild type and transgenic lines stained by toluidine blue at 20 days post-anthesis (DPA). C, Cuticle thickness measured on the the thinner zone as displayed by arrowhead 2 in A (n = 60).[21]

1.3.3.2 Protection against UV light

As described previously, flavonoids and aromatic waxes were proven to play a role in the UV protection provided by the cuticle. Additionally, as described in section 1.3.1, cutin possesses a phenolic acid monomer fraction which contributes to the UV-protection as well. These aromatic monomers have also been shown to have an impact

in the UV absorption properties of the cuticle of apple fruits.[12] Specifically, covalently bound aromatic compounds have been found to bear the major responsibility for the UV-B absorption. On the other hand, flavonoids and other aromatic wax constituents have been accounted for the UV-A absorption properties of the cuticles.[12]

1.3.3.3 Organ fusion

Cutin plays a key role in the definition of plant organs boundary. As stated previously, cutin deficiency in arabidosis is often paired with ectotopic organ fusion, as depicted in Figure 1.9.[13–15,34,57–61] Analysis of the fusion area by light microscopy shows that the polysaccharide fraction of the cell wall of the adjoining cells merges with no visible cuticular membrane.[58,62] The presence of non-functional stomata in some fusion zone indicates that despite the occurrence of fusion between tissue, tissue differentiation still exists between the two adjacent epidermal cell layers.[62]
This phenotypes was also observed in some wax deficient mutants but, to our knowledge, it seems to be far less common[13,63] while almost all permeable cuticle arabidopsis mutants seems to present some degree of organ fusion.[64] The fusion phenotype was also observed on cutinase expressing *Arabidopsis thaliana* mutants, further proving the importance of the cuticle in preventing organ fusion.[16,62]

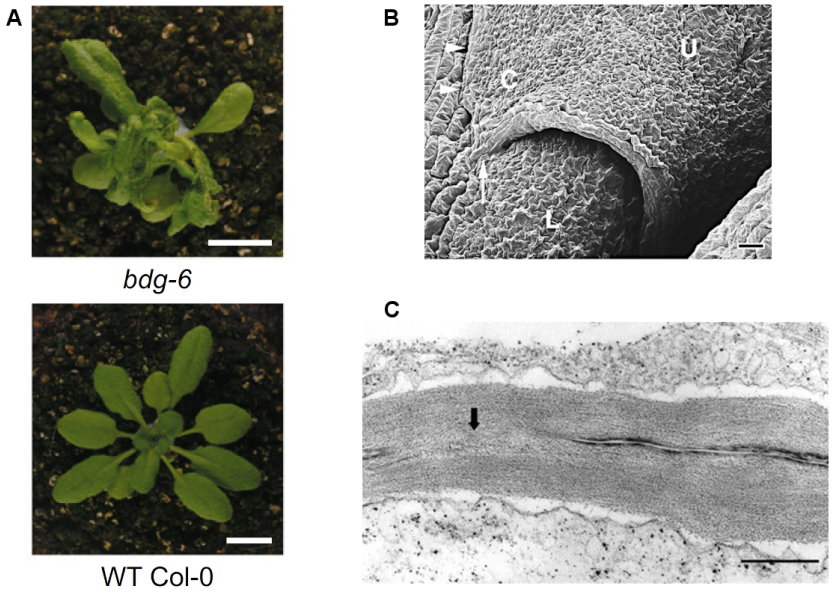

Figure 1.9: Exemple of organ fusion. A, visual phenotypes of organ fusion observed on a bodyguard (*bdg*) arabidopsis mutant compared to Columbia (Col-0) wild type (WT); bar = 5 mm.[65] B, scanning electron microscopy (SEM) of the fusion point between two rosette in a cutinase expressing arabidopsis plant. Arrowheads indicate fusion zone with hidden cell contacts; arrow indicates fusion zone with visible cell contacts; C, leaf corner; L, lower leaf; U, upper leaf; bar = 50 µm.[62] C, light microscopy at the point of organ fusion between two fused leaves of a arabidopsis *bdg* mutants; arrow indicates a point of fusion where the cuticular layer is missing; bar = 500 nm.[58]

1.3.3.4 Mechanical and rheological properties of cutin

Another important aspect to consider when talking about the cuticle and cutin itself, is the mechanical and rheological behavior of cutin. The mechanical properties of cutin and of the cuticle are of importance for biological research, as it could play a key role in organs and plants growth by limiting the expansion of internal tissues through tension.[66] Additionally, these properties are of importance for industrial and economical application as the integrity of cutin and the cuticle plays an important role in fruits shelf life.[67,68] A study has shown that in the case of several cultivars of *Solanum lycopersicum*, the cuticle is responsible for 25 to 50% of the strength of the fruit skin.[69] Biomechanical studies of the whole cuticle proved that the cuticle possess 2 different behavior. Under small stresses, the cuticle reacts as an elastic material (reversible deformation), while at higher stresses, it behaves more as a viscoelastic material (time dependant irreversible deformation).[10,31,70]

The cuticle is a complex composite material, and it has been observed that the cuticle and isolated cutin have very different mechanical properties.[70] A studies showed that, by removing the polysaccharide fraction of isolated tomato cuticle, through the use of anhydrous hydrofluoric acid in pyridine, a decrease in the elastic modulus of the cuticle was observed. The elastic modulus, or Young's modulus, is a value that represents the resistance to the deformation of a material as a response to a force applied to this material. It can be measured as the slope of a stress-strain curve depicted in Figure 1.10. This decrease in elastic modulus indicates that the carbohydrate fraction of the cuticle is responsible for the stiffness and rigidity of the whole cuticle while the cutin matrix is accounted for the viscoelastic behavior.[70,71]

Additionally, it was proposed that the amounts of phenolic compounds also impacts the stiffness of the cuticle. This hypothesis is supported by the increase in stiffness of the cuticle during ripening of tomato fruits, which is accompanied by an increase in the amounts of phenolic compounds.[29,67,70,72] Additionally, a studies performed on a variety of tomato genotypes, presenting a varied amount of flavonoids at the red ripe stage, showed that ripened tomatoes possessing less flavanoid typically have mechanical properties that are similar to that of mature green tomatoes. This further confirms the theory that the flavonoids and other phenolics might play a role in cuticle rigidity.[73]
Furthermore, dewaxing of the cuticle results in a reduction of the elastic modulus as well as a decrease of the fracture force of the cuticle.[71] These results suggests that the waxes acts as polymer fillers, reducing the free space and increasing the rigidity of

the polymer matrix.[10,71,74] In contrast, hydration plays a different role as it was shown that at higher humidity level, for both isolated cutin and the cuticle, shows a decrease in stiffness and strength as depicted in Figure 1.10. This observation hints at the fact that water might act as a plasticiser.[29,70,71] The inclusion of polysaccharides and waxes allows the cuticle to be a more adaptable material. This adaptability was suggested to be beneficial for the plants growth and development. A young plant or fruit would benefits from a more flexible cuticle which would offer the opportunity for expansion. However, as the plant mature, the presence of a more rigid and strong cuticle is more desirable. One could draw some similarity between the cuticle and its adaptable mechanical properties to the presence of the primary cell wall that offer flexibility to the cell and the secondary cell wall that offer a strong and rigid structure to the cell once the maturity is reached.

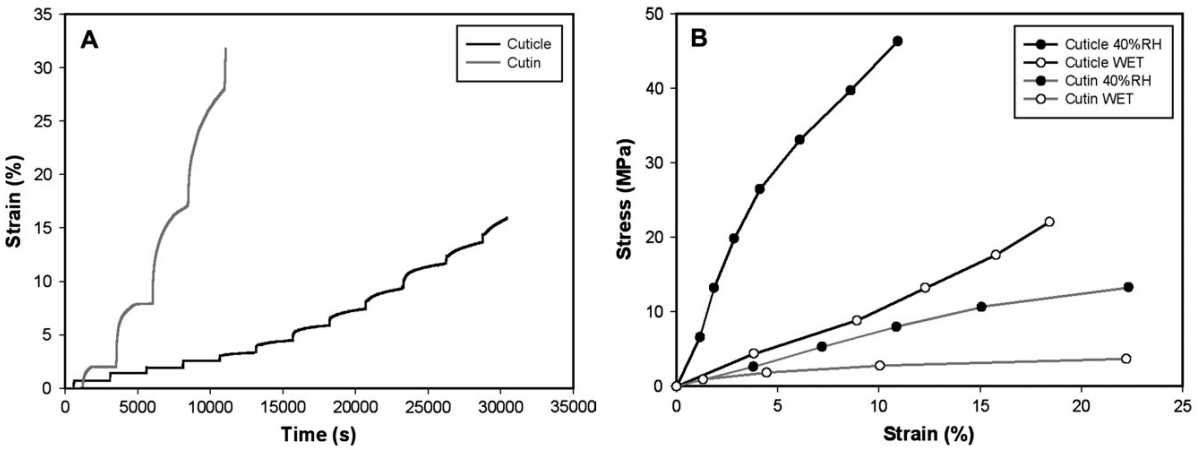

Figure 1.10: Mechanical study of red ripe tomato fruit cuticle and cutin under tensil stress at 23 %. (A) Strain-time curve of isolated cuticle (black line) and cutin (grey line) at 40% relative humidity (RH). (B) Stress–strain diagrams of isolated cuticle (black line) and cutin (grey line) at 40% RH (black circle) and wet conditions (white circle).[70]

As written earlier, cutin is responsible for the viscoelastic properties of the cuticle. Indeed this assumption is supported by different studies performed on the fruit of a large population of *Diospyros kaki* cultivars[75] and on *Sonneratia alba* leaves.[74] These studies have shown that the amount of cutin is related to the viscoelasticity of the cuticle, further proving that cutin is accounted for the viscoelastic behavior of the cuticle.

It is important to note that the composition of cutin may greatly affect its mechanical properties. It was reported that more rigid cuticle could be correlated to cutin rich in C16 monomers while more elastic cuticles would corresponds to cutin with a C16/C18 mixed monomeric profile.[29,76] However, to our knowledge, a comparison

between composition and mechanical properties of isolated cutin has not been reported to date.

Cutin has recently gained the interest of scientist as a potential biodegradable polymer. A recent review by Heredia-Guerrero *et al.*[77] discusses this topic and compares the properties of cutin with those of usual polymers such as high density (HDPE) and low density polyethylene (LDPE), polystyrene (PS), acrylonitrile-butadiene rubber (NBR) and many others. Tomato fruit cutin presents a low stress at break and Young's modulus compared to polymers like HDPE, polypropylene and polyethylene terephthalate (PET) and is more comparable to polymers like LDPE and NBR. However, the latter displays elongation at break that is far superior to that of cutin. In this regard, cutin is more comparable to more rigid polymers such as PS and polymethyl methacrylate (PMMA). Thermal degradation of watermelon cutin has been measured at 200 °C according to thermogravimetric analysis, which is appreciably high and similar to that of polyethylene and rubber.[78] Taking into account all of those parameters, and judging by the high biodegradability of cutin, most of the proposed industrial applications of cutin so far revolves around packaging. However, it is important to note that the properties of cutin can be tuned by the presence of other components such as the cell wall carbohydrates and the cuticular waxes. Hence, understanding exactly how these components changes the properties of cutin can be of great interest for future industrial applications of cutin.

1.3.3.5 Barrier against pest and pathogens

The cuticle is the first line of defense against external stresses. It acts as a chemical barrier and, in parts due to its mechanical properties, allows the plant to withstand some low levels mechanical stresses. But cutin itself plays a role in the defense against pathogens. As an example, the cutin deficient tomato mutants *cd1*, *cd2* and *cd3* presents a higher susceptibility to the fungus *Botrytis cinerea* compared to the control fruit M82.[54] A similar results was observed through the comparison between fruits from the tomato cultivar *delayed fruit deterioration* (*dfd*) and aisla craig (AC) as the red ripe fruits from AC, which possesses a lower amount of cutin, were more susceptible to the *B. cinerea* fungus. Conversly, if the integrity of the cuticle was comprimised, the suceptibility of both cultivar to *B. cinerea* was equivalent.[38]

While the comparison between mutants and cultivars can be very informative, they are typically not good enough to draw definitive conclusions. However, to further prove the claim that cutin acts as a primary defense against pathogen, the inhibition

of a cutinase found in the fungus *Colletotrichum gloeosporioides* proved to eliminate the ability of the fungus to infect papaya fruit in places where the cutin layer remained intact. Additionally, the infection was observed when the tissue was mechanically breached even in the presence of the cutinase inhibitors.[79]

Surprisingly, in the case of cutin *A. thaliana* mutants, a significant increase in their resistance against *B. cinerea* was observed.[80–84] This increased resistance is thought to arise from a better diffusion of either antifungal compounds or external elicitors that would promote the formation of the antifungal compounds. In support of this hypothesis, the presence of anti-fungal activity in leaf extracts (or diffusates) of arabidopsis permeable cuticle mutants (*lacs2* and *bdg*) as well as in a cutinase-expressing mutant was confirmed.[81,84] It is important to note that this anti-fungal activity is selective as the cutinase-expressing and *lacs2* mutants showed no improved resistance to other fungal infection.[81] Additionally, *lacs2* mutant presents an increased suceptibility to a typically avirulent bacteria, *Pseudomonas syringae*.[80] This last observation further proves that cutin plays a role as a primary barrier but also hints at the fact that cutin might also play a role in secondary defense mechanisms. As an example of the potential role of cutin in secondary defense mechanism, it was found that cutin monomers acts as elicitors of plant defense in various plants such as rice and barley,[85] potato[86] and cucumber.[87] Taking into account that cutin monomers are released during the enzymatic degradation of cutin, it is not surprising that some plants have developed a damage-associated defense mechanism triggered by the presence of cutin monomer.

1.3.4 The biosynthesis of cutin

Despite its unusual composition of cutin monomers, *A. thaliana* has proven to be a valuable model organism in unraveling the intricacies of cutin biosynthesis owing to clear phenotypes observed on arabidopsis cutin mutants such as organ fusion and permeability to toluidine blue. Much progress have been made through the genetic studies of *Arabidopsis thaliana* in conjunction with *Solanum lycopersicum*. This next section will focus on the different aspects of cutin biosynthesis, including the synthesis of cutin precursors and their transport, the polymerization of the precursors and the regulation of cutin biosynthesis. A general overview of cutin biosynthesis can be found on Figure 1.11.[31]

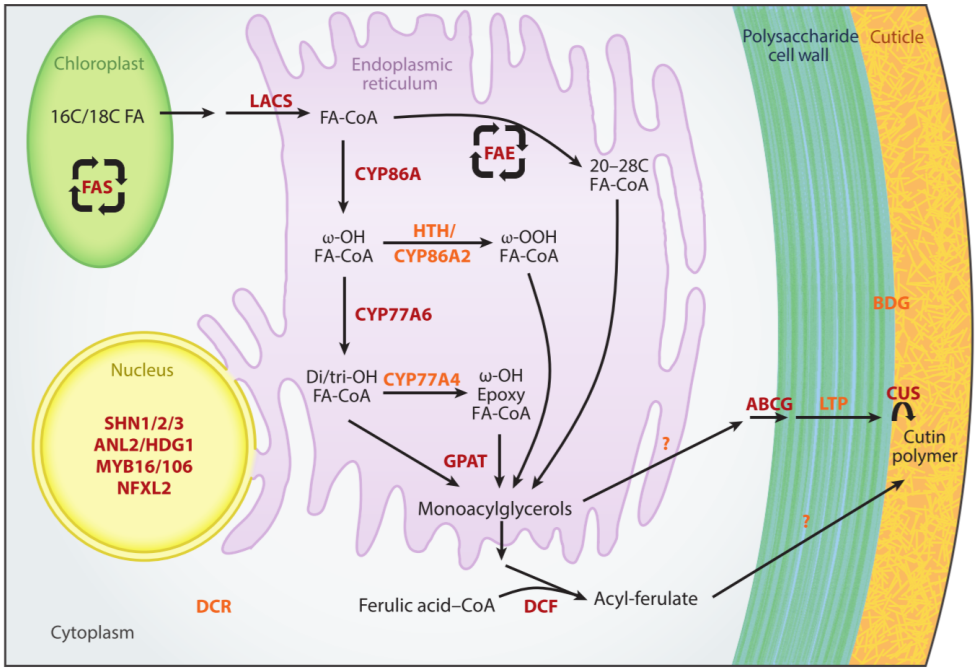

Figure 1.11: Representation of the known biosynthetic pathway leading to cutin formation. Names in red represent enzyme or protein complex with a known function; names in orange represent protein with putative or unknown function. In the case were several paralogs are relevant, only the gene subfamily is shown. Abbreviations: C, carbon; CoA, coenzyme A; FA, fatty acid; FAE, fatty acid elongase complex; FAS, fatty acid synthase complex.[31]

1.3.4.1 Synthesis of cutin monomer

The synthesis of cutin precursors starts from C16 and C18 fatty acid (FA) produced in plastids. These acids are transported to the endoplasmic reticulum (ER) where they are enzymatically transformed into oxygenated monoacyl glycerol. Several processes are involved in this transformation. The first step is thought to involve long-chain acyl-CoA synthetase (LACS) enzymes. In particular, LACS1 and LACS2 have been shown to be responsible for the formation of C16 precursors and are thought to activate the fatty acid into acyl-CoA.[88] Those two enzymes seems to have a redundant function as some pleiotropic effect like organ fusion only appears in the case of *lacs1-lacs2* double mutants.[61] Interestingly, mutation of LACS1 affects the production of C16 monomers but also affects the production of waxes. A substantial decrease in wax contents, at the exception of VLCFA waxes that shows a drastic increases, was observed in both *lacs1* and *lacs2* mutants.[61,88] Furthermore, LACS1 possesses a high affinity for C30 FA with C16 only coming second hinting at the fact that while LACS1 has a definitive effect on cutin biosynthesis, it also activates VLCFA for further enzymatic treatments in wax biosynthesis.

The next step in cutin biosynthesis is the oxidation of the precursors. Two different oxidation, namely terminal ω-oxidation and mid-chain oxidation, can take place and are thought to be carried out by different subfamilies of the cytochrom p450 enzymes. The CYP86A subfamily is accounted for the ω-hydroxylation as indicated by the altered cutin composition of *cyp86a2*, *cyp86a4* and *cyp86a8* mutants[34,83,89,90] as well as the *in vitro* ω-oxidation activity of *CYP86A2*, *CYP86A4* and *CYP86A8* transcripts.[57,91,92] Owing to the fact that a member of the CYP86A subfamily found in *Petunia hybrida* shows a lower affinity for fatty acids than for their Acyl-CoA derivatives, the terminal oxidation steps is thought to happen after the LACS CoA activation.[93] Formation of diacid monomers such as the one presents in arabidopsis cutin would require further oxidation of the ω-carbon. No enzymes have been directly tied to this advanced oxidation step, however, due to the monomeric profile impoverished in diacids of their respective mutants, both CYP86A and an oxidoreductase named HOTHEAD have been considered as likely candidates.[89,94]

Mid-chain oxidation is carried out by the CYP77A subfamily of cytochrom P450 enzymes.[6,31] At the time of writing, only one of those enzyme, CYP77A6, has been directly linked to cutin synthesis, and is accounted for the mid-chain oxidation leading to the formation of 10(9),16-dihydroxypalmitate monomer in cutin petals.[34] Contrastingly, CYP77A4 was found to catalyze the *in vitro* epoxidation of unsaturated C18 fatty acids but its implication in cutin biosynthesis has not been proven yet.[95] Interestingly, CYP77A6 was found to catalyze the mid-chain oxidation of ω-hydroxypalmitic acid but not of the non-hydroxylated palmitic acid. Additionally, arabidopsis mutants of the *cyp77a6* gene possess a cutin composition enriched in 16-hydroxy palmitic acid and in 1,16-dicarboxylic C16 monomers but no 10,16-dihydroxy palmitic acid. These two lines of evidence indicates that the ω-oxidation occurs prior to the mid-chain oxydation.[34]

Another enzyme family is involved in the preparation of cutin precursors, the glycerol-3-phosphate acyl transferase (GPAT) enzymes. In particular, the arabidopsis GPAT4, GPAT6 and GPAT8 are required for cutin biosynthesis.[34,40] GPATs enzyme typically catalyze the sn-1 acylation of glycerol-3-phosphate leading to the formation of lysophosphatidic acid. However, GPATs involved in cutin biosynthesis acylates glycerol on the sn-2 position over the sn-1 position. Additionally, GPAT4 and GPAT6 possess an active phosphatase domain. This bifunctional activity allows for the synthesis of 2-monoacylglycerol (2-MAG), which are believed to be the actual cutin precursors as already described in section 1.3.1,[44] as observed by in vitro assays.[96,97]

1.3.4.2 Cutin precursor transportation

The next important steps in cutin deposition is the transport of the monomers from the ER to the site of polymerization. This mechanism is still largely unknown and represents an interesting field of research for scientists. However, several mechanism have been postulated.[98] One such mechanism would be through the use of ATP-binding casette (ABC) transporters, a family of transmembrane proteins. This theory is supported by the reduced cutin load of *wbc11*, a line of arabidopsis T-DNA insertional knock-out mutants targeted at ABCG11, a member of the ABC transporters.[59] Additionally, mutation of the ABCG13 transporter resulted in both a floral cutin load decrease along with flower organ fusion while ABCG32 mutations proved to induce a reduction in arabidopsis petal cutin deposition and an increased resistance to *B. cinerea* all of which are typical cutin defficiency phenotypes.[82,99]

Another family of transporters, the lipid transfer proteins (LTP), has been proposed to play a role in cutin deposition based on their *in vitro* binding properties with lipids including fatty acid precursors of cutin.[100] Two different LTPs, LTP1 and LTP2, were shown to be involved in cuticular wax transport, but no evidence of such activity were found for cutin monomers.[101–103]

Another transport mechanism hypothesis relies on the transport of monomers through the formation of exocytotic vesicles. This mechanism would in term allows for the transport of a much larger quantity of monomers at once, however, to our knowledge, there is no evidence to support this theory.[98]

1.3.4.3 Polymerisation of cutin

The last step in cutin biosynthesis is the polymerization of the monomers into a polymeric scaffold. The mechanism of polymerization has been a long-standing question. The original work from Croteau and Kolattukudy in 1974 was the first experience that hinted at an enzymatic acyltransferase polymerization mechanism.[104] More recently, an acyltransferase named defective in cuticular ridges (DCR) was tied to the cuticle biosynthesis due to the lack of 9(10),16-dihydroxy-hexadecanoate monomer in the floral cutin composition of its respective arabidopsis mutants.[105] However, the cytosolic localization of this enzyme combined with its *in vitro* diacylglycerol acyltransferase activity leading to the formation of triacylglycerol is not consistent with its proposed role as a cutin polymerase.[46] At the time of writing, the role of DCR in cutin biosynthesis is still not well understood.

Another enigmatic enzyme that has been proposed as a cutin polymerase is the *A. thaliana* BODYGUARD (BDG), an α/β hydrolase that is expressed in epidermal cells as well as in root endodermis.[58,65] An *Arabidopsis thaliana bdg* mutant shows a disrupted cuticular organization but an increased cutin deposition.[58] Interestingly, another study showed that two different *bdg* mutants present a reduced cutin deposition for young leaves while the overexpression of *BDG* leads to a drastic increase in cutin load.[65] Unless a yet to be discovered overcompensation regulation mechanism between BDG and redundant enzymes exists, the increase in cutin deposition of *BDG* null mutant is not consistent and BDG most likely contributes to the cuticule formation through an unknown mechanism.[6]

In recent years, lipases/esterases possesing a glycine - aspartic acid - serine - leucine motif (GDSL motif) have been growing in popularity as candidates for cutin polymerisation. This popularity was triggered by the discovery of the induced expression of a gene encoding for a putative GDSL lipases/esterase by WAX INDUCER 1 (WIN1), also called SHINE1 (SHN1), a transcription factor known to be implicated in cutin biosynthesis.[106] Additionally, several GDSL-motif lipase/esterase were found to be expressed preferentially in the epidermal layer of tomato fruits.[107]

The involvement of GDSL esterases in cutin biosynthesis was confirmed in 2012, when two research groups independently discovered the existence of a tomato GDSL lipase whose expression level affects cutin deposition.[21,44] One of these research group relied on the formation of RNA interference mutants targeted at reducing the expression of the *GDSL1* gene (also known as *CD1*). These mutant lines showed a drastic reduction in cutin deposition and a high perturbation of the cuticular matrix at drastically low expression level. The other research group focussed on the study of *cutin deficient 1* (*cd1*), a tomato null mutant which fruits only possess about 5% of wild type tomato M82 and which was found to accumulate 2-mono-(10,16-dihydroxyhexadecanoyl) glycerol (2-MHG), the glycerol precursor to tomato cutin main monomer (see section 1.3.1). Immunolocalization of the transcripts of *CD1*, a GDSL-lipase named CD1 and later renamed cutin synthase-like 1 (CUS1),[108] showed that this protein was primarily expressed in the epidermis and more particularly, in the cuticle. Furthermore, recombinant CUS1 was found to catalyze the *in vitro* polymerization of synthetic 2-MHG into linear oligomers.[44,108] However, this might differ for the *in vivo* polymerization as an unpublished study indicates that CUS1 might be responsible for mid-chain acylation.[31] The polymerization is believed to occur through the formation of an acyl-enzyme intermediate in a ping-pong bi-bi fashion as depicted in Scheme 1.1. How-

ever, no experimental evidence have been found to confirm this mechanism at the time of writing.[108] Interestingly, orthologs of CUS1 were found in both, Arabidopsis and the moss *Physcomitrella patens*, indicating that CUS1 is part of a well conserved family of enzymes.[108] Additionally, the existence of another CUS enzymes, CUS2, was confirmed in arabidopsis, unfortunately, the difference in role between the different members of the CUS familly is currently not well understood.[36]

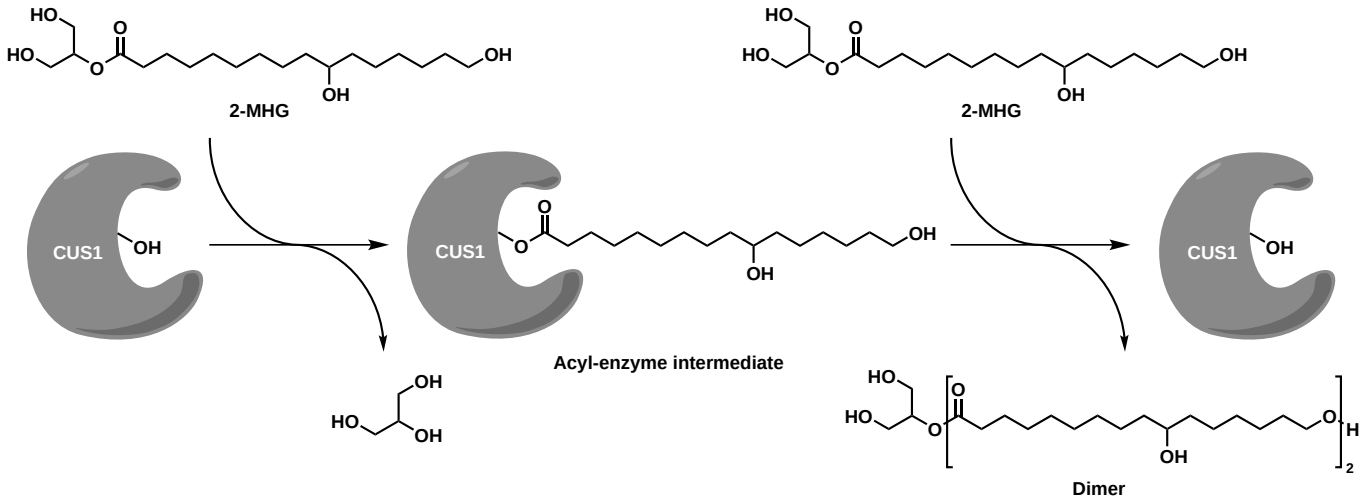

Scheme 1.1: Proposed mechanism for the CUS1-catalyzed 2-MHG dimerization. Further polymerization occurs by using the newly formed dimer as a substrate for an additional acyl trasfer. Recreated from Yeats *et al.* 2014[108]

The discovery of CUS enzymes is still rather new and several questions still surrounds its mechanism of action, its specificity and selectivity as well as its three-dimensional structure. The presence of a small cutin deposition in the null mutant *cd1* is also intriguing as it opens the door for potential new enzymes as well as for different compensating mechanisms. The research on cuticle formation, a critical and ubiquitous step of land plants formation, would greatly benefits from a better understanding of cutin synthase-like enzymes. Furthermore, the formation of the cuticle has a huge impact on the conservation of plants and fruits as demonstrated in section 1.3.3, and improving our knowledge of cutin formation could potentially have an impact from an industry point of view. Hence, the study of CUS enzymes might be a critical field of research for both biological research as well as industrial applications.

1.4 Suberin

As described in section 1.3.1, cutin is not the only plant polyester. This section will focus on the second plant polyester, suberin, and attempt at comparing plant polyesters

in their function and composition.

Suberin is an extracellular polymeric matrix similar to cutin, but contrarely to cutin, suberin layers are deposited primarily on the periderm, the exodermis of roots, as well as the endodermis of roots where it covers the cells of the casparian strip.[18,109–116] Suberin is also deposited in wounded tissue,[117,118] in the bundle sheath of monocots, and it is the main components of cork.[119] Similarly to cutin, suberized layers are also associated with a mixture of organo-soluble waxes.[118] Suberin associated waxes comprise a variety of compounds such as very long chain alkanes (From C17 to C35), fatty acids and fatty alcohols (from C16 to C28), ω and 2-hydroxy fatty acids (C16 to C22), α,ω-dicarboxylic acid (C16 to C22), hydroxyaromatic acids, 2-hydroxy fatty acids and sterols.[8,120]

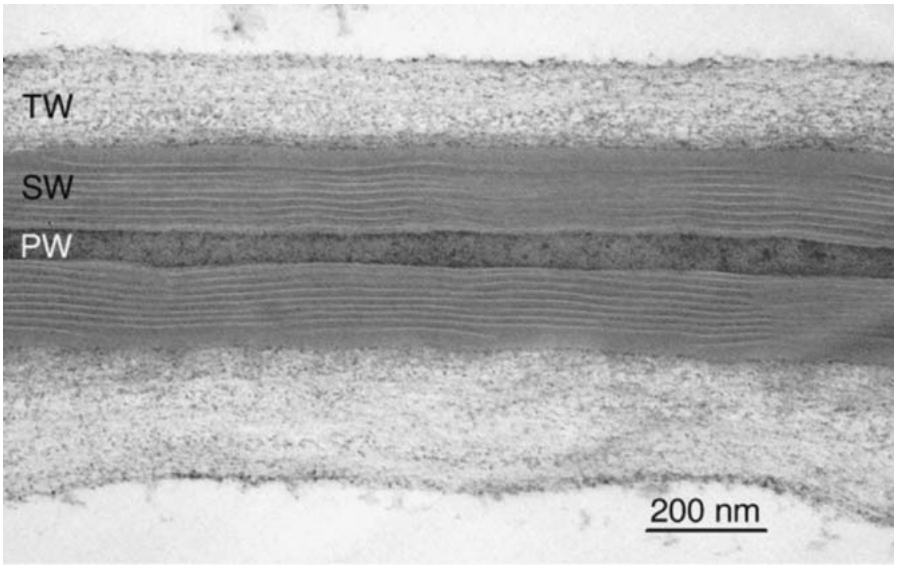

Figure 1.12: Ultrastructure of Suberin as observed by TEM of the cork cell wall. PW, Primary cell wall; TW tertiary cell wall; SW Suberized secondary wall.[121]

While cutin is deposited on the outer face of the cell wall of epidermal cells, suberin is typically located on the inner face of the primary cell wall or in the secondary cell wall.[18,42,122]

Similarly to the cuticle, suberin and the associated waxes provides a protection against uncontrolled water and solutes diffusion while acting as a primary defense barrier against pathogen. In the case of root exodermis and endordermis, suberin is essential in regulating apoplastic water movement.[18,116,119,123,124] Additionally, suberin plays an important role in wound healing and in the abscission process.[117–119]

Microscopic analysis of suberin by TEM, depicted in Figure 1.12, shows that suberin forms poly-lamellate structures of light, electron translucent, and dark, electron opaque, lamellae. This structure have long been used to define the suberin layer but some species seems to possess suberin layers that do not comply to that structure.[125]

1.4.0.1 Composition and structure

It is commonly accepted that the lamellate structure of suberin arises from its composition. Indeed, suberin presents a monomeric composition that differs substantially from cutin yet still reamains similar. Two main families of monomer can be observed by the depolymerization of suberin, the aliphatic monomers and the aromatic monomers.[18,111,114,119]

Aliphatic monomers can be easily studied via depolymerization by methanolysis. A summary of the composition of suberin obtained through methanolysis for three distinct species can be found on Table 1.2. Suberin aliphatic fraction is mainly composed of α,ω-dicarboxylic acid as well as glycerol. The presence of *n*-alcohols, fatty acids, and ω-hydroxy fatty acids was also observed in various amounts among different species. The chain length of suberin aliphatic monomers is typically longer than that of cutin monomers and generally varies between C16 and C30. Unsaturated and oxygenated diacids and ω-hydroxy fatty acids can be found with chain length of 18 carbons.[18,122,126,127]

As indicated in Table 1.2, the presence of phenolic acids such as ferulic acid have been observed using methanolysis. However, only a low amounts of aromatic is observed through this method as it was observed that majority of the aromatic fraction is resistant to transesterification and has been estimated to make up for around 31% of the weight for potato periderm.[119,128–130] Due to its high chemical resistance, the nature of the polyaromatic fraction is less defined than its aliphatic counterpart. The use of harsh depolymerization methods such as alkaline nitrobenzene oxidation lead to the assimilation of the polyphenolic fraction of suberin with lignin, another plants polyaromatic polymer.[131] However, solid state ^{13}C NMR analysis of wound-induced potato suberized tissue have indicated that the major components of suberin aromatic fraction are hydroxycinnamic acids, and derivatives, held together through non-ester covalent linkages.[129] To date, the nature of those covalent bonds is still to be determined.

A general belief is that the translucid lamellate is chiefly composed of aliphatic compounds while the electron dense lamellate is made of aromatic monomers. Taking into account this hypothesis, the monomeric composition of suberin and the potential

Table 1.2: Comparison of the suberin monomeric composition of three different species as analyzed after methanolysis depolymerization.[122,126,127]

Compound class	Features	*P. menziesii* % (w/w)	*Q. Suber* % (w/w)	*S. tuberosum* % (w/w)
Glycerol 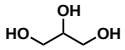		26	14.2	22
Phenolics 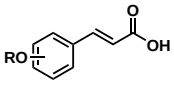		0.8	0.8	1
n-alcohols 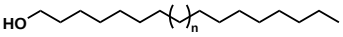	C18–C26	0.6	0.4	2.5
Fatty acids 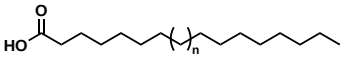	C16–C22	3.6	1	0.7
	C23-C30	1.6	0.1	7.7
ω-Hydroxyacid 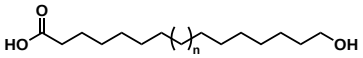	C16	4.3	0.4	1.3
	C22	1.7	7.9	0.6
	C18, C20, C24–C28	3.5	3.1	0.8
	C18:1	1.7	5.4	12.1
	9-epoxy C18	-	7.3	-
	9,10-dihydroxy C18	0.2	2.2	-
α,ω-diacid 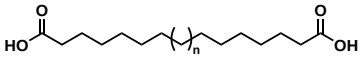	C16	18.7	2	0.7
	C22	1.6	4.5	-
	C18, C20, C24, C26	8.9	2.2	1.1
	C18:1	9.1	6.2	30.1
	9-epoxy C18	-	22.9	-
	9,10-dihydroxy C18	1.6	7.7	0.1
other unidentified		2.2 13.9	1 10.7	- 19.3

interaction between monomers, a hypothetical structure of suberin, depicted in Figure 1.13, has been proposed.[119,122] This proposed structure have not been proven experimentally but is supported by the correlation observed between suberin monomer length and the thickness of the electron translucent lamellae.[132] Furthermore, the presence of glyceryl-DCA-glyceryl and DCA-glyceryl-DCA trimer was confirmed by par-

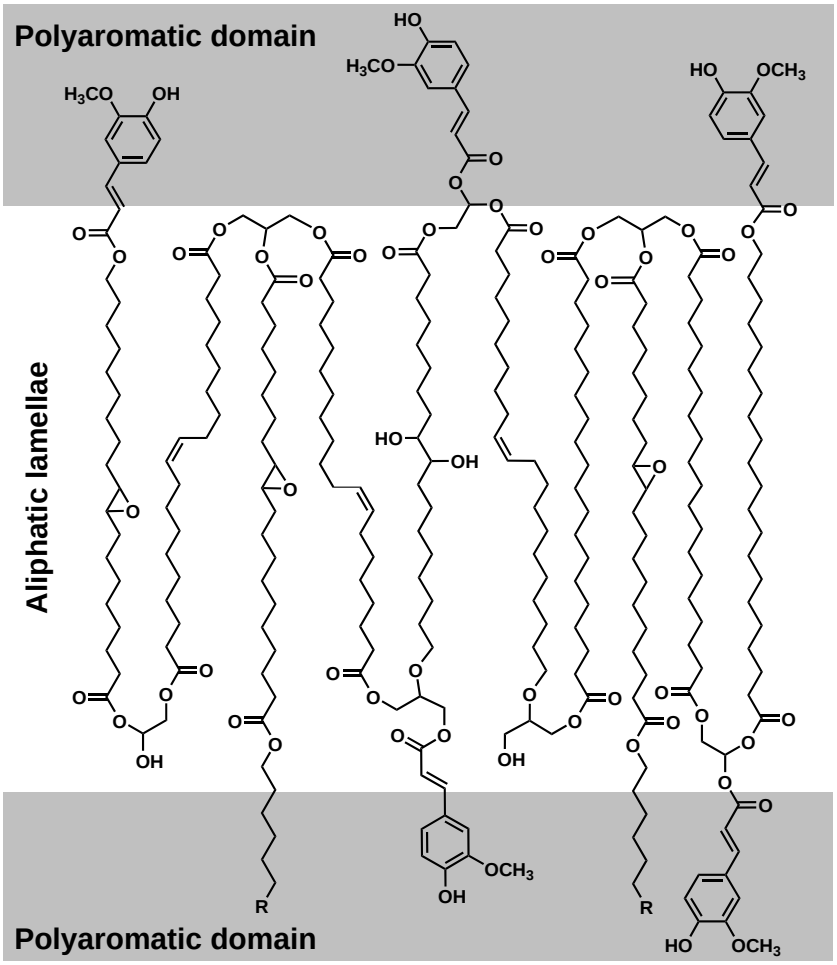

Figure 1.13: Proposed structure of suberin inspired from Graça *et al.* 2007[122]

tial depolymerization.[133] Finally, solid-state NMR proved the existence of two different aliphatic carbon types, a more flexible one comprised of short chains alkyl corresponding to the glycerol backbones, and a more rigid domain corresponding to the long alkyl chains.[134,135]

1.4.1 The biosynthesis of Suberin

The biosynthesis of suberin major aliphatic monomers follows a very similar pathway to the one of cutin. An overview of the biosynthetic pathway can be found on Figure 1.14 For the sake of simplification, the formation of the aromatic domain as well as the preparation of aromatic monomers will not be discussed here.

Suberin monomers synthesis starts with fatty acids produced in plastids. These differ-

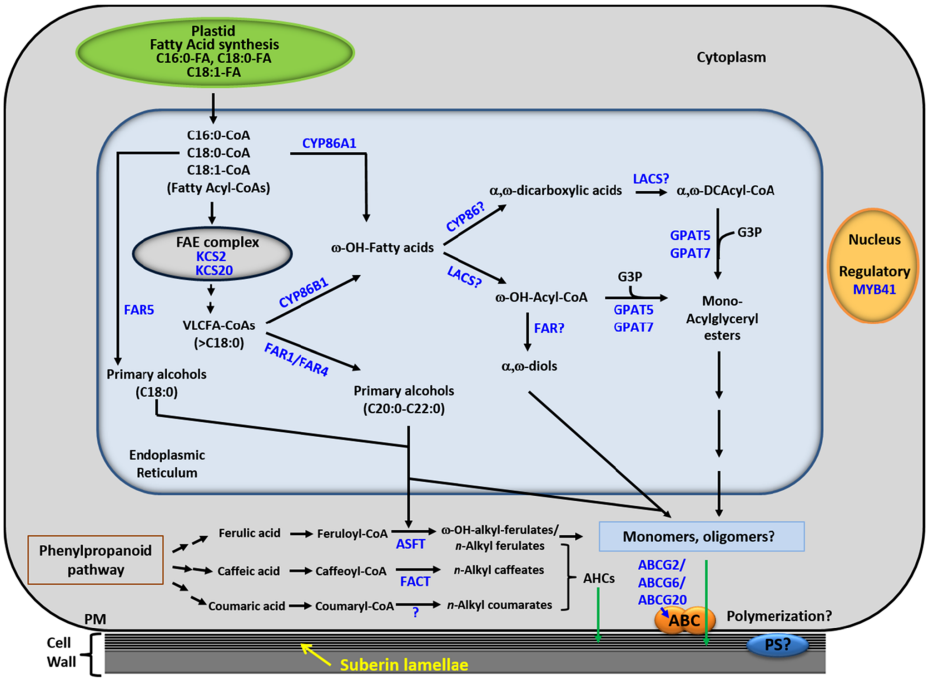

Figure 1.14: Overview of the known suberin biosynthetic pathway.[136]

ent precursors are transported to the ER where they undergo several transformations such as elongation, oxidation or reduction and glycerol esterification.

Enzymes such as CYP86A1 has been tied to the ω-oxidation of small chain monomers with chain length ranging from C12 and C18 according to *in vitro* studies,[137] while CYP86B1 is accounted for the terminal oxidation of C22 and C24 monomers.[138,139] To the best of our knowledge, no enzymes responsible for the mid-chain oxidation have been discovered. Additionally, the oxidation of the ω-carbons leading to the formation of carboxylic acid remains an open question.

GPAT enzymes are also involved in suberin synthesis. In particular, GPAT5 was found to be responsible for the sn-2 acylation of long chain monomers (C20–C24).[40,96] Overexpression of GPAT5 lead to the formation of sn-2 MAG, however, in contrast with cutin-related GPATs, recombinant GPAT5 was proven to lack the phosphatase activity. This results indicated that external phospholipases might be necessary for the preparation of suberin monomers. It is important to note that *gpat5* mutants only showed a decrease in very long chain monomers, indicating that other GPAT enzymes might be involved in the preparation of shorter length precursors.[96] In this respect, the wound-induction of GPAT7 expression and the presence of suberin-like monomers when overexpressed indicates that this enzyme is tied to wound-induced suberin pro-

duction.[97]

The involvement of GPAT enzymes hints at the potential existence of suberin-related LACS enzymes. To the best of our knowledge, no specific LACS enzymes were associated with suberin biosynthesis up to date, however, the cutin-related LACS2 enzyme might also play a role in suberin synthesis (Isabel Molina, unpublished data[140]).

The alcohols monomers are prepared through the reduction of the activated fatty acyl. Enzymes involved in this process are called fatty acyl reductases (FARs). In the case of suberin synthesis, three different FAR have been identified, FAR1, FAR4 and FAR5.[120,141] Mutation of the related genes shows that the three reductases are chain-length specific: FAR1 is related to C22-OH formation, FAR4 reduces C20 monomer and FAR5 is responsible for C18-OH production.[141] Triple mutation of the *FAR* genes lead to a decrease in *n*-alcohols monomer of about 70 to 80% without affecting the other main monomers. This decrease in alcohol monomers proved to be detrimental to the permeability of seed coat, indicating that the presence of these monomers might play a big role in suberin permeability.[120]

The starting precursors of suberin monomers are C16 and C18 monomers, however, suberin is characterized by longer chain monomers. The elongation of fatty acids is catalyzed by a complex of enzymes called fatty acid elongase (FAE).[142] The elongation process is controlled by β-ketoacyl-CoA synthase (KCS), the enzyme responsible for the first reaction of the elongation process.[143] Two different KCS enzymes are involved in the elongation of C20 suberin fatty acid, KCS2 and KCS20.[101,144] The composition of the arabidopsis *kcs2* and *kcs20* null-mutant is impoverished in C22 and C24 fatty acid derivatives and enriched in C20 monomers. This effect is even more drastic for the *kcs2-kcs20* double mutants, indicating that KCS2 and KCS20 is mostly functionally redundant.[101] In potato, StKCS6 was accounted for the preparation of C28 monomers and higher chain length.[121]

Transport of the monomer through the plasma membrane requires ABCG transporters. In particular, suberin monomer transport requires ABCG2, ABCG6 and ABCG20. Mutation linked phenotypes could only be observed via the simultaneous mutation of the three transporters, which suggests that these transporters are functionally redundant.[146]

The last step in the biosynthesis of suberin is its assembly from the monomers. Un-

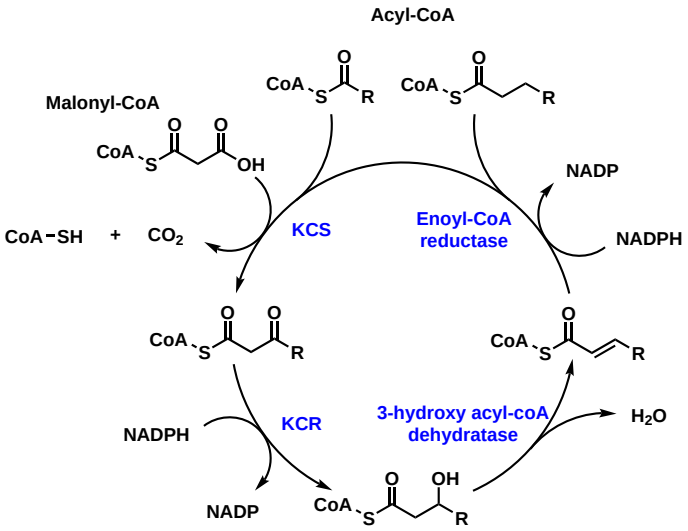

Scheme 1.2: Representation of the elongation cycle of the fatty acid elongase complex.[145]

fortunately, at the time of writing, researchers were not able to identify any suberin synthases (SUS). Cutin and suberin shares a lot of similarities. These similarities lead scientists to believe that the formation of cutin and suberin arises from a common plant functionality and diverged over time. This theory is further supported by the suberin-like cutin composition of arabidopsis. In this context, GDSL lipases are under investigation for potential SUS. The identification of a GDSL lipase/esterase type suberin synthase would prove to be a valuable evidence towards the common plant functionality theory.

1.5 Chemical synthesis of cutin monomer: state of the art

In order to study some cutin-related phenomena, several groups have synthesized cutin monomers. As an example, as a mean to study the effect of cutin monomers on the activation of a lipid-activated protein kinase from *Colletotrichum trifolii*, Ahmed *et al.* devised an asymmetric synthesis of 10,16-dihydroxyhexadecanoic acid (**6**), the main repeating units of tomato cutin.[147]

The first part of the synthesis, depicted in Scheme 1.3, relies on the benzyl protection of 5-hexynol followed by coupling with 10-undecenal to obtain propargylic alcohol **2** as a racemic mixture. Assymetry is then obtain by the oxidation of the mid-chain alcohol into a ketone that can be reduced using chiral alpine borane allowing for the

formation of both, **(R-)2** and **(S)-2**.

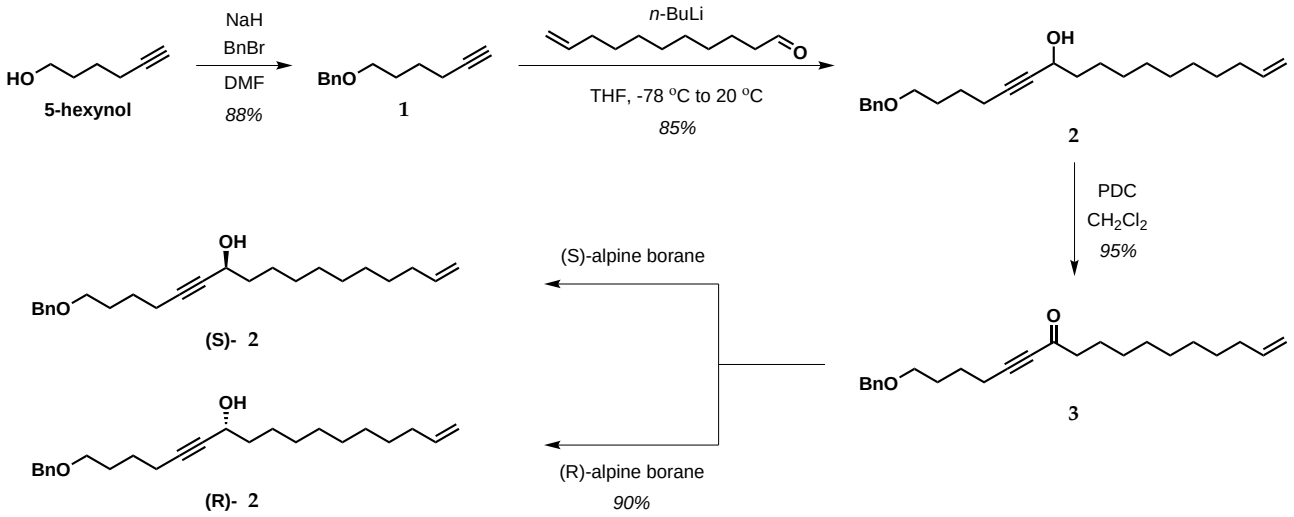

Scheme 1.3: Formation of intermediates **2** as two separate enantiomer.[147]

Both of the enantiomer can undergo ozonolysis in the presence of methanol followed by an acetylation of the mid-chain alcohol to afford propargylic ester **4**, as depicted in Scheme 1.4. Hydrogenation of the triple bond and hydrogenolysis of the benzyl group can be achieved by the subsequent treatment of compound **4** by Pt/C and Pd/C int the presence of H_2. Finally, target molecule **6** can be obtained through the saponification of compound **5** using aqueous NaOH.

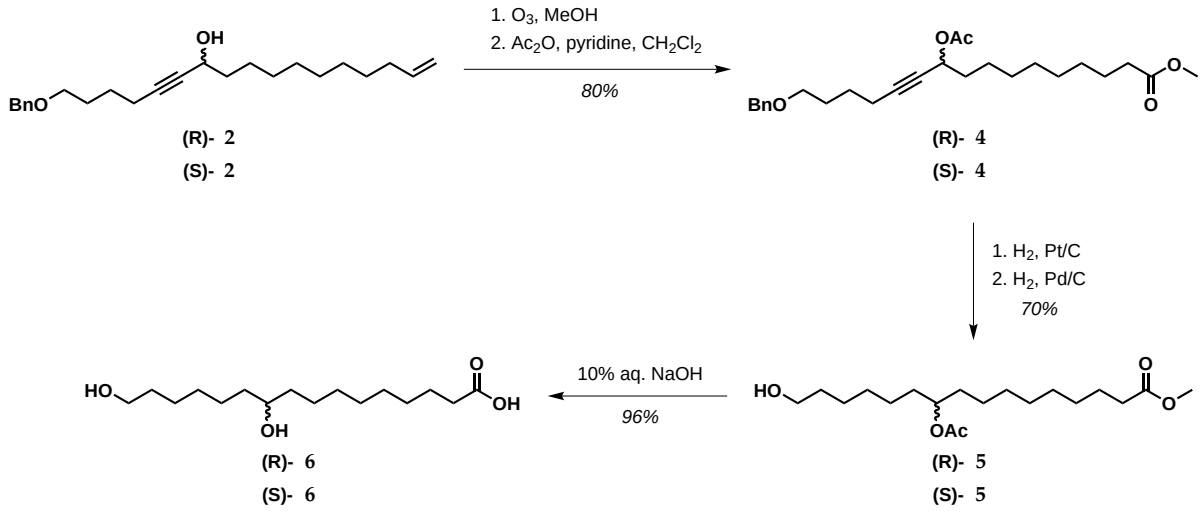

Scheme 1.4: End of the synthesis of 10,16-dihydroxyhexadecanoic acid.[147]

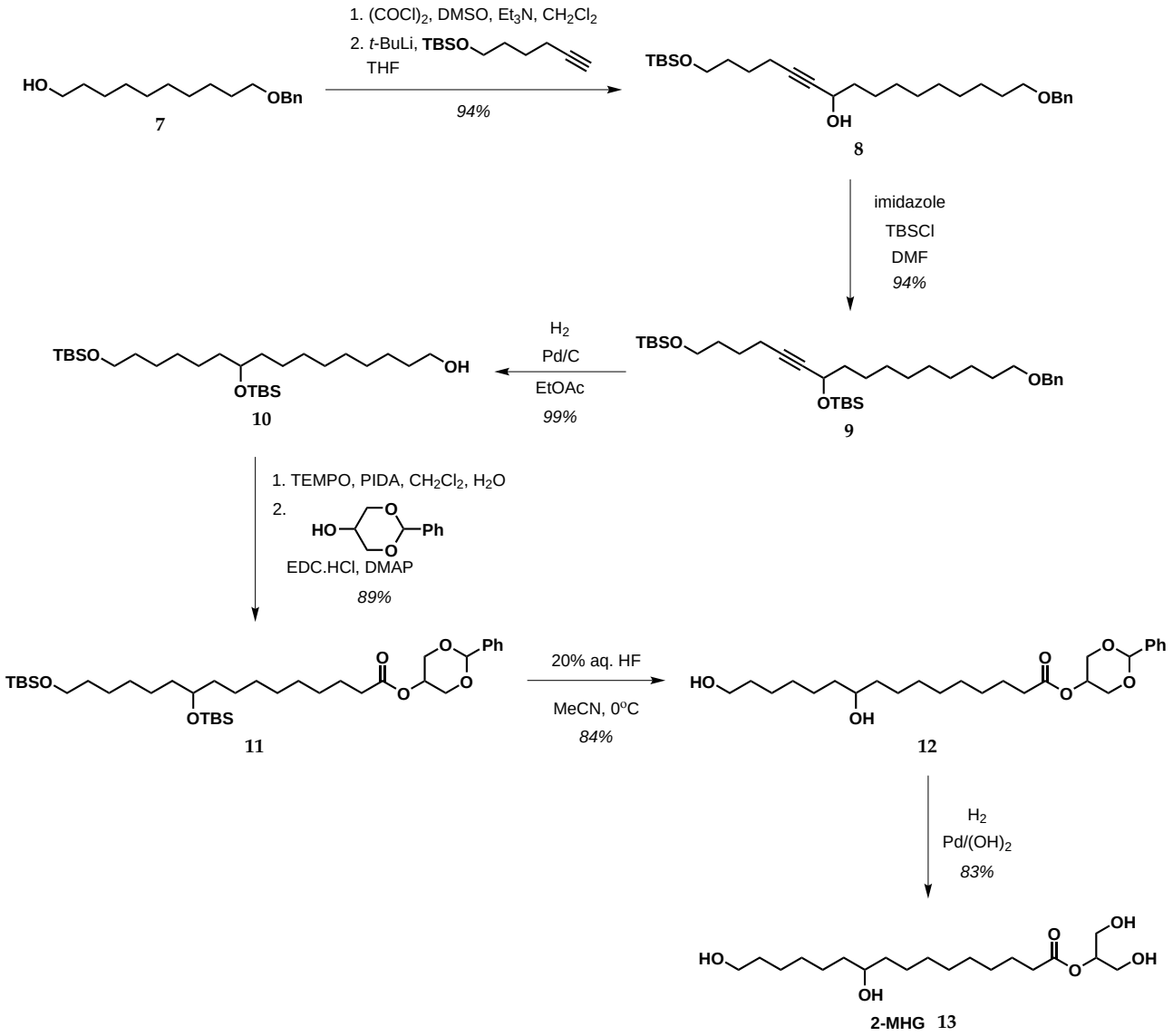

Scheme 1.5: Synthesis of 2-MHG.[44]

The identification of CUS1 was part of a collaborative work between the group of Prof. Jocelyn K. C. Rose at the Cornell University (CU) and Prof. Mads H. Clausen at the Technical University of Denmark (DTU).[44] In order to confirm the polymerase activity of CUS1, 2-mono(10,16-dihydroxyhexadecanoyl)glycerol have been chemically synthesized and used in a polymerization assay.[44] The synthesis of 2-MHG, depicted in Scheme 1.5, starts by the coupling between 10-(benzyloxy)decan-1-ol **7** and the lithium acetylide of 6-((tert-butyldimethylsilyl)oxy)hex-1-yne to afford alcohol **8**. The latter can undergo a TBS protection followed by a concomitant palladium catalyzed hydrogenation and hydrogenolysis to afford compound **10**. Oxidation of the free alcohol to

the carboxylic acid followed by a Steglich esterification gave a fully protected derivative of 2-MHG. Finally, 2-MHG can be obtained by a 2 step global deprotection using first aqueous HF followed by a hydrogenolysis catalyzed by Pearlman's catalyst.[44]

One of the main difficulties of working with sn-2 glyceryl esters lies on their tendency to migrate to the thermodynamically favored sn-1 position. This synthesis relies on the use of cis-5-hydroxy-2-phenyl-1,3-dioxane, a 1,3-protected glycerol that is only released at the very last step using mild hydrogenolysis conditions in order to overcome this issue. Due to the acid-induced lability of benzylidene acetal, another key step in the 2-MHG synthesis is the TBS deprotection leading to precursor **12** which is performed using 20% aq. HF at 0 °C. According to the author, stronger HF solutions and higher temperature promotes the combined removal of the benzylidene acetal and migration of the glycerol moiety.

Chapter 2

Synthesis and Investigation of the Bio-polymerization of Cutin Monomers and Derivatives - A Chemical Approach

2.1 Towards an enantioselctive synthesis of a CUS1 Monomer

2.1.1 Objectives

Following its discovery in 2012, the question of CUS1 specificity and stereospecificity remained open. CUS1 was proven to catalyze the *in vitro* oligomerization of 2-MHG. In nature, different positional isomers of 2-MHG were found. One of the major 2-MHG isomer is 2-mono(9,16-dihydroxyhexadecanoyl)glycerol, depicted in Figure 2.1, which will be referred to as 9-OH-2-MHG. The objective of this project was to developed a novel synthesis of 9-OH-2-MHG which will be further used in enzymatic assays to investigate CUS1 specificity. Additionally, the proposed synthesis, despite not being enantioselective, has been developed in a way that could allow for enantioselectivity. Synthesizing both enantiomers would allow us to assess if each enantiomers are substrates of CUS1.

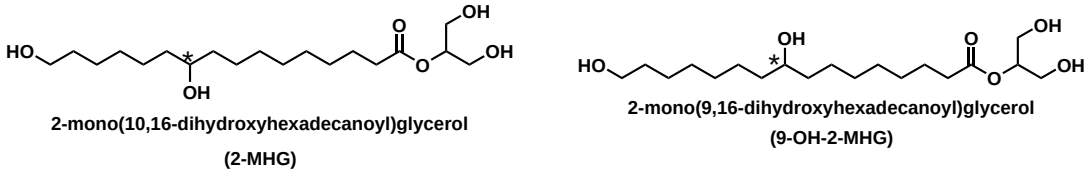

Figure 2.1: Structure of 2-MHG and its positional isomer 9-OH-2-MHG. The chiral center is denoted by the star.

2.1.2 Synthetic strategy

The proposed synthetic strategy is depicted in Scheme 2.1. Target compound 9-OH-2-MHG (**14**) would arise from a global deprotection of the fully protected precursor **15** similarly to what has already been reported for the synthesis of 2-MHG.[44] Compound **15** was thought to be obtainable through the esterification between 1,3-*O*-benzylideneglycerol and acid **16**, and the latter would be prepared from a benzyl deprotection

followed by oxidation of benzyl ether **17**. This protected triol was thought to be obtained from the alcohol protection and selective reduction of β-hydroxy ketone **18**. This β-hydroxy ketone motif can be obtained through an aldol condensation between ketone **20** and aldehyde **19** which both could be formed from commercially available 1-methyl-1-cyclohexene (**22**) and 1,9-nonanediol (**27**) respectively. The choice of using an aldol reaction is key here as it would allow us to use an assymetric versions of this coupling reaction in the future.[148] Additionally, the protecting group strategy have been developed in order to simplify several protection and deprotection steps which have already been developed for similar compounds in the original 2-MHG synthesis.

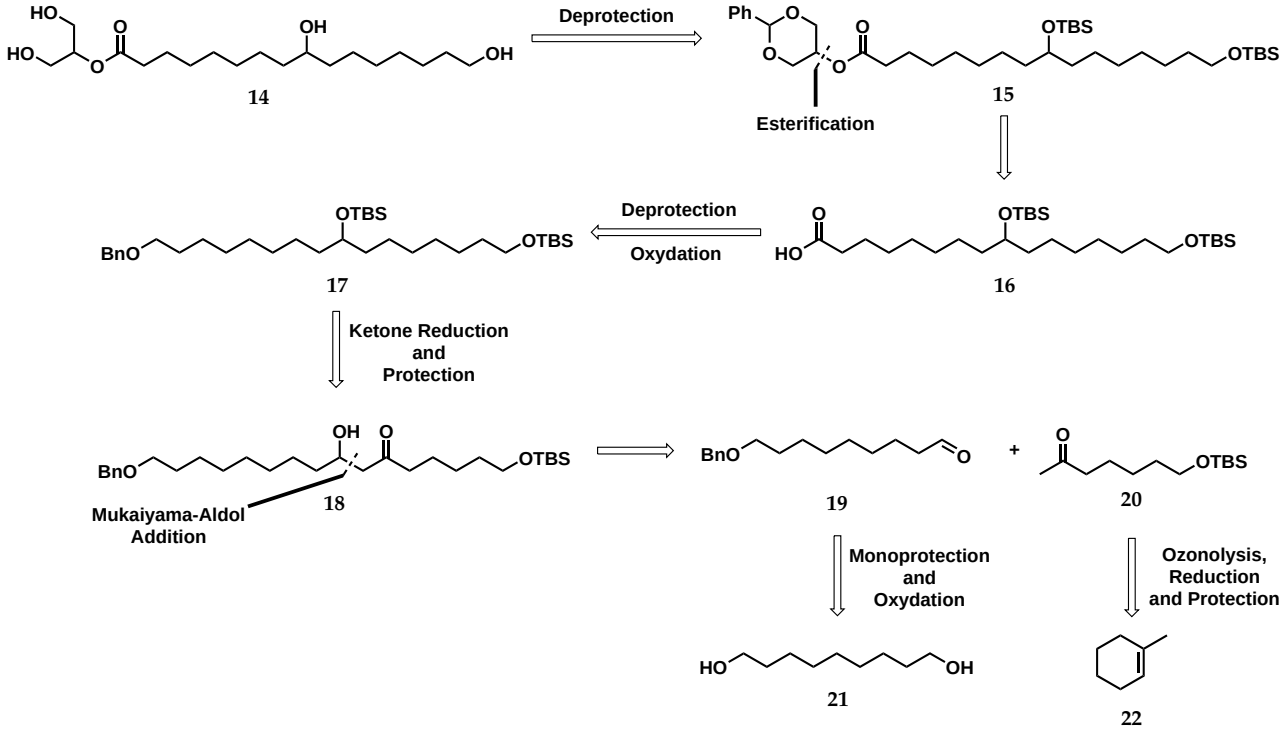

Scheme 2.1: Proposed retrosynthesis of 9-OH-2-MHG.

2.1.3 Results and discussions

2.1.3.1 Synthesis

As described on the former section, we intended to use ozonolysis of 1-methyl-1-1-cyclohexene (**22** to produce keto-aldehyde **23**. This reaction was performed according to McMurry *et al.* 1978,[149] however, the reaction afforded an inseparable mixture of compounds. NMR analysis of the crude mixture indicated the presence of the desired compound as well as impurities, however, the desired compound could not be

isolated. Similar results were observed when using triphenylphosphine instead of dimethylsulfide as a reducing agent.

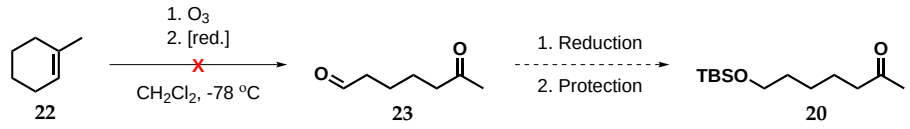

Scheme 2.2: Tentative synthesis of ketone **20** via the ozonolysis of 1-methyl-1-cyclohexene (**22**).

Due to the unsucessful purification of the ozonolysis products, an alternative synthetic route, displayed in Scheme 2.3, was developed for the synthesis of ketone **20**. This synthetic route starts with a lactone opening of ε-caprolactone using *N*,*O*-dimethylhydroxylamine hydrochloride in the presence of trimethylaluminium.[150] This step was directly followed by a TBS protection of the hydroxy group affording Weinreb amide **25** in high yield. The Weinreb ketone synthesis was then achieved by the treatment of the Weinreb amide with a solution of methylmagnesium bromide followed by the hydrolysis of the hydroxylamine in mild acidic conditions in order to obtained desired ketone **20**. The use of mild acidic condition was key here as the use of a stronger acid mixture lead to a major deprotection of the TBS group

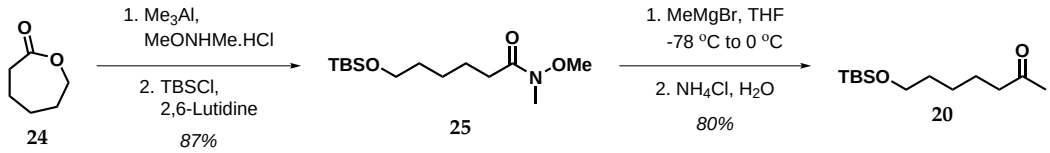

Scheme 2.3: Synthesis of ketone **20** through Weinreb ketone synthesis followed by the formation of the kinetic silyl enol ether.

Next, the preparation of aldehyde **19** was undertaken. This compound was prepared in two steps from commercially available 1,9-nonanediol (**27**) as depicted in Scheme 2.4. This synthesis revolved around the monoprotection of 1,9-nonanediol to afford alcohol **28**. This synthesis was performed using half an equivalent of benzyl bromide compared to the starting diol in order to reach an optimal ratio of monoprotected with respect to the bis-protected diol. This step was followed by oxidation of the free hydroxy group using Dess-Martin periodane (DMP) as a mild oxidative agent. This aldehyde was found to be unstable and was always prepared and used for the next step on the same day.

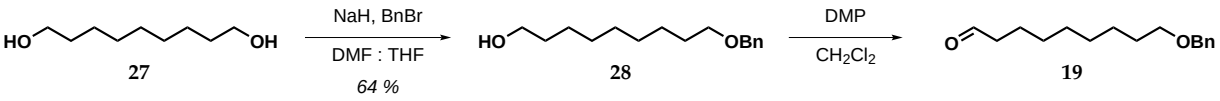

Scheme 2.4: Synthesis of aldehyde fragment **19**.

With the two aldol fragments in hand, the next step in the synthesis was the aldol reaction. In particular, the Mukaiyama aldol addition was chosen for the ease of preparation of the desired kinetic aldol addition product. For this purpose, the formation of the trimethylsilyl (TMS) enol ether **26** was necessary. This was achieved via the use of lithium diisopropylamide, a strong and bulky base. The first attempt at coupling silyl enol ether **26** with aldehyde **19** in the presence of boron trifluoride etherate lead to the formation of a complex mixture dominated by the presence of ketone **20**. This result was thought to arise from the premature degradation of the TMS enol ether. Alternatively, a slow reaction rate of could be accounted for those results.

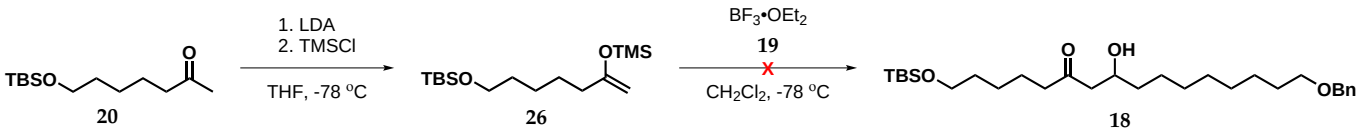

Scheme 2.5: Preparation of TMS enol ether **26** and first attempt at aldol coupling between the latter and aldehyde **19**

In this context, the preparation of the more resistant the *t*-butyldimethylsilyl (TBS) enol ether (**29**) was attempted, as depicted in Scheme 2.6.[151] Unfortunately, treatment of the lithium enolate with TBSCl led to no further reaction while using TBSOTf led to the formation of a 1 : 1 mixture of kinetic and thermodynamic enolate according to crude NMR analysis. The formation of the TBS enol ether was left without further investigation.

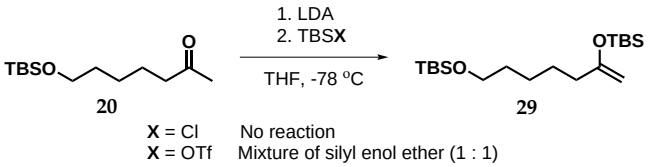

Scheme 2.6: Tentative preparation of TBS enol ether **29**.

To increase the rate of the aldol addition reaction, the reaction was perfomed using $TiCl_4$, as depicted in Scheme 2.7. This successfully catalyzed the formation of desired aldol product **18**, although in 34% yield. The low yield is partially explained by the presence of a large amount of TBS-deprotected aldol product arising from the strong acid conditions of the reaction.

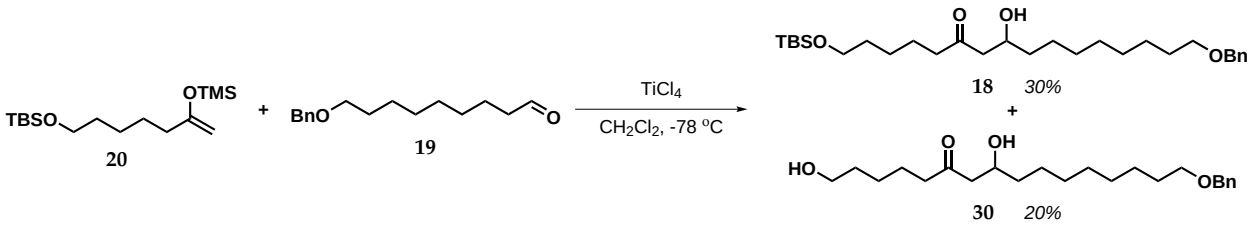

Scheme 2.7: Aldol coupling between **26** and **19**.

Subsequently, the protection of the mid-chain hydroxy group by treating compound **18** with TBSCl in the presence of imidazole failed. In light if this, the protection of the hydroxy group was pushed to a later stage in the synthesis. The next key step for the proposed synthesis was the ketone removal. We envisioned that this could be achieved via the formation of a thioketal followed by Raney-nickel mediated desulfurization. The formation of the thioketal derivative of aldol **18** was undertaken as displayed in Scheme 2.8. Treating the aldol abduct with 1,3-propanedithiol and boron trifluoride etherate lead to the formation of a small amount of the TBS deprotected thioketal **32** as well as a large amount of TBS deprotected aldol abduct **30**. Once again proving that TBS group is too labile in the employed acidic conditions.

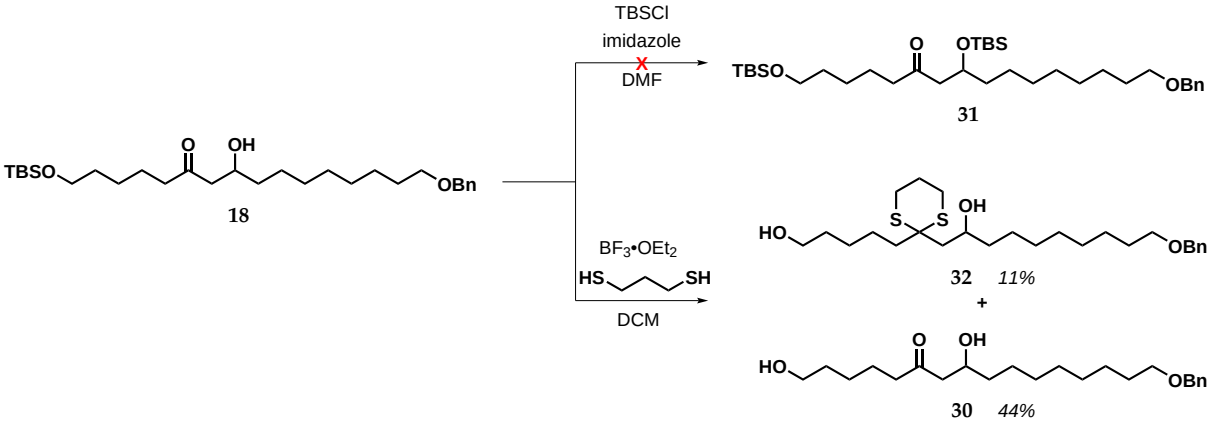

Scheme 2.8: Attempt at protecting the mid-chain alcohol of compound **18** and thioketal formation.

Attempt at protecting both alcohol using TBSCl in the presence of imidazole, depicted in Scheme 2.9, proved to be inefficient as no conversion was observed.
In order to determine optimal conditions for the thioketal formation, and due to the small amount of **30** in hand at that time, a few test reactions were performed on simpler substrates. The impact of the acid catalyst was investigated as depicted in Table 2.1. $TiCl_4$ (entry 1) lead to the formation of the TBS deprotected thioketal while PPTS (entry 2) was not strong enough to catalyze the thioketal formation. In order to

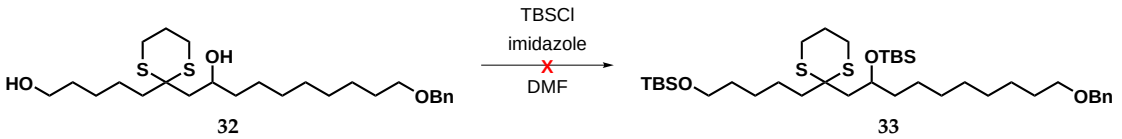

Scheme 2.9: Attempt at protecting both alcohol of thioketal **33** using TBSCl in the presence of imidazole.

avoid the presence of protic acid produced by the hydrolysis of $TiCl_4$, titanium (IV) isopropoxide was used as a catalyst (entry 3). Similarly to PPTS, Ti(O*i*Pr)$_4$ proved to be inefficient as no conversion of the starting material was observed.

Table 2.1: Effect of the acid on the thioketal formation.

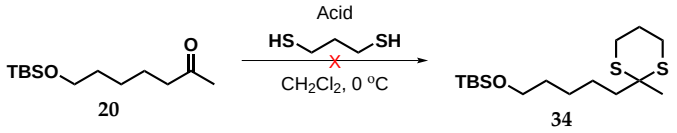

Entry	Acid	Comments
1	$TiCl_4$	TBS-deprotected thioketal as major product (74 %)
2	PPTS	No conversion
3	Ti(O*i*Pr)$_4$	No conversion

Due to the major issue linked to the protecting group strategy, and more specifically, the use of TBS protecting groups in acid catalyzed reactions, this proposed synthetic route was discontinued and the project was left asides in favor of a different synthesis of 9-OH-2-MHG.

2.2 Synthesis of a CUS1 monomer and isotopically labeled monomer for CUS1 specificity

2.2.1 Objectives

The cutin composition of angiosperm is dominated by dihydroxy-palmitic acids.[6,18,152] Additionally, fragmentation analysis of cutin depolymerization products via gas chromatography mass spectrometry (GC-MS) has proven that 10-16,dihydroxypalmitic acid is the main isomer that constitutes this specific type of monomer for a lot of plants including tomato fruits.[152] However, little is known about how this selectivity arises. Hypothetically, polymerase enzymes might play a pivotal role in this positional isomer dominance by means of enzymes intrinsic selectivity. In this context, analyzing the selectivity of CUS1 might provide us with some insight into this particular aspect of the monomer composition of tomato cutin. The analysis of choice to asses CUS enzymes *in vitro* polymerization product is MALDI-TOF mass spectrometry. Theoretically, performing a polymerization assay with an equimolar mixture of potential monomers and analyzing the oligomer mixture by MALDI-MS would allow us to see which monomers are preferentially included within the polymer matrix by the polymerase. Unfortunately, MALDI-MS suffers from very little fragmentation, if any at all, and does not allow for the differentiation between different positional isomers that possess the same mass. One way to work around this limitation would rely on the formation of isotopically labeled positional isomers. This would allow us to differentiate positional isomers by mass spectrometry and investigate the selectivity of CUS1 for these different positional isomers.

In particular, this project aims at synthesizing both, 9-OH-2-MHG and an isotopically labeled version of 9-OH-2-MHG, more specifically, 2-mono(9,16-dihydroxyhexadecanoyl)glycerol-10,10,11,11-d_4 (**35**). These compounds will then be co-polymerize with 2-MHG and the deuterated version of 2-MHG, both prepared by Ph.D. student Ignacio Martínez San Segundo, in order to assess the selectivity of CUS1.

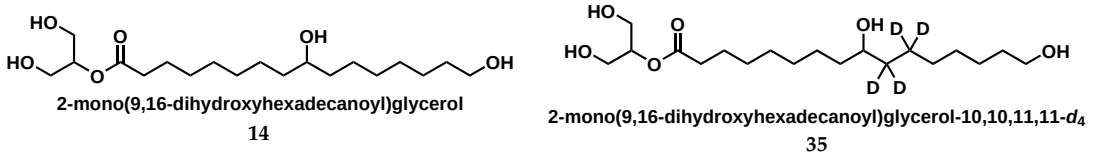

Figure 2.2: Target compounds for CUS1 selectivity studies

2.2.2 Synthetic strategy

The proposed synthetic strategy, depicted in Scheme 2.10 is an adaptation of the original 2-MHG synthesis. Both the non-deuterated and deuterated target compounds, **14** and **35**, are believed to be obtainable via common precursor **36**. Retaining the triple bond up to the very last stage of the synthesis is one of the main difference compared to the original synthesis, and is crucial as it will act as a handle for deuterium insertion. Precursor **36** is thought to be obtainable through esterification of acid **37** with 1,3-*O*-benzylideneglycerol. This acid can be formed through protection, deprotection and oxidation of the terminal alcohol of compound **38**. Protection of the terminal alcohol as a 2-naphtylmethyl (NAP) ether is a second major difference with the original 2-MHG synthesis. The change from the benzyl to the NAP protecting group was motivated by its ability to be removed under oxidative conditions which would allow us to keep the propargylic triple bond intact. Similarly to what has been done in the 2-MHG synthesis, C16 precursor **38** is thought to be afforded by the acetylide coupling between mono NAP protected diol **39** and TBS protected alkyne **40** which are both believed to be obtainable from commercially available 1,9-nonanediol (**41**) and 6-heptyn-1-ol (**42**) respectively.

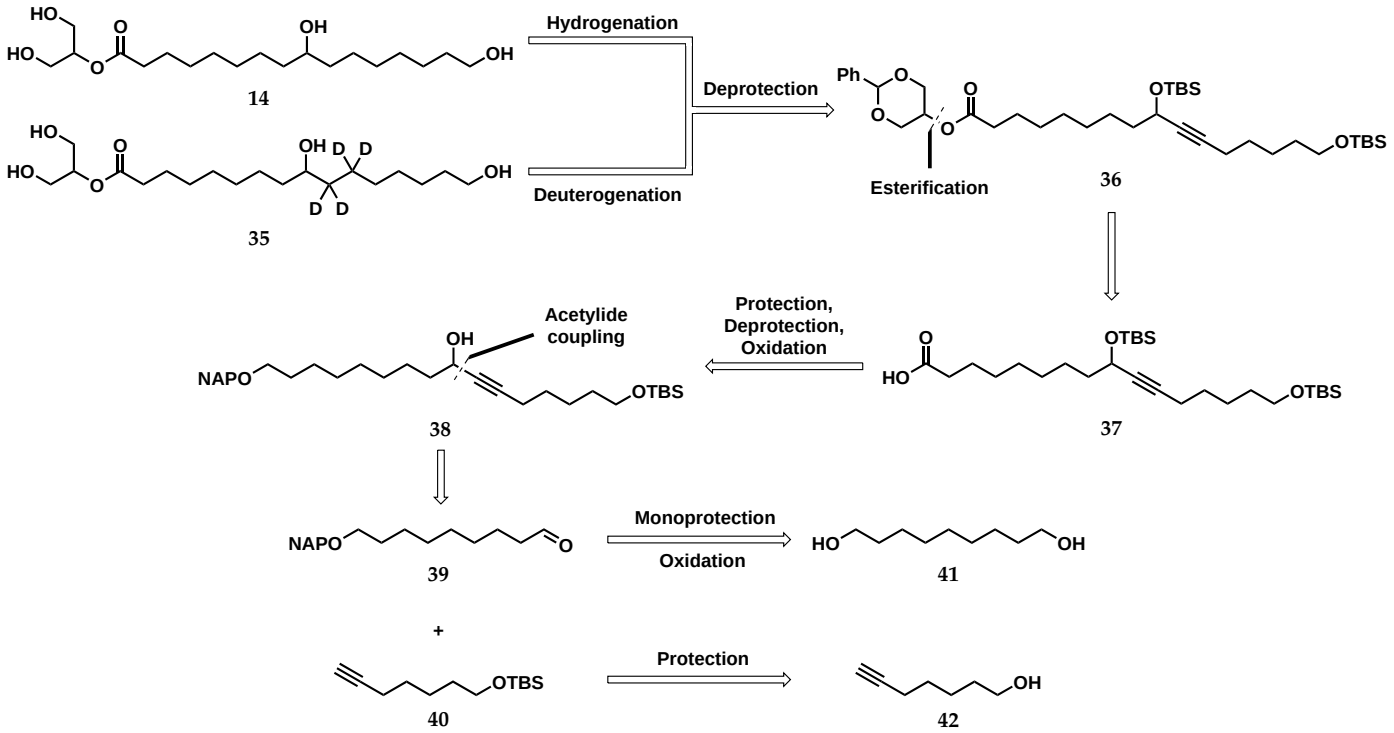

Scheme 2.10: Retrosynthetic analysis of 9-OH-2-MHG and 9-OH-2-MHG-d_4.

2.2.3 Results and discussions

2.2.3.1 Synthesis

The synthesis of 9-OH-2-MHG started by the formation of the NAP protected diol and resemble the benzyl protection seen on Scheme 2.4 in section 2.1.3.1. The remaining free hydroxyl group was then oxidized using the Dess-Martin reagent to afford the first acetylide coupling fragment, aldehyde **39**, as depicted in Scheme 2.11.

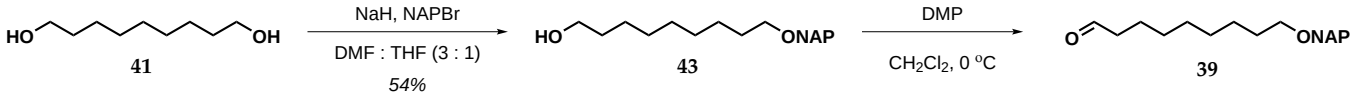

Scheme 2.11: Formation of aldehyde **39** from **41**.

The other fragment was synthesized by the imidazole mediated TBS protection of commercially available **42** as depicted in Scheme 2.12. Treatment of the latter with *n*-BuLi followed by the addition of aldehyde **43** lead to the formation of alcohol **38** in good yield. The newly formed hydroxy group was then treated with TBSCl in the presence of imidazole yielding the fully protected compound **44**.

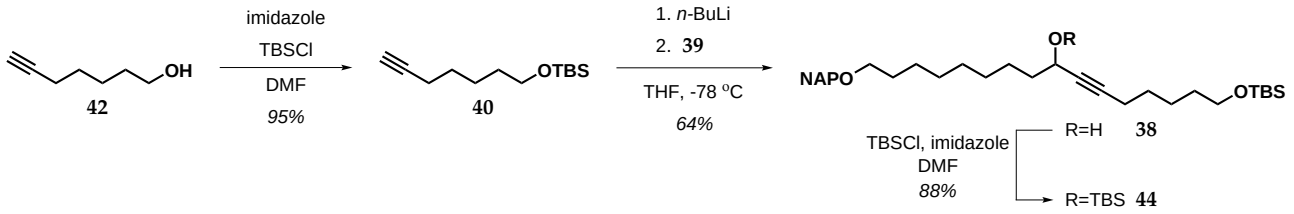

Scheme 2.12: Formation of precursor **44** via acetylide coupling.

The deprotection of the NAP group was performed by treating the compound with 2,3-dichloro-5,6-dicyano-1,4-benzoquinone (DDQ) as shown in Scheme 2.13. However, the yield of the reaction is inconsistent and ranges from 30 to 60 %. Thes results were thought to arise from the precipitaton of 2,3-dichloro-5,6-dicyanohydroquinone byproducts rendering the workup tedious. Despite the use of different workup strategies, including filtration over celite and the use of saturated aqueous sodium hydrogenocarbonate and the use of a citric acid and ascorbic acid buffer, the yield and consistency of this reaction could not be improved.[153]

The unprotected alcohol was then oxidized in a two-step procedure using Dess-Martin oxidation followed by a Pinnick-Lindgren oxidation to afford acid **37** as depicted in Scheme 2.14. This two step oxidation was necessary as it was previously demonstrated

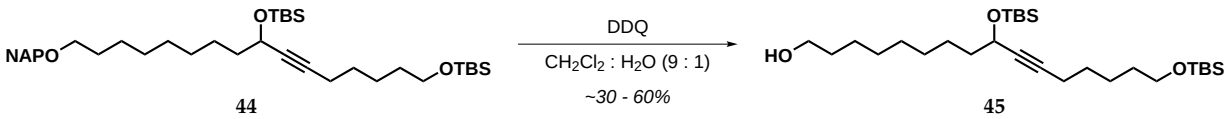

Scheme 2.13: DDQ mediated deprotection of the NAP group.

in our group that the direct oxidation to the carboxylic acid using TEMPO/PIDA oxidation, which directly, used in the synthesis OF 2-MHG, gives low yields when the triple bond is present (unpublished results). Subsequent Steglich esterification between the newly formed acid and 1,3-*O*-benzylideneglycerol, mediated by DMAP and EDC · HCl afforded ester **36**. Removal of both TBS protecting group was performed by treating precursor **36** with aqueous hydrofluoric acid at 0 °C affording intermediate **46**.

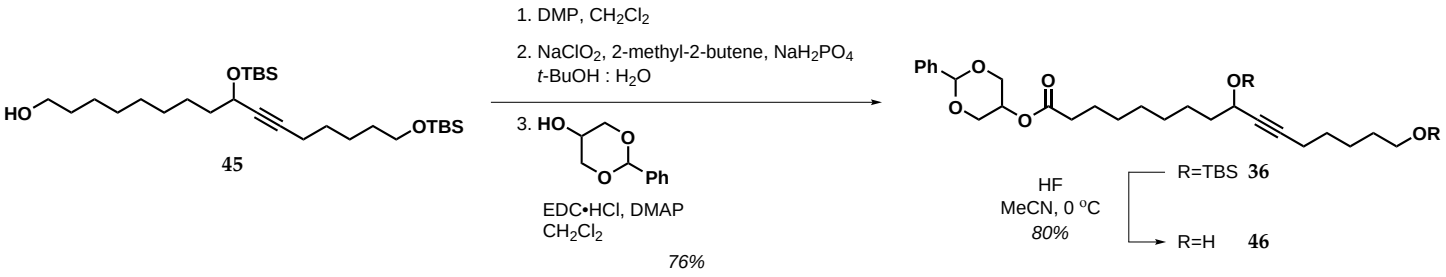

Scheme 2.14: Two step oxidation of **45** and subsequent Steglich esterification of the formed acid followed by the TBS deprotection of both alcohols.

Compound **46** was subjected to two different reaction conditions as depicted in Scheme 2.15. On the one hand, benzylidene acetal **46** was treated with Pearlman's catalyst in the presence of hydrogen gas in order to obtain fully saturated target compound **14**. On the other hand, compound **46** was treated with the same catalyst but in the presence of deuterium gas in order to allow for the insertion of deuterium atom and obtain deutero-compound **35**.

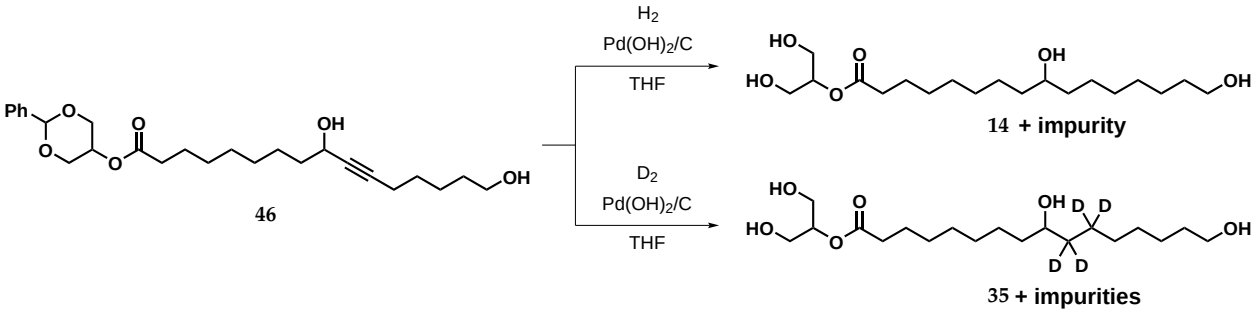

Scheme 2.15: Reduction of the triple bond and concomitant benzyl removal using hydrogen and deuterium gas.

To our surprise, under these conditions, the apparition of signals characteristic to an unknown ketone was observed in both carbon and proton NMR spectra. Every attempt at purifying the compounds by recrystallization failed and the lability of the glycerol moiety does not allow for column chromatography purification. This ketone formation is believed to arise from a Meyer-Schuster rearrangement.[154] If this assumption is correct, this would imply that the ketone would be the results of the migration of the alcohol from C9 to C11. At the exception of the signals corresponding to the protons α to the ketone, all the other proton signals are merging with the signals of 9-OH-2-MHG on the proton spectra. Additionally ^{13}C NMR shows that all of the carbons spectra were only slightly shifted for the unknown compound. These results suggest that the the ketone possess a similar structure than 9-OH-2-MHG. Taking into account these observations, the proposed structure for the ketone can be found on Figure 2.3.

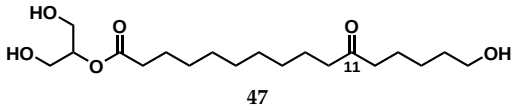

47

Figure 2.3: Potential structure of the unknown ketone as would be obtained through a Meyer-Schuster rearrangement.

Despite the ketone contamination, 9-OH-2-MHG and deutero compound **35** were subjected to the enzymatic polymerization using recombinant CUS1 enzymes provided by the group of Prof. Jocelyn K. C. Rose at Cornell University, NY, USA. The results of this polymerization assay will be presented in details in the next section. However, it was observed that compound **35**, asides from the presence of the ketone, was also isotopically impure. Indeed, peaks ranging from the mass of the non deuterated to the tetra deuterated monomers were observed in the enzymatic assay product as displayed on Figure 2.4.
The presence of this distribution of isotopically labeled monomer is undesirable and is thought to arise from a deuterium-hydrogen exchange between the atmosphere and the catalyst. To the best of our knowledge, this exact phenomenon was not reported. However, a similar reverse exchange has been described in the literature where D_2O is used as to produce deuterium gas, in a Pd/C catalyzed deuterium-hydrogen exchange, which is subsequently used for a dehalogenation deuterium-insertion.[155,156] In light of these findings, the use of the triple bond as a deuterium-insertion handle was found to be problematic and a new synthetic route was developed for the formation of 9-OH-2-MHG as well as a deuterium labeled variant of the latter.

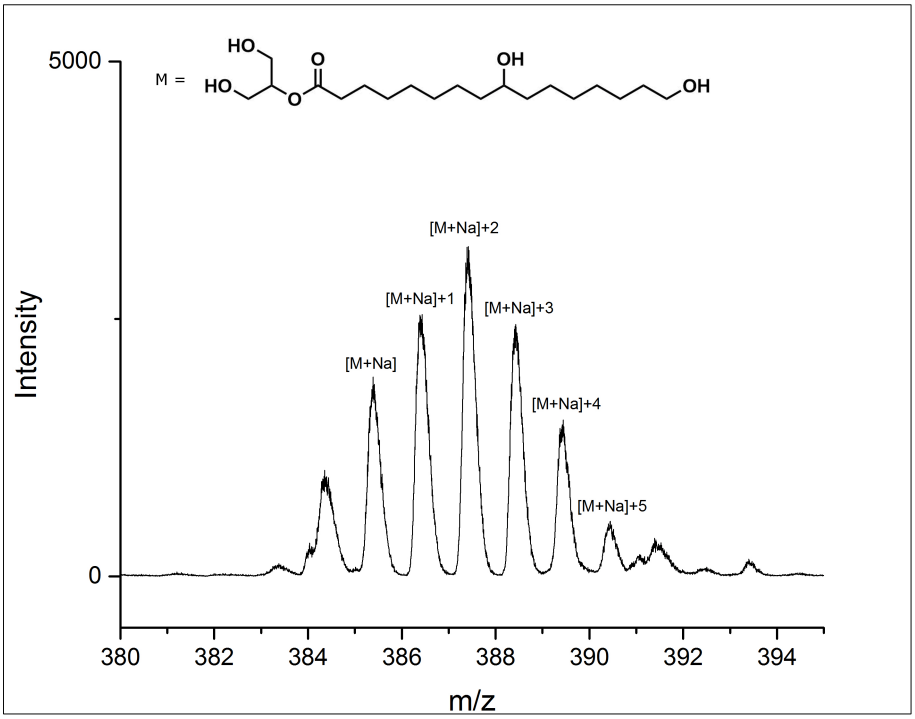

Figure 2.4: MALDI-TOF analysis of the deuterogenation product.

Due to its tendency to from degradation by-products, the hydrofluoric acid-mediated TBS deprotection depicted in Scheme 2.14 was sometimes halted before completion. By taking advantage of this issue, mono-deprotected compound **48**, depicted in Scheme 2.16, was isolated. This compound was then subjected to a poisoned palladium catalyst in the presence of hydrogen gas. To our surprise, this reaction led to the formation of the fully reduced triple bond instead of the initially expected corresponding alkene.

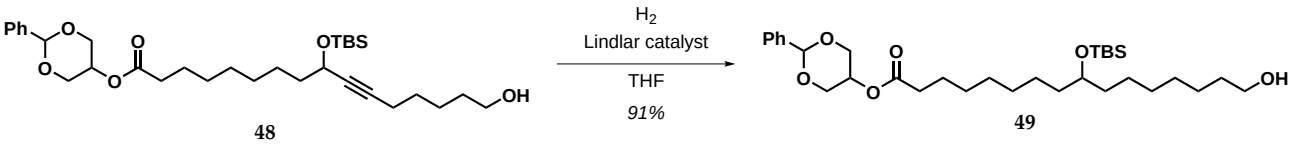

Scheme 2.16: Reduction of the triple bond

This compound was then oxidized to corresponding aldehyde **50** using the Dess-Martin reagent. This aldehyde was used as a handle in order to insert a single deuterium atom using sodium borodeuteride to afford compound **51**. The latter was treated with HF to afford deuterated benzylidene acetal **52**.

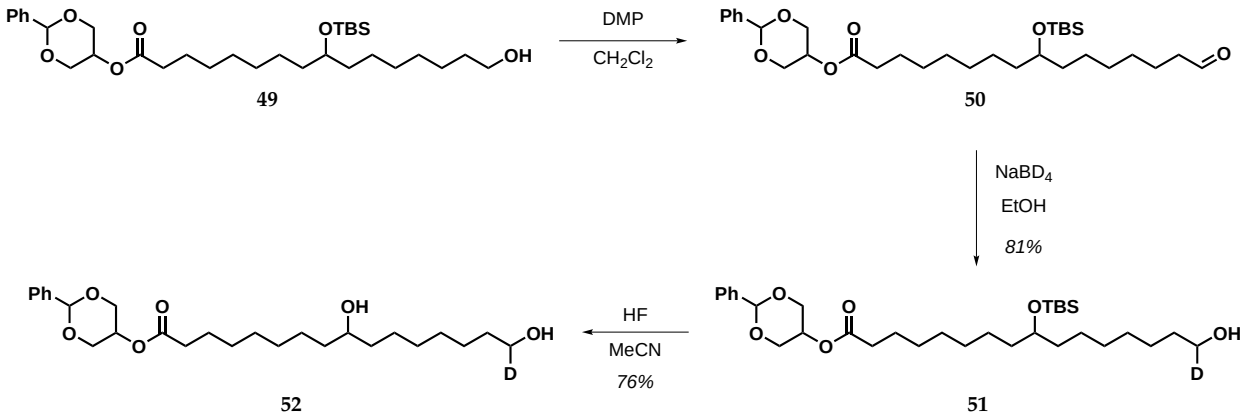

Scheme 2.17: Formation of deuterated precursor **52** from compound **49**.

Compound **49** was also treated with HF to promote the removal of the TBS group and obtain acetal **53** as depicted in Scheme 2.18.

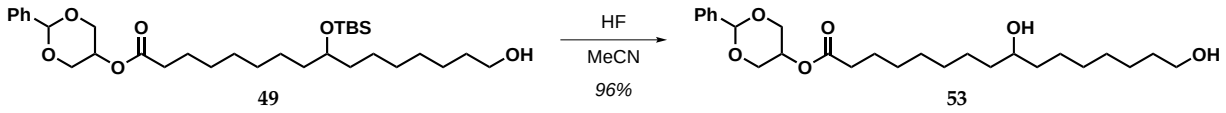

Scheme 2.18: TBS removal of compound **49** for the formation of non-deutarated precursor **53**.

Finally, both target molecules **14** and **54** were successfully synthesized through the hydrogenolysis of benzylidene acetals **52** and **53** as shown on Scheme 2.19.

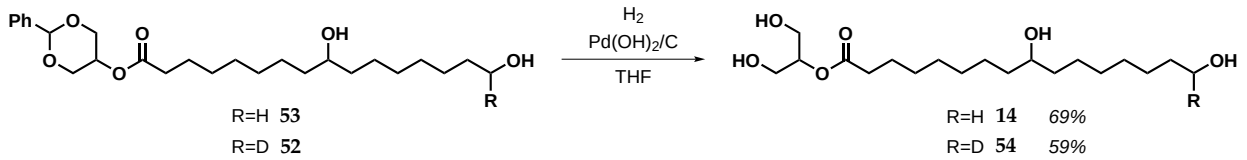

Scheme 2.19: Final hydrogenolysis of precursor **53** and deuterated precursor **52** to obtain target compounds **14** and **54**.

2.2.3.2 Enzymatic assay

The synthesized compound were used in various enzymatic assays. First, to assess that 9-OH-2-MHG is a potent substrate of CUS1, an enzymatic polymerization of this compound with CUS1 was performed. The MALDI-TOF analysis of the polymerization product, depicted in Figure 2.5, allowed us to confirm that CUS1 is indeed capable of polymerizing 2-mono(9,16-dihydroxyhexadecanoyl)glycerol.

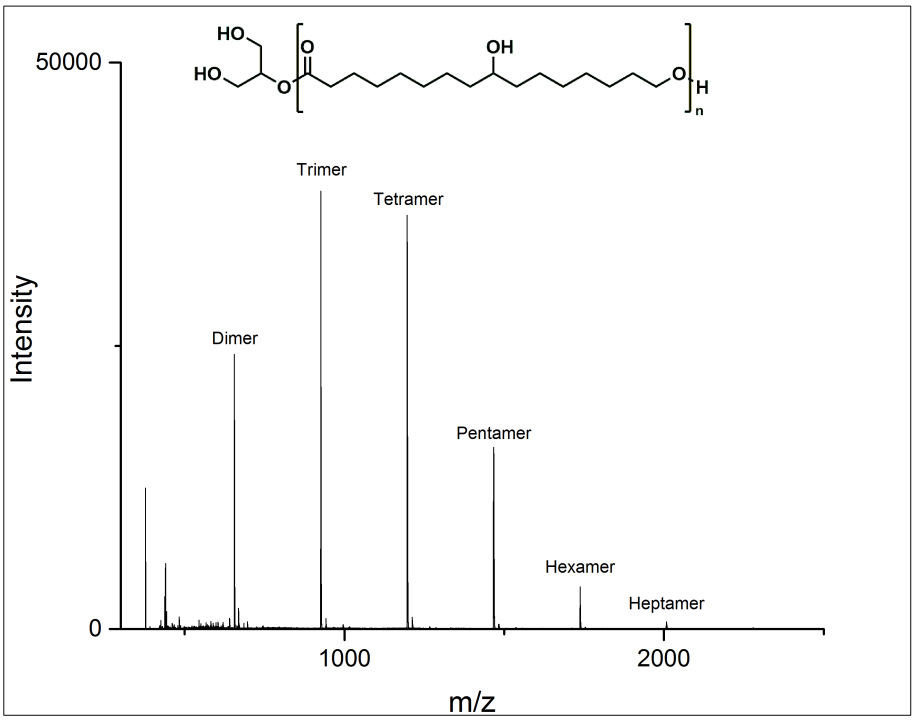

Figure 2.5: MALDI-TOF analysis of the polymerization product of 9-OH-2-MHG with recombinant CUS1. Each oligomers are present as their respective sodium abduct.

Polymerization assays were also performed on the mixture of 9-OH-2-MHG and unknown ketone **47**. Interestingly, this analysis demonstrated that CUS1 is also able to polymerize the unknown ketone as seen by the inclusion of ketone in trimers, depicted in Figure 2.6B. This inclusion of ketone was observed for all of the oligomer peaks on the mass spectra, proving that CUS1 might possess a broad range of substrates. This result indicates that CUS1 might be responsible for the inclusion of most of the C16 cutin monomers.

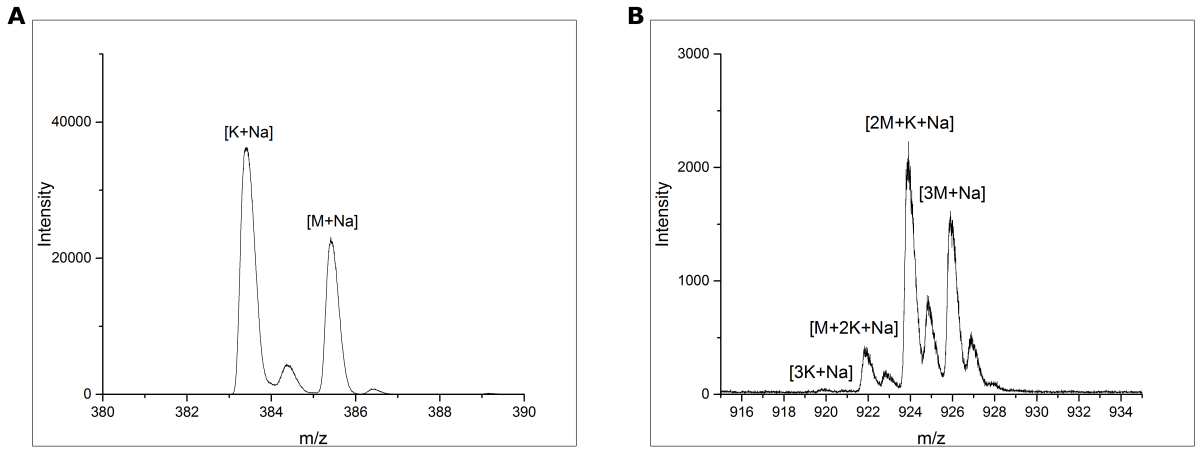

Figure 2.6: MALDI-TOF analysis of the polymerization product of a mixture of 9-OH-2-MHG and ketone **47** with recombinant CUS1. A, zoom of the monomer region; B, zoom of the trimer region; M, 9-OH-2-MHG; K, ketone.

To assess for the selectivity of CUS1 between the two positional isomers, 2-MHG (**13**) and 9-OH-2-MHG (**14**), competition assays have been performed. For those competition experiments, 2-MHG and a deuterated version of 2-MHG were necessary. Both of these compound were provided by Ph.D. student Ignacio Martínez San Segundo. The structure of deutero-2-MHG **55** can be found on Figure 2.7.

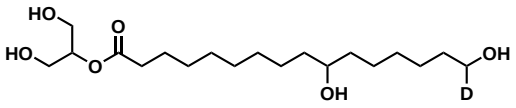

55

Figure 2.7: Structure of deutero-2-MHG **55**.

A comparison between the MALDI-TOF spectra of the polymerization product of 2-MHG, deutero-9-OH-2-MHG (**54**), and an equimolar mixture of both of these compounds is shown on Figure 2.8. This comparison suggests that the amount of monomer consumed is higher for the deuterated monomer than for the non-deuterated monomers. Additionally, the dimer and trimer peaks for the mixture suggests that more deuterated oligomers are incorporated within the structure. However, taking into account that the larger the molecule is, the more probable it is to contain one or several isotopes, this apparent preference for deuterated monomers might arise from the natural occurrence of isotopes.

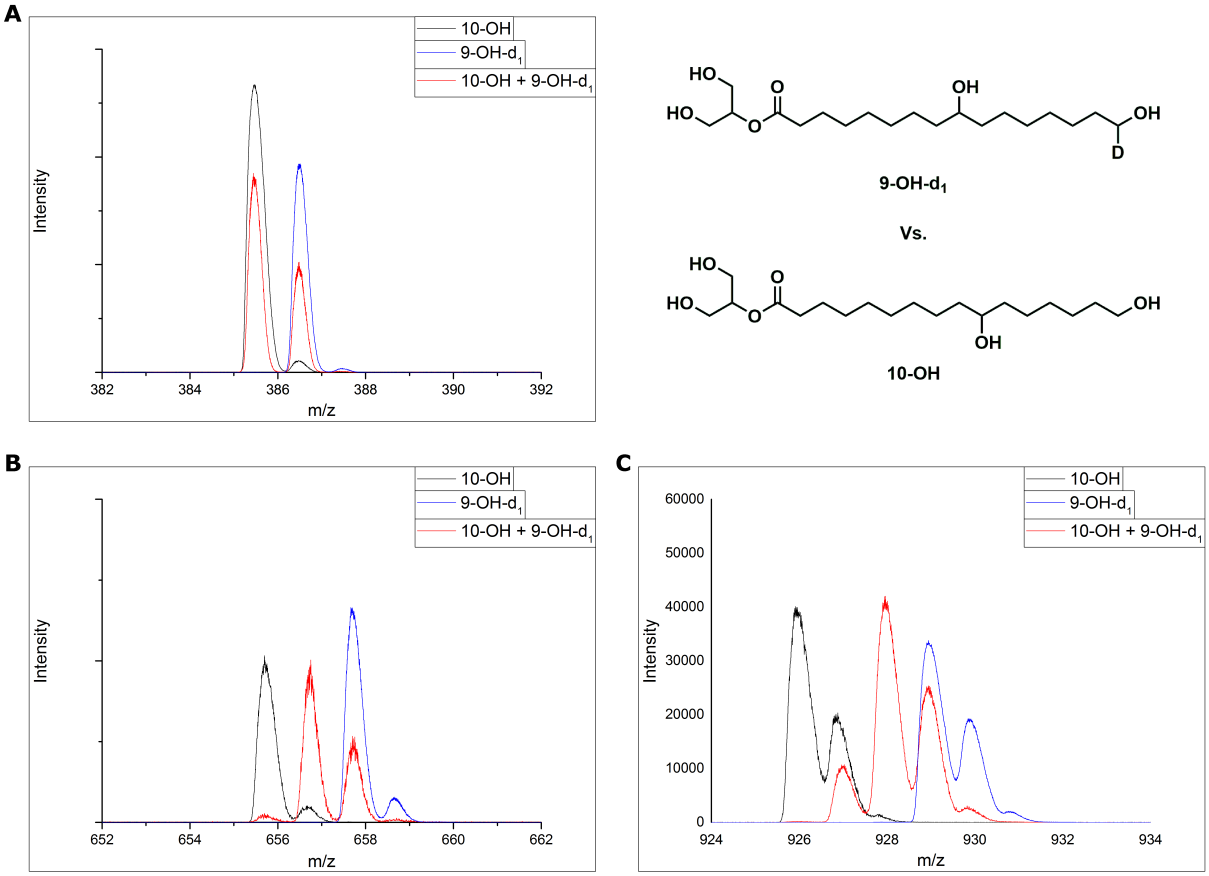

Figure 2.8: Comparison between the CUS1-mediated polymerization product of 2-MHG (**13**), Deutero-9-OH-2-MHG (**54**) and an equimolar mixture of both monomers. A, zoom of the monomer region; B, zoom on the dimer region; C, zoom on the trimer region.

To confirm this theory, the same experiment was carried out with deuterated 2-MHG **55** and the natural 9-hydroxy ester **14**. This experiment demonstrate that the inclusion of monomers are in favor of the deuterated species independently of the nature of the deuterated species, as displayed on Figure 2.9. This result further prove the aforementioned claimed that this pattern is due to the natural occurrence of isotopes. Alternatively, a secondary kinetic isotopic effect might also take place.

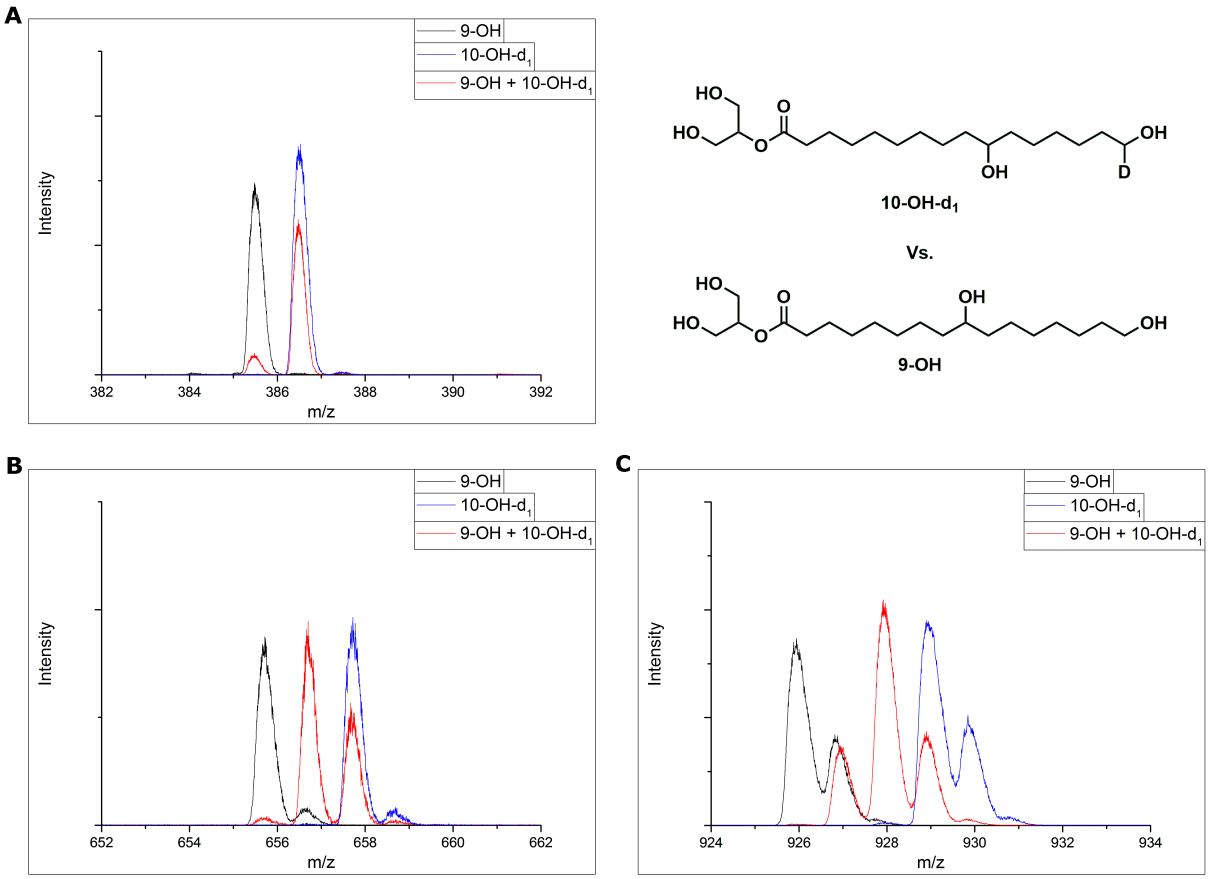

Figure 2.9: Comparison between the CUS1-mediated polymerization product of deuterated 2-MHG **55**, 9-OH-2-MHG (**14**) and an equimolar mixture of both monomers. A, zoom of the monomer region; B, zoom on the dimer region; C, zoom on the trimer region.

2.2.4 Conclusions and Perspectives

To further our understanding of CUS1 and the selectivity of CUS1, the synthesis of the cutin monomer 2-mono(9,16-dihydroxyhexadecanoyl)glycerol **14** as well as its teradeutero derivative 2-mono(9,16-dihydroxyhexadecanoyl)glycerol-10,10,11,11-$d_4$6 (**35**) was initiated. Due to issues linked to the reduction of the propargylic triple bond and the inefficient deuterogenation of this triple bond in our initial synthetic route, an alternative route had to be developed. This alternative synthesis was found to be successful and allowed us to isolate both 2-mono(9,16-dihydroxyhexadecanoyl)glycerol (**14**) and 2-mono(9,16-dihydroxyhexadecanoyl)glycerol-16-d_1 (**54**). These two compounds, along with 2-MHG (**13**) and its deuterated derivative (**55**) were all used in polymerization assays using CUS1. The various experiments demonstrated that 2-mono(9,16-dihydroxyhexadecanoyl)glycerol as well as the unknown ketone are both substrates of CUS1, suggesting that CUS1 might have a large scope of monomers and might be

responsible for the inclusion of most of the C16 monomers. Additionally, the competition experiments indicates that CUS1 might not favor any of the two positional isomers. However, to confirm this theory, further competition assays between a natural monomer and its deuterated needs to be performed to confirm that the pattern observed is independent of the nature of the monomers used.

To further our understanding of the scope of CUS1, the behavior of CUS1 towards C18 monomers is still unknown. Hence, the synthesis and CUS1-mediated biopolymerization of C18 monomers would be of interest.

2.3 Synthesis and investigation of a putative CUS1 ligand

The following section will present a project that started as a bachelor thesis. This project was initiated by student Maria Holm Rautenberg who successfully developed the synthesis of intermediate **59**. This project was subsequently carried on by the author of this thesis. This synthesis was also repeated by external student Judith Bastien who performed some of the optimization reactions.

2.3.1 Objectives

The tertiary and quaternary structure of an enzyme is directly associated with the enzymatic activity. In this context, the discovery of the three-dimensional structure of an enzyme is important for the establishement of the enzyme-substrates interaction as well as its mechanism of action. To obtain a protein three-dimensional structure, scientists can rely on two different methods, NMR spectroscopy and X-ray diffraction (XRD). XRD is a technique that takes advantage of the interaction between X-rays and the electronic density of atoms. More specifically, spatially organized matter, crystals, will allow to diffract X-rays in a way that will create a diffraction pattern. This diffraction patterns is typical of the three-dimensional organization of the analyzed crystals. Hence, the diffraction pattern of a protein can be used and analyzed to unfold the tertiary structure of this specific protein and unravel specific interactions between an enzyme and its substrates.[157–159]

Unfortunately, due to the extremely high degree of freedom of macromolecules, protein crystallization is a very complex process where a variety of parameters, such as protein and salt concentration, cation and anion nature, and pH has to be taken into account. In this context, protein crystallization generally require intensive screening. Due to the screening nature of the process, a large amount of enzyme is often needed and obtaining diffraction-quality crystals can be long and tedious.[159,160] The use of ligand and inhibitors, which can interact with and stabilize the enzyme, have been proven to facilitate the protein crystallization.[160] Additionally, the obtention of a crystal-ligand structure where the ligand shares structural similarities with the enzyme natural substrates can help delineate the nature of the enzyme-substrate interactions.

In this context, and taking into account the lack of information on CUS1 three-dimensional structure, the synthesis of a CUS1 ligand or inhibitor to facilitate CUS1 crystallization is of interest. Among esterase inhibitors, carbamates have been found to be potent, additionally, several drugs have carbamates incorporated to inhibits esterases and deacetylases.[161–163] For this reason, the objective of this study was to synthesize a carbamate derivative of 2-MHG, depicted in Figure 2.10. Additionally, the inhibition potential of this compound will be assessed by competition enzymatic assays.

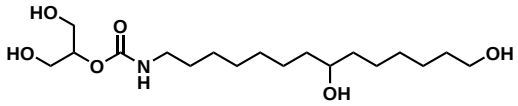

56

Figure 2.10: Structure of the target carbamate.

2.3.2 Synthetic Strategy

The proposed synthetic strategy, depicted in Scheme 2.20, starts by the global deprotection of carbamate **57** to afford target compound **56**. The fully protected carbamate is believed to be obtainable through the carbamate formation between 1,3-*O*-benzylideneglycerol and amine **58**, which is believed to be affordable through the amine conversion of alcohol **59**. This compound is similar to alcohol **10** found in the original synthesis of 2-MHG and is believed to be formed through the reduction of alkyne **60**. This alkyne is believed to be the product of the acetylide coupling between TBS-hexynol **62** and C8 aldehyde **61**, which are both believed to be obtainable from commercially available 1,8-octanediol (**63**) and 5-hexyn-1-ol (**64**).

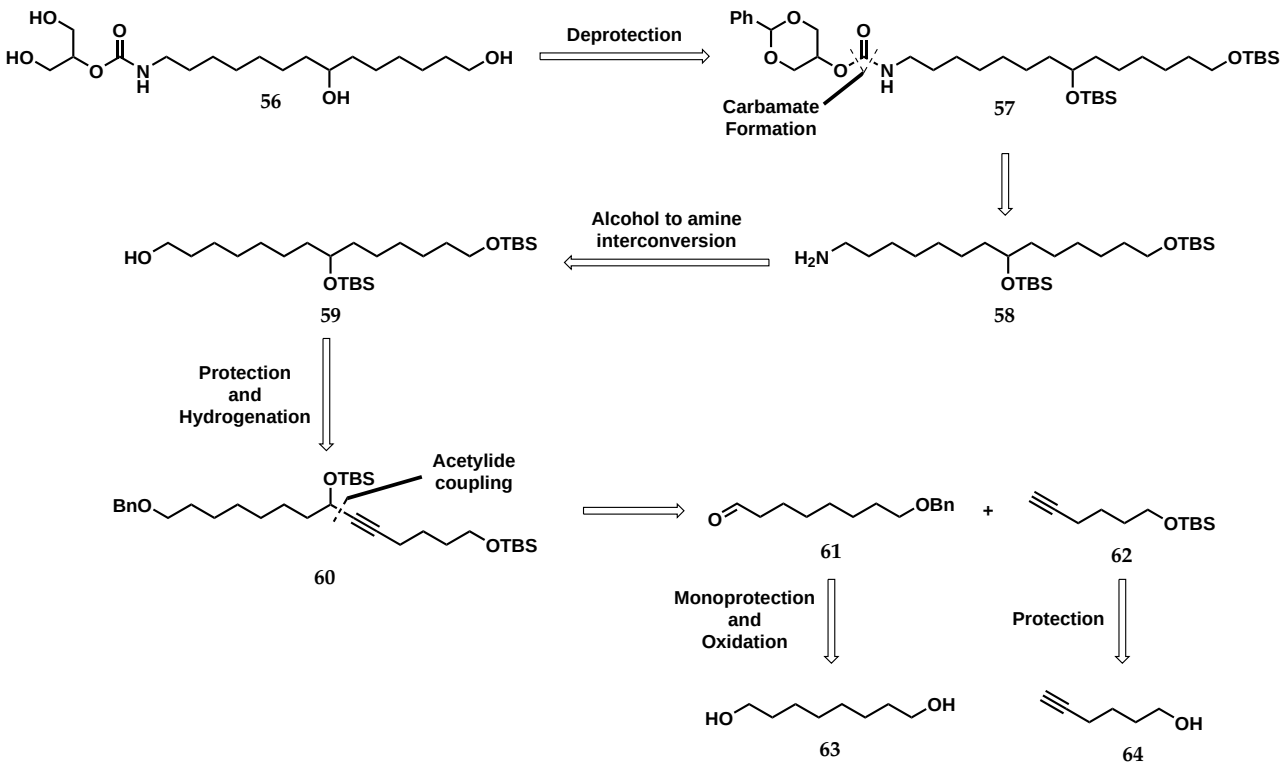

Scheme 2.20: Retrosynthetic analysis of 9-OH-2-MHG and 9-OH-2-MHG-d_4.

2.3.3 Results and Discussions

2.3.3.1 Synthesis

Similarly to what has been reported for the synthesis of 2-MHG shown in Scheme 1.5, the synthesis of aldehyde precursor **61**, depicted in Scheme 2.21, was performed through the mono benzyl protection of 1,8-octanediol (**63**) affording alcohol **7**. The latter was subsequently oxidized into the desired aldehyde **61**.

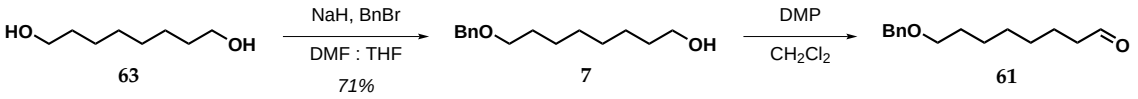

Scheme 2.21: Formation of aldehyde **61** from commercially available 1,8-octanediol.

5-Hexyn-1-ol was protected to afford TBS-protected alkyne **62**. Acetylide coupling between the latter and aldehyde **61** afforded C14 coupling product **65** as shown on Scheme 2.22. This abduct was then subjected to the standard TBS protection conditions to obtain mid-chain alkyne **60**.

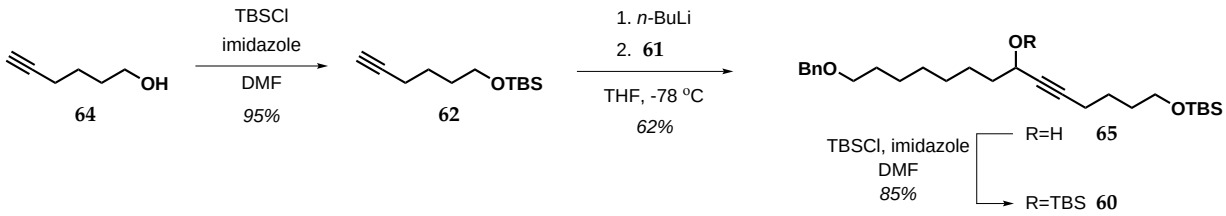

Scheme 2.22: Formation of precursor **60** via acetylide coupling.

Concomitant hydrogenolysis of the benzyl group and reduction of the triple bond was performed smoothly under classical palladium catalyzed hydrogenation, affording alcohol **60** as depicted in Scheme 2.23.

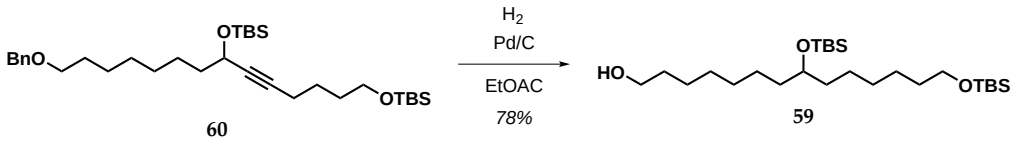

Scheme 2.23: Formation of **59** via the concomitant hydrogenation of the triple bound and hydrogenolysis of the benzyl group.

One of the key transformation of this synthesis was the transformation of terminal alcohol **59** into desired amine **58**. The first attempt at performing this transformation relied on the mesylation of the alcohol, turning this alcohol in a good leaving group. This leaving group was then intended to be substituted using a nucleophilic amine source such as benzyl carbamate as depicted in Scheme 2.24. Unfortunately, this reaction did not lead to the formation of the desired compound according to UPLC-MS and the corresponding mesylate was observed as the major peak, indicating that either the deprotonation did not occur as planned or the deprotonated carbamate was not reactive enough.

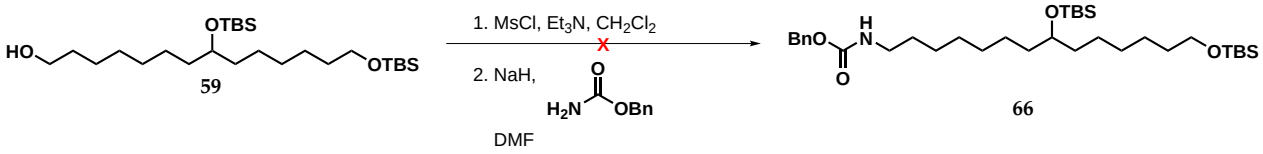

Scheme 2.24: Attempt at forming benzyl carbamate **66**.

Following this finding, the substitution reaction was performed using potassium phtalimide as a nitrogen source as depicted in Scheme 2.25. This reaction allowed the formation of desired phtalimide **67**, though, in low yield. One potential explanation for low yield lies in the difficulty to distinguish the starting alcohol from its corresponding mesylate by TLC due to their similar polarity making it impossible to follow

the reaction. Addition of a large excess of mesyl chloride did not improve the yield which suggest that the low yield might not arise from the formation of the mesylate.

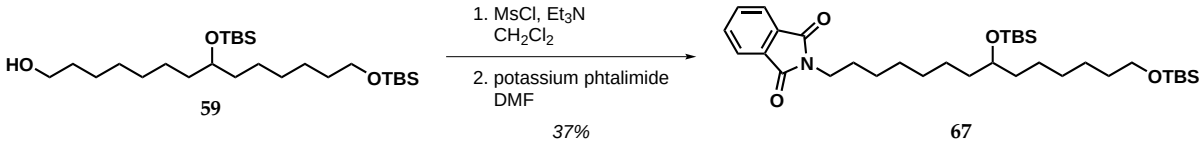

Scheme 2.25: Synthesis of phtalimide **67** from alcohol **59**.

Removal of the phtalimide was attempted using both, hydrazine and methylamine at room temperature and in refluxing ethanol. Unfortunately, in all of these cases, no conversion was observed.

Table 2.2: Attempt at releasing amine **58** from phtalimide **67** using different conditions.

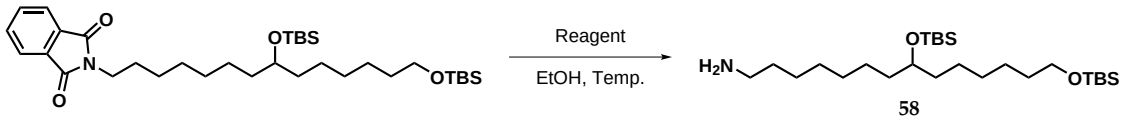

Entry	Reagent	Temperature	Comments
1	$NH_2NH_2 \cdot H_2O$	21 °C	No reaction
2	$NH_2NH_2 \cdot H_2O$	70 °C	No reaction
3	$MeNH_2$	21 to 70 °C	No reaction

One of the main issue linked to the use of the mesylation lies in the difficulty to differentiate the starting material from the mesylate by TLC making it difficult to troubleshoot this first step. For this reason, the formation of tosylate **68** was performed as depicted in Scheme 2.26. This tosylate was then treated with sodium azide, a strong nucleophilic nitrogen source to afford organo azide **69** in high yield.

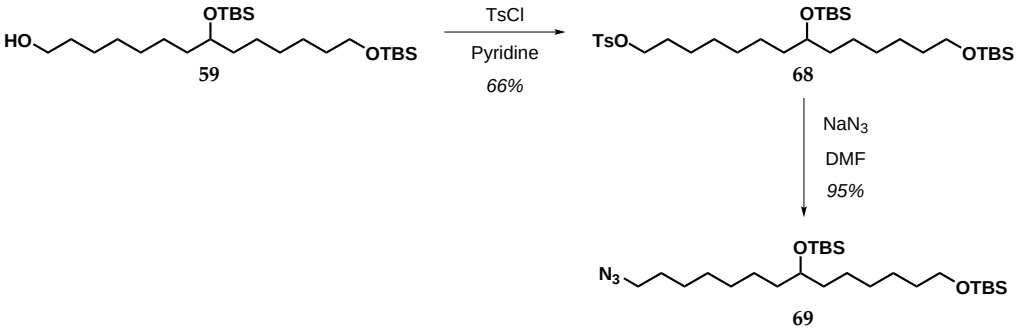

Scheme 2.26: Two step fromation of azide **69** from alcohol **59**.

Then, the latter was subjected to palladium catalyzed hydrogenation. These conditions provided desired primary amine (**58**) in low yield. To our surprise, the presence of secondary amine **70**, where two carbon chains are attached to the same amine, was also observed. This dimerization process was described in two different studies and seems to be less prevalent at lower temperature and diluted conditions.[164,165] In order to test this out, the hydrogenation was carried on at 0 °C and at a starting material (SM) concentration of 0.05 M (Table 2.3, Entry 2). As expected, under these conditions, the yield of primary amine **58** was substantially improved, while the yield of the secondary amine was reduced.

Table 2.3: Impact of temperature and concentration on the palladium catalyzed reduction of organo azide **69**.

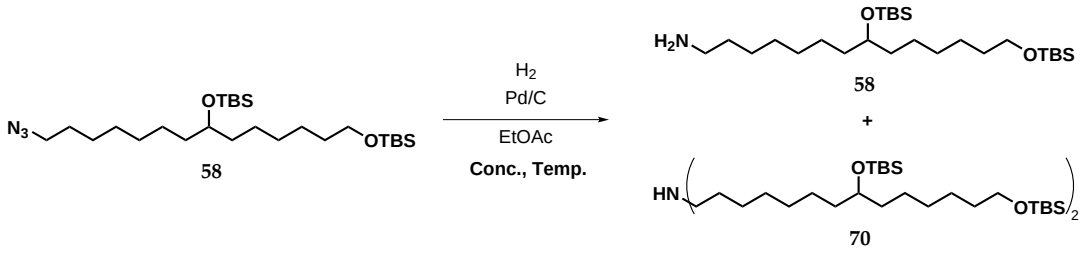

Entry	Concentration (M)	Temperature (°C)	**58** Yield (%)	**70** Yield (%)
1	0.1	21	51	20
2	0.05	0	69	14

To synthesize carbamate **57** from amine **58**, a benzylideneglycerol carbonyl acceptor was required. Different way to prepare this kind of reagent exists such as treating the desired alcohol with phosgene or derivatives. However, due to the high toxicity of phosgene and the fact that this synthesis was first part of a bachelor project, safer options were first investigated. The first acceptor investigated was para-nitrophenolate carbonate **72** depicted in Scheme 2.27. This mixed carbonate was then allowed to react with primary amine **58**. Surprisingly, this reaction lead to the formation of both, benzylidene glycerol carbamate **57** as well as nitrophenyl carbamate **73**. The latter was readily converted to the desired compound using the benzylidine glycerol alkoxide as a nucleophile. However, the presence of this undesirable carbamate as a major product suggests that the para-nitrophenolate is not a good leaving group with respect to the benzylidene glycerol.

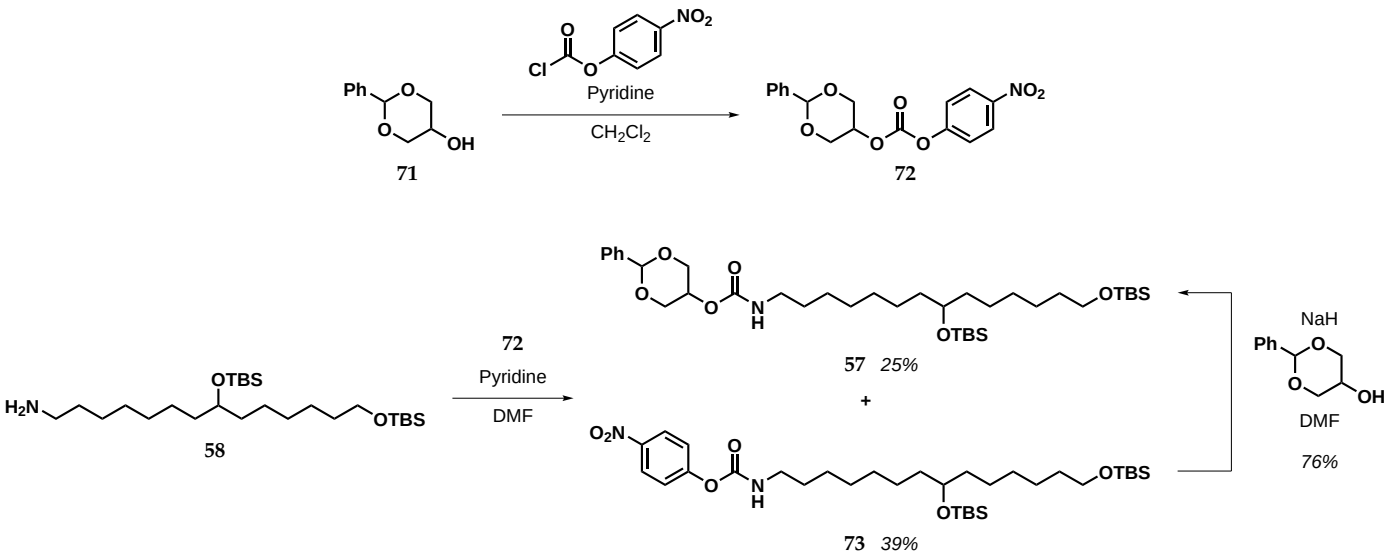

Scheme 2.27: Synthesis of mixed carbonate **72** and subsequent carbamate formation yielding desired carbamate **57** and the nitrophenolate **73**.

To try to improve the yield of the carbamate formation, the use of different carbonyl acceptors was studied. Formation of benzylidene glycerol chloroformate **74** using triphosgene was unsuccessful due to the lack of reactivity of alcohol **71** as depicted in Scheme 2.28.

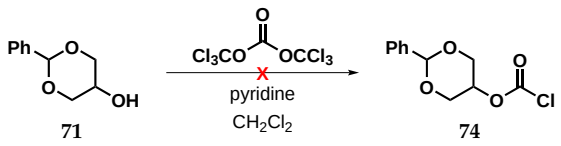

Scheme 2.28: Attempt at making benzylidene glycerol chloroformate **74** using triphosgene.

Following this result, another approach was tested where 1,3-*O*-benzylideneglycerol was treated with 1,1'-carbonyldiimidazole (CDI) allowing the formation of imidazole carbamate **75** which was then subjected to amine **58** affording carbamate **57** in high yield, as depicted in Scheme 2.29.

Due to the low solubility of the fully protected carbamate in acetonitrile, the removal of the TBS groups was first performed in THF. Unfortunately, the rate of the reaction in THF is very slow and after 24 hours of stirring in THF, nearly full conversion of the starting material was observed, however, a large majority of the mono-deprotected moiety was still present. The crude mixture was purified and the mixture of fully protected and mono-deprotected carbamate was subjected to the HF-mediated deprotection in acetonitrile, which yielded precursor **76** in good overall yield. The use of a

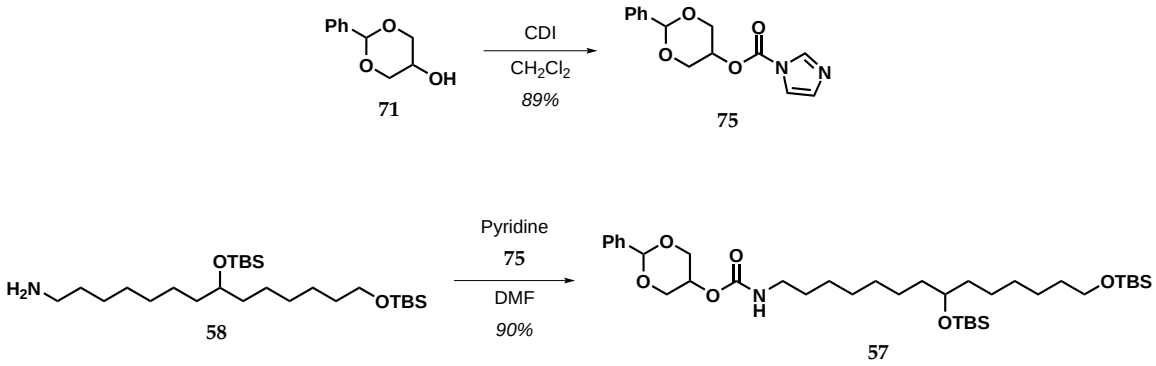

Scheme 2.29: Optimization of the formation of carbamate **57** using CDI-mediated carbamoylation.

THF : MeCN solvent mixture could potentially alleviate the need for a two step deprotection process. This was attempted by a student and a one step deprotection was achieved but with a lower overall yield.

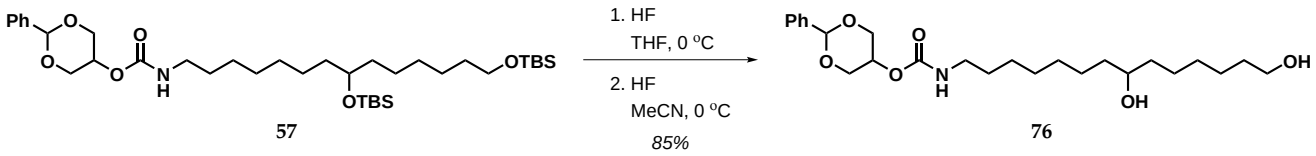

Scheme 2.30: Two steps TBS removal using hydrofluoric acid in THF then acetonitrile.

Final hydrogenolysis of the benzylidene acetal afforded target carbamate **56** in good yield.

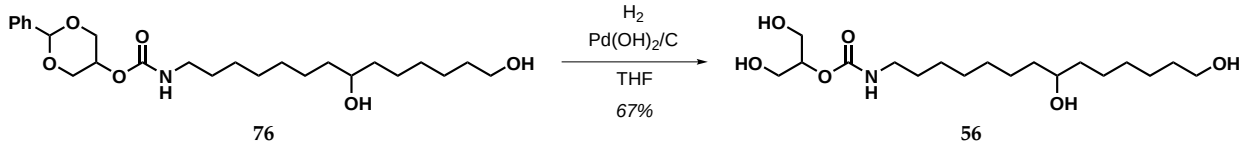

Scheme 2.31: Final hydrogenolysis affording target compound **56**.

2.3.3.2 Enzymatic assay

To assess if carbamate **56** could be used as a CUS1 ligand, several polymerization assays have been performed. Firstly, carbamate **56** was subjected to the polymerization conditions to assure that carbamate **56** is not a substrate of CUS1. As depicted in Figure 2.11, the MALDI-TOF analysis of the carbamate incubation product shows that CUS1 is unable to polymerize the carbamate on its own as no oligomers peaks were observed.

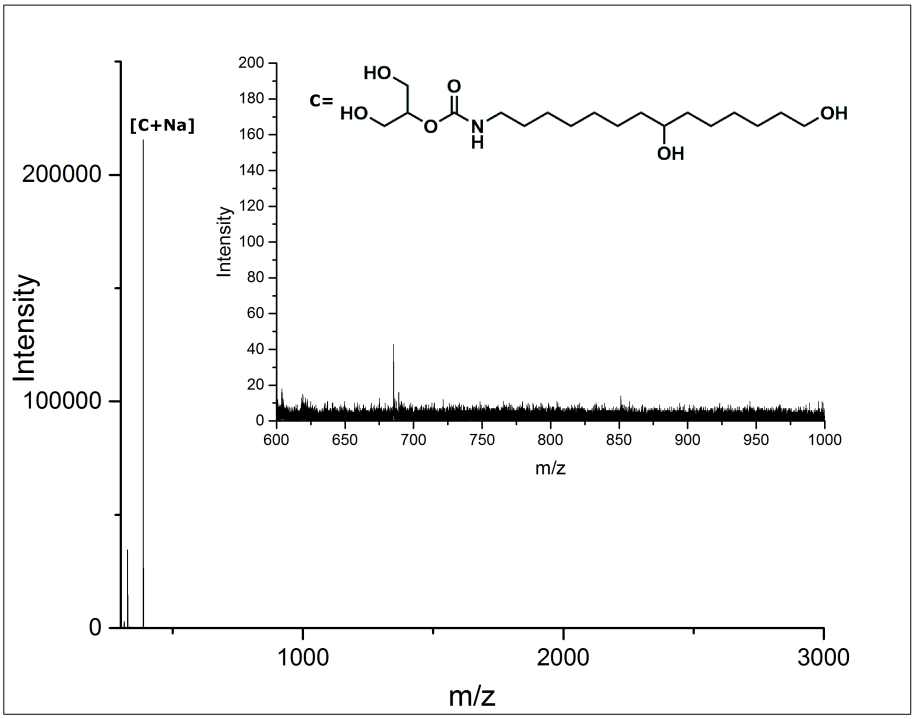

Figure 2.11: MALDI-TOF analysis of the carbamate incubation product.

A direct competition experiments between carbamate **56** and 2-MHG was performed by incubating an equimolar amount of both compound with CUS1 for 24 hours. MALDI-TOF analysis of the resulting mixture suggests that the polymerization is hindered by the presence of the carbamate as indicated by the lower intensity of each oligomer peaks and the absence of oligomers above the tetramer. To our surprise, the inclusion of one single carbamate repeating unit within the oligomers was observed as major products, indicating that the carbamate is interacting with CUS1. In light of this finding, two different theories are proposed. First, the carbamate could act as a capping reagent by adding itself onto a growing oligomeric chain and blocking the polymerization of this specific chain due to its lower elecrophilicity at the carbonyl site. Alternatively, the carbamate could interact strongly with the enzyme and act as a ”seed” for the chain to grow. Understanding how this carbamate insertion works could shed some light on the polymerization mechanism and more specifically, the direction of chain growth. To assess if the carbamate acts as a capping agent, one could incubate some monomer with the enzyme until full conversion and subsequently, add the carbamate to the oligomer mixture. If the carbamate acts as a seeding agent, no carbamate insertion should be observed, contrastingly, if the carbamate acts as a cap-

ping agent, carbamate insertion will be present. Unfortunately, due to time restriction, such experiments could not be performed at the time of writing.

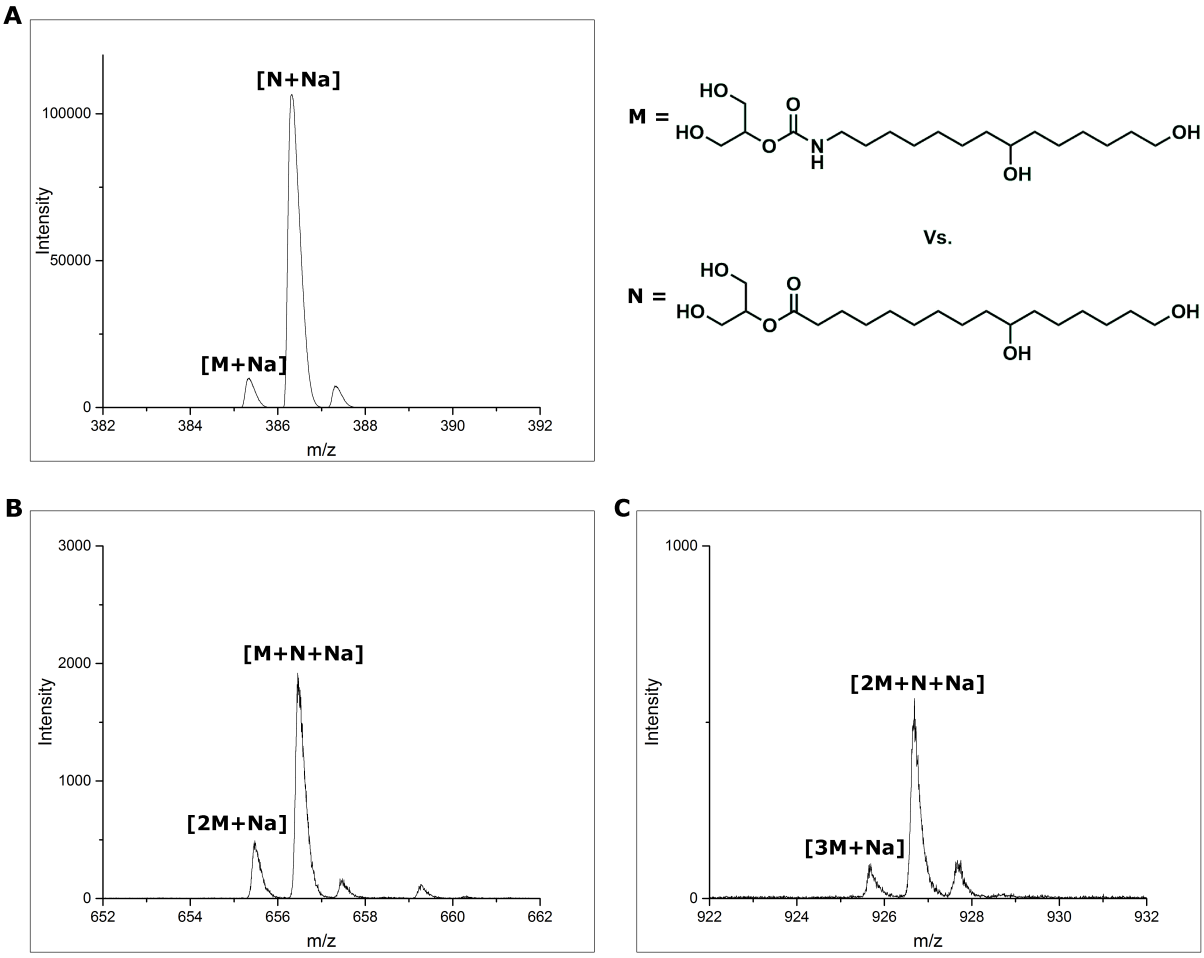

Figure 2.12: MALDI-TOF analysis of the direct competition experiments. A, zoom of the monomer region; B, zoom on the dimer region; C, zoom on the trimer region.

To try to optimize the carbamate-induced inhibition, a delayed competition experiments was set up. CUS1 was incubated with carbamate **56** for 2 hours prior to the addition of 2-MHG. However, pre-incubation of the carbamate did not allow to improve the inhibition of the polymerization as the presence of dimer, trimer and tetramer are still observed.

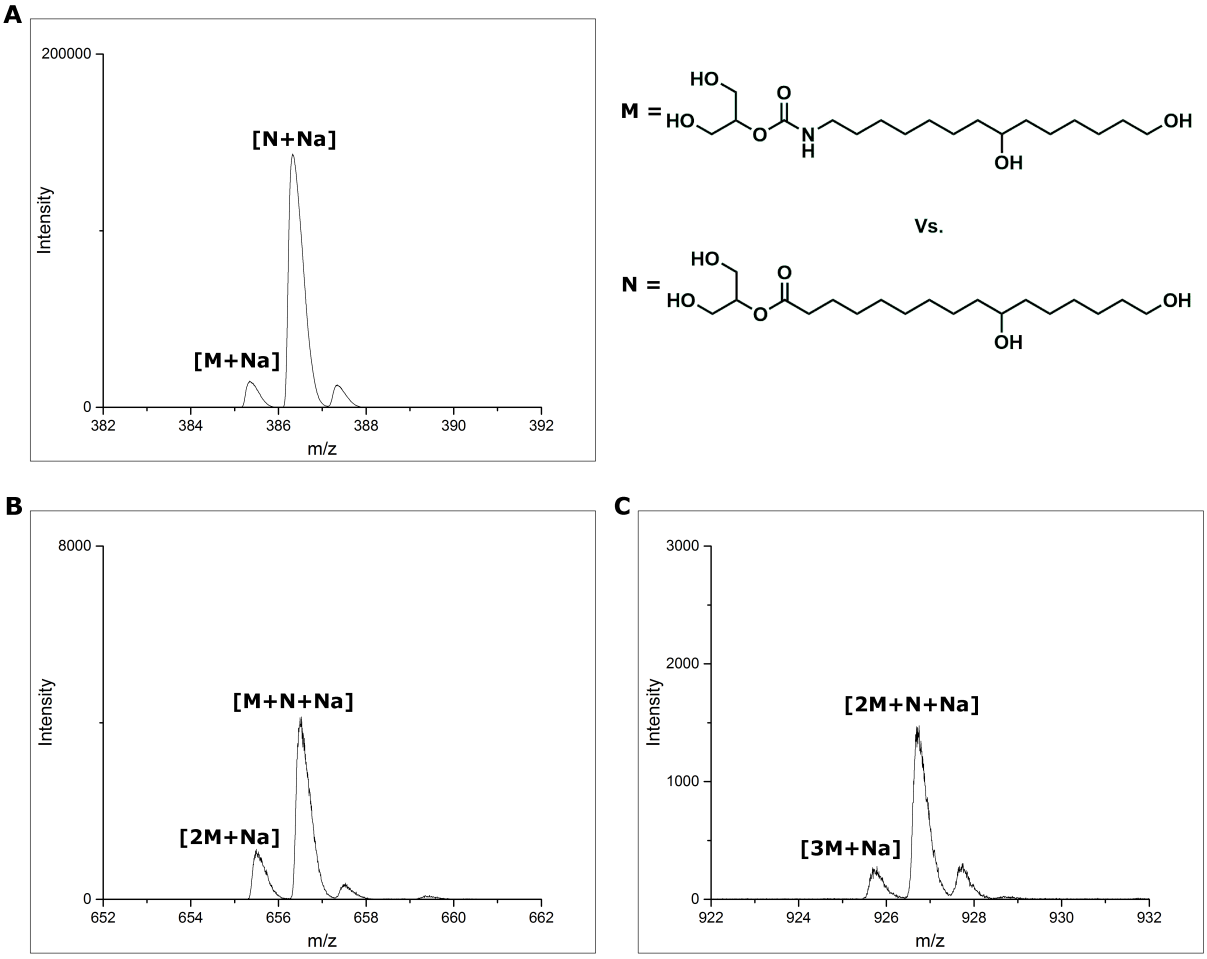

Figure 2.13: MALDI-TOF analysis of the delayed competition experiments. A, zoom of the monomer region; B, zoom on the dimer region; C, zoom on the trimer region.

2.3.4 Conclusions and perspectives

A robust synthesis for target carbamate **56** was developed. Enzymatic assays using this carbamate proved that CUS1 is not able to polymerize this compound on its own. However, subjecting an equimolar mixture of 2-MHG and carbamate **56** to CUS1-mediated polymerization indicates that the carbamate might hinder the polymerization of 2-MHG. Unfortunately, incubating the carbamate with CUS1 prior to the addition of 2-MHG does not seems to improve the polymerization inhibition.

Interestingly, the insertion of one single molecule of carbamate was observed for a series of oligomers. MALI-TOF analysis indicates that co-oligomers are the major product of the enzymatic polymerization of the mixture. Two different theories have

emerged to explain this result, the seeding theory and the capping theory. Understanding the mechanism of insertion of the carbamate within the oligomer could offer valuable information on the mechanism of CUS1-mediated polymerization. However, to confirm the nature of the formation of this co-oligomers, further enzymatic tests needs to be performed.

If carbamate **56** is found to be a potent CUS1 ligand, co-crystallization of CUS1 and the carbamate will be investigated. If the co-crystalization is successful, the crystals will be analyzed by XRD to delineate the tertiary structure of CUS1.

2.4 Selectivity of CUS1 - Headgroup Modification

The next section presents a project undertaken by Sara Britta Riehm Pedersen as part of her master thesis. This project was supervised by both, Ph.D. student Ignacio Martínez San Segundo and the author, Ph.D. student Gauthier Scavée. All of the chemistry presented has been performed by the master student while the enzymatic assays has been performed by Ph.D. student Nicholas Segerson at Cornell University, NY, USA.

2.4.1 Objectives

The selectivity of enzymes towards different substrates is often guided by a series of interactions between the enzyme and the substrates. Due to the unknown tertiary structure of CUS1, it is difficult to obtain information on the recognition pattern between CUS1 and its substrates. The aim of this project was to assess the selectivity of CUS1 regarding monomers headgroup in hope to provide more information on the recognition process between CUS1 and its substrates. In this context, the synthesis of four different 10,16-dihydroxypalmitic esters, depicted in Figure 2.14 has been undertaken.

First, the synthesis of 1-mono(10,16-dihydroxyhexadecanoyl)glycerol (**77**; 1-MHG) was planned. This thermodynamically favored compound, with respect to 2-MHG, is often formed by the migration of the glycerol moiety of 2-MHG when the latter is incubated in protic solvent. Secondly, the synthesis of ethylene glycol ester **78** and isopropyl ester **79** were envisaged to assess for the importance of the hydroxyl group in the recognition pattern of CUS1. Finally, 1,3-dimethylglycerol ester **80** would allow us to assess if the hydrogen donating properties of the hydroxyl groups is required for the recognition of 2-MHG as a CUS1 substrate.

In terms, we hope that differences in the polymerization of these various esters will allow us to draw some conclusion on the required features of the headgroup for the recognition between CUS1 and its substrates.

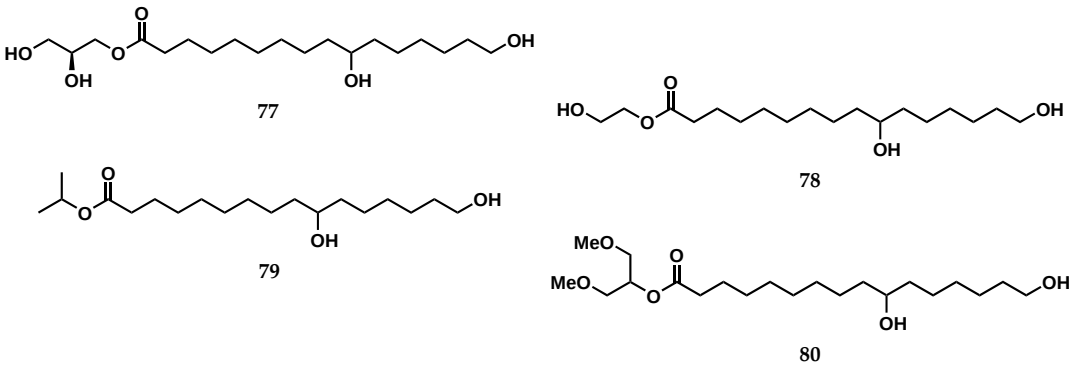

Figure 2.14: Target 10,16-dihydroxypalmitic esters.

2.4.2 Synthetic Strategy

The target compounds should all be obtainable through the oxidation, esterification and global deprotection of precursor **10** using different alcohols during the esterification process. Alcohol precursor **10** is one of the intermediates of the original 2-MHG synthesis whose synthesis has already been described in section 1.5.[44]

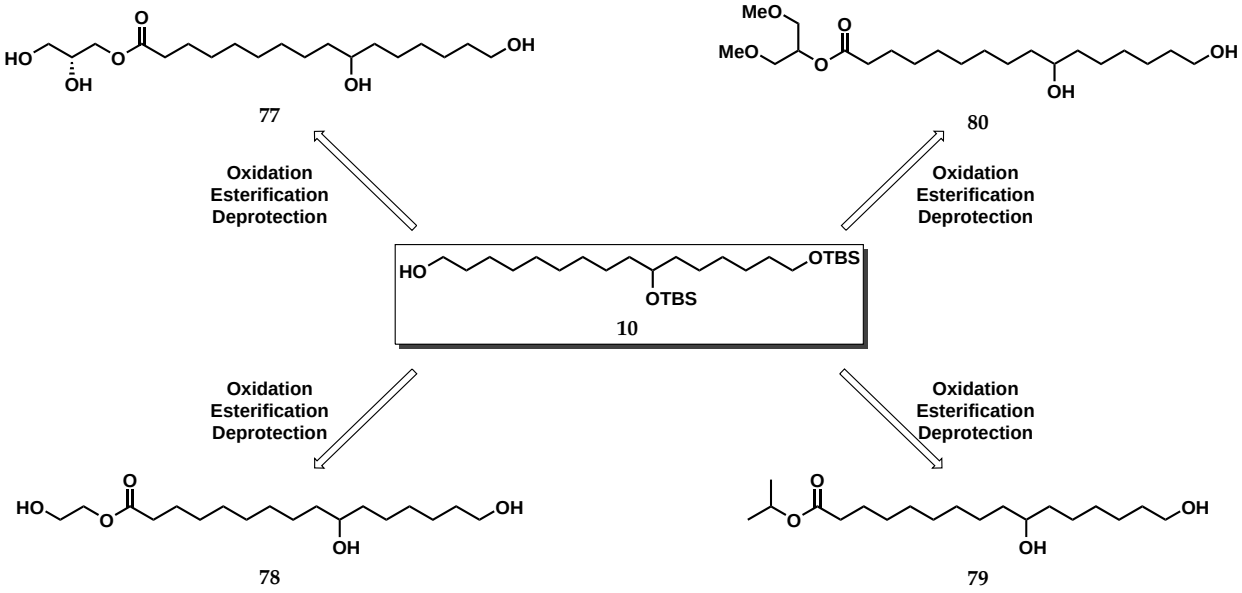

Scheme 2.32: Retrosynthetic analysis of the four target esters.

2.4.3 Results and discussion

2.4.3.1 Synthesis

The synthesis of precursor **10** has already been described in Scheme 1.5 in section 1.5 and will not be discussed here. This precursor was oxidized using either a one-step oxidation using PIDA in the presence of TEMPO, or a two-step procedure via Dess-Martin oxidation and subsequent Pinnick-Lindgren oxidation to afford carboxylic acid **81**. The latter was then subjected to four Steglich esterification reaction using (S)-2,3-Bis(benzyloxy)propan-1-ol, 2-(benzyloxy)ethan-1-ol, isopropanol and 1,3-dimethoxypropan-2-ol affording protected esters **82**, **83**, **84** and **85**.

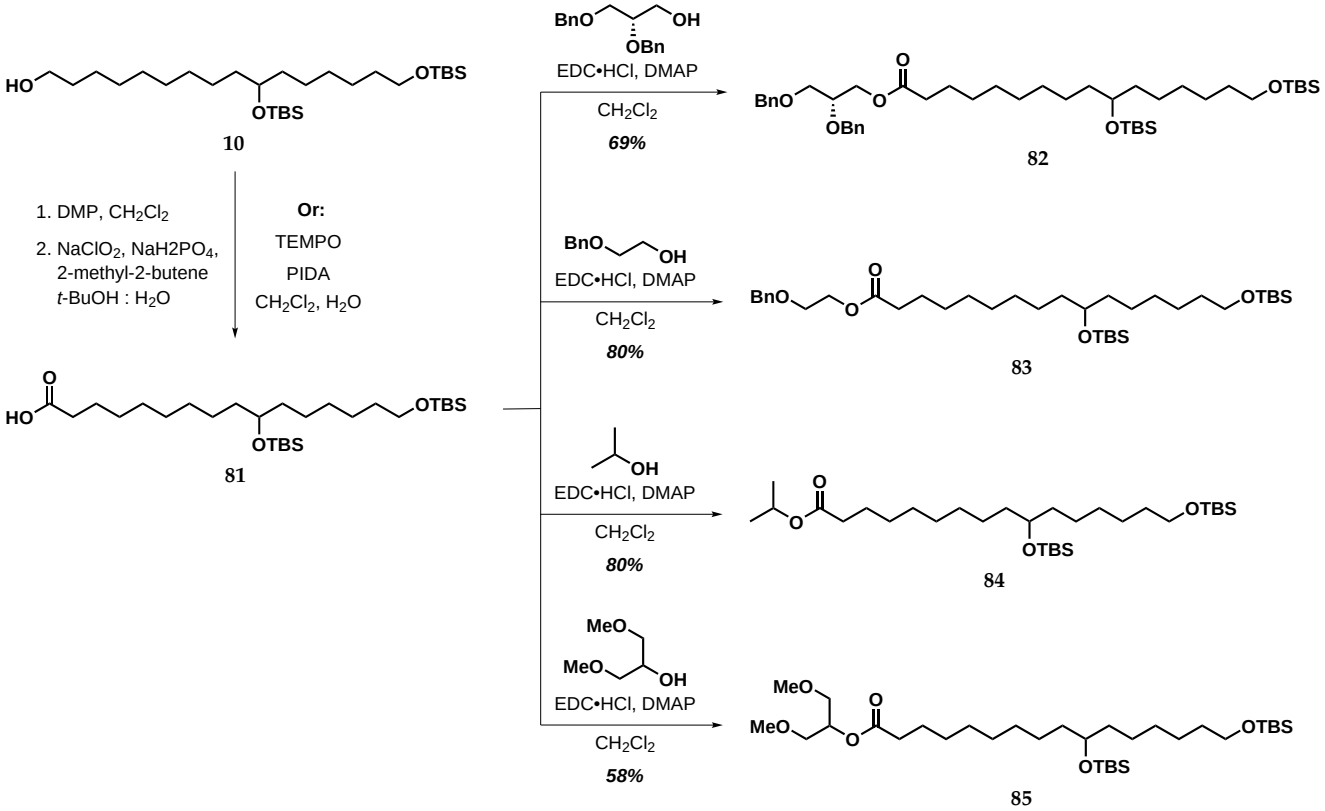

Scheme 2.33

Removal of the TBS protecting groups for both, 1-MHG precursor **82** and ethylene glycol ester **83** afforded intermediates **86** and **87** respectively. The latter were subjected to hydrogenolysis conditions using Pearlman's catalyst affording the target compounds **77** and **78**. Similarly, target compounds **79** and **80** were obtained from intermediates **84** and **85** via the HF-mediated TBS deprotection.

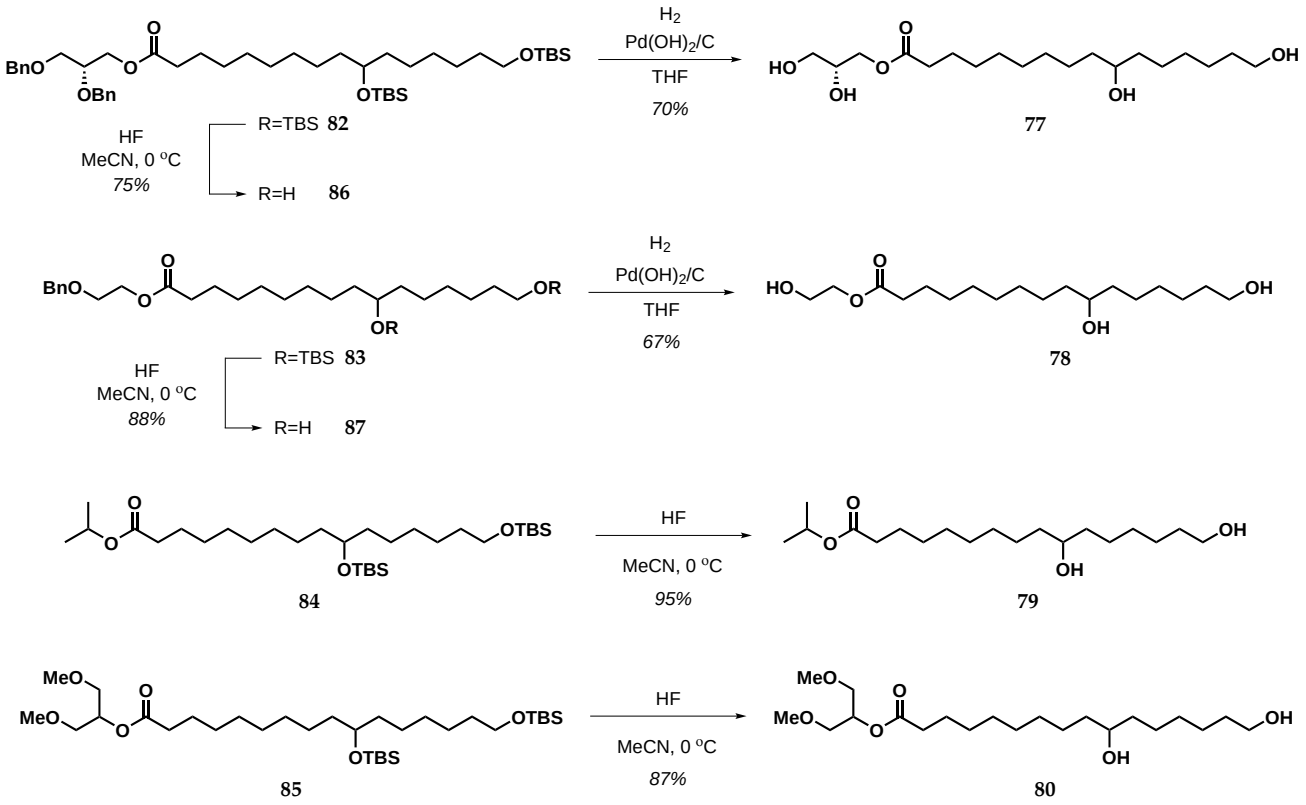

Scheme 2.34: Final deprotection of intermediates **82**, **83**, **84** and **85** affording target esters **77**, **78**, **79** and **80**

2.4.4 Enzymatic assay

Each of the synthesized esters were subjected to a 24 hour incubation with CUS1 and analyzed by MALDI-TOF. The results are shown on Figure 2.15 to Figure 2.18 and indicates that CUS1 is relatively permissive regarding the monomer headgroup. Of all the synthesized compound, 1-MHG was found to polymerize the best, tightly followed by both, 1,3-dimethoxypropanol ester **80** and ethylene glycol ester **78**. Conversely, isopropyl ester **79** was found to polymerize poorly and did not produce any oligomer longer than the dimer. This indicates that the presence of the oxygen atom plays an important role in the recognition of CUS1 substrates. Interestingly, in the case of 1,3-dimethoxypropanol ester **80**, the presence of hydrolyzed dimers was observed, suggesting that the presence of the methyl groups might promote the hydrolysis of the headgroup.

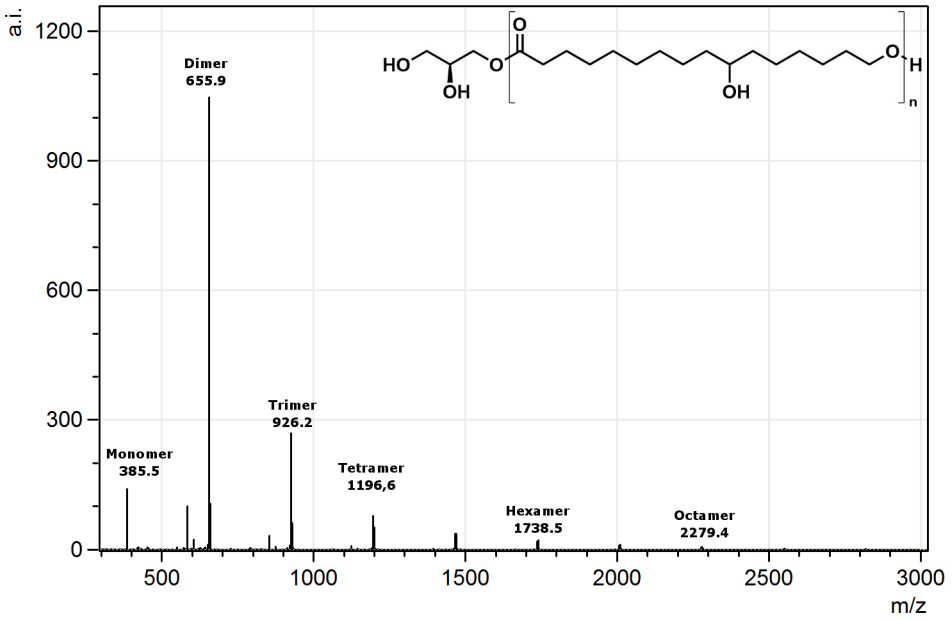

Figure 2.15: MALDI-TOF analysis of the polimerization product of sn-1 glycerol ester **77**.

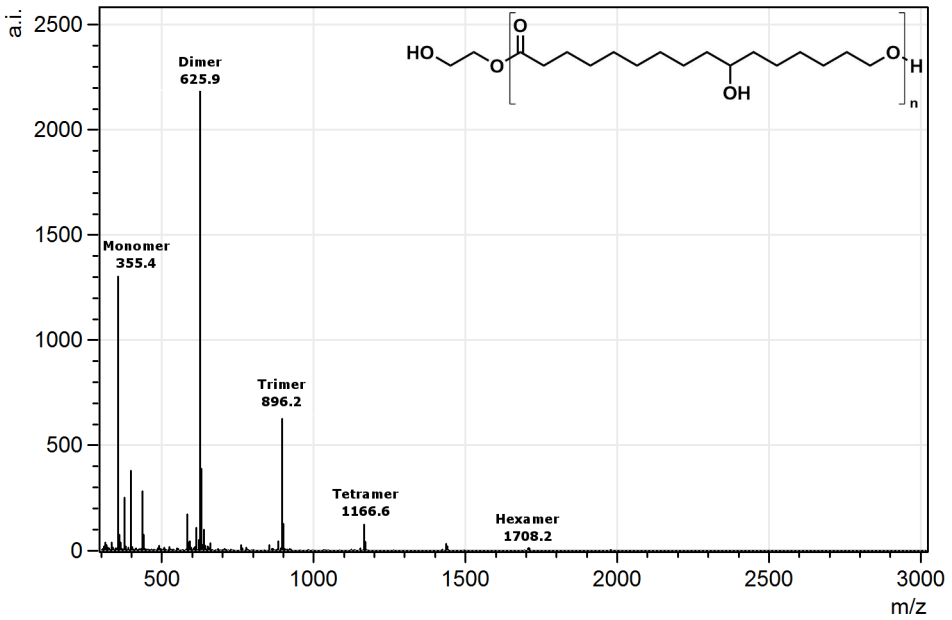

Figure 2.16: MALDI-TOF analysis of the polimerization product of ethylene glycol ester **78**.

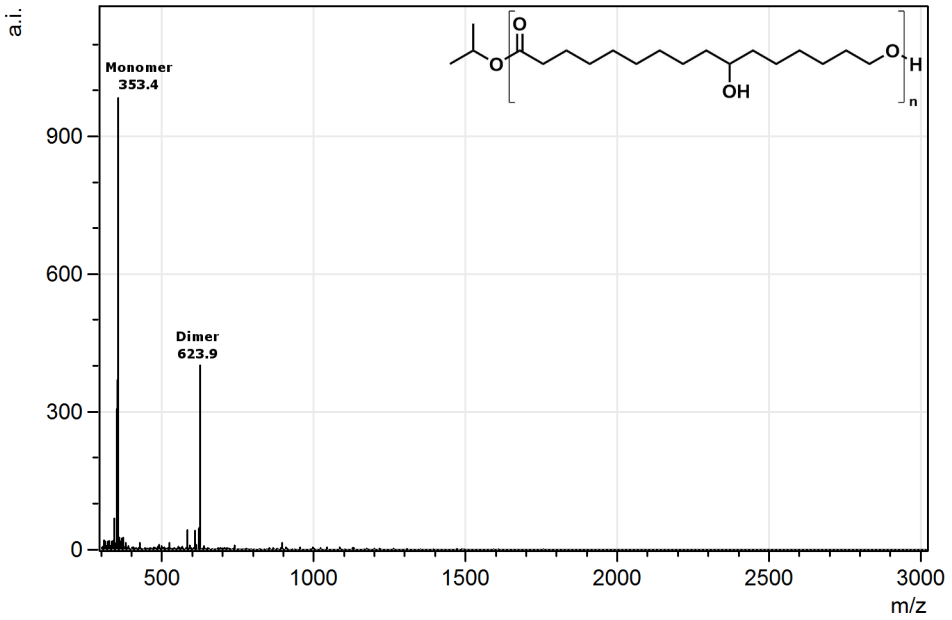

Figure 2.17: MALDI-TOF analysis of the polimerization product of isopropyl ester **79**.

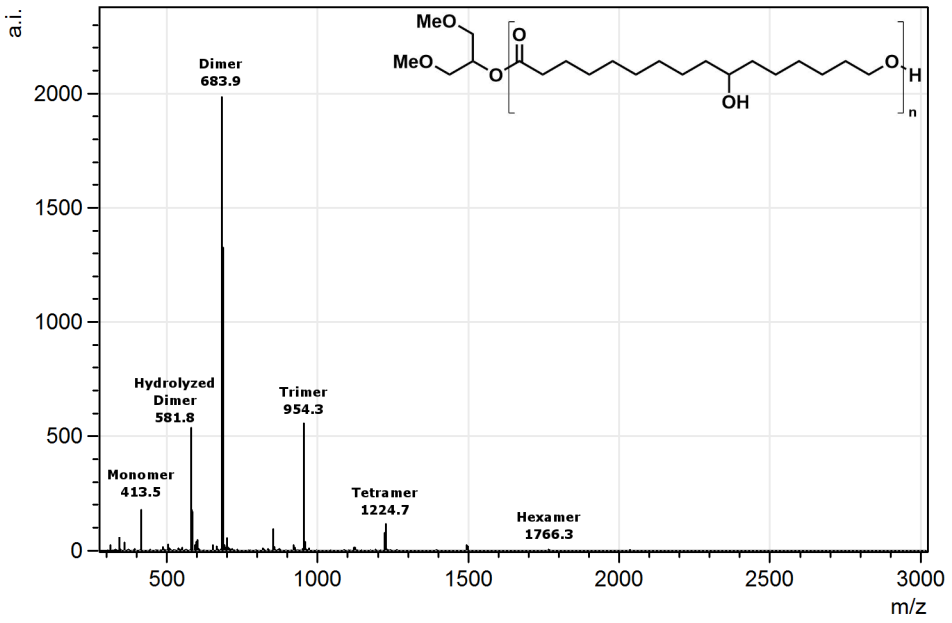

Figure 2.18: MALDI-TOF analysis of the polimerization product of dimehtylglycerol ester **80**.

2.4.5 Conclusions and perspectives

To assess the behavior of CUS1 with respect to different headgroup, four different 10,16-dihydroxyhexadecanoic esters, compound **77**, **78**, **79** and **80** were synthesized through a divergent synthetic route. These different esters were subjected to CUS1 mediated polymerization and proved to be potent substrates for CUS1 at the exception of isopropanol ester **79**, highlighting the importance of the hydroxy groups for CUS1 substrates recognition. Additionally, the presence of methyl groups on the glycerol moiety did not inhibit polymerization, suggesting that the headgroup hydroxyl groups interact as hydrogen bond acceptor with CUS1.
The synthesis and investigation of the biopolymerization of these four esters proved to be a fast and efficient way to shed some light on the potential recognition mechanism between CUS1 and its substrate.

Chapter 3

Experimental

3.1 General considerations

Starting materials, reagents and solvents were purchased from commercial suppliers and used without further purification. All solvent are HPLC-grade and anhydrous solvent were obtained from Inovative Technology PS-MD-7 Pure-Solv solvent purification system except for pyridine which was dried over 4 Å activated molecular sieves for a minimum of 24 h (according to standard procedure).[166] All reactions requiring anhydrous conditions were carried out in flame-dried glassware under inert atmosphere. Thin-layer chromatography (TLC) was performed on Merck Aluminum Sheets pre-coated with 0.25 mm silica gel C-60 F_{254} plates. The plates were visualized under UV irradiation at 254 nm and/or by heating after dipping in a suitable developing reagent. Eluent systems are specified for each R_f-value and ratios are given as volume ratios. Evaporation of the solvent was performed on a Heidolph laborota 4000 efficient under reduced pressure (*in vacuo*) at temperature ranging from 20-40 °C. Flash column chromatography was performed using Geduran silica gel 60 Å (35-70 µm) as the stationary phase by the general procedure developed by Still *et al.*[167] Dry column Vacuum chromatography (DCVC) was performed according to litterature procedure.[168] The eluent systems for both, flash chromatography and DCVC, are specified under the protocol for each synthesis. Eluent ratios are given as a volume ratios. NMR spectras were recorded on a Bruker Ascend 400 spectrometer with a Prodigy cryoprobe. Chemical shifts (δ) are reported in ppm downfield from TMS (δ = 0) using solvent resonance as the internal standard (chloroform – d, ^{1}H: 7.26 ppm, ^{13}C: 77.16 ppm; Methanol – d_4 ^{1}H: 4.87 ppm, ^{13}C: 49 ppm; benzene – d_6, ^{1}H: 7.16 ppm, ^{13}C: 128.06 ppm). The annotation (2C) and (3C) indicates when two or three carbon signals are totally overlapped. Coupling constants (*J*) are reported in Hz and the field is reported in each case. Multiplicities are reported as singlet (s), broad singlet (br. s), doublet (d), doublet of doublets (dd), doublet of triplets (dt), doublet of doublet of doublets (ddd), doublet of doublet of triplets (ddt), triplet (t), triplet of doublets (td), quartet (q), pentet (p) and multiplet (m). HRMS analysis were performed on either on a UHPLC-QTOF system (Dionex ultimate 3000 and Bruker MaXis) with an electrospray ionization (ESI) source or a MALDI-TOF system (Bruker Solarix XR 7T) and controlled using Data Analysis 4.2 software. Melting points were measured on a Stuart melting point SMP30 and reported in °C uncorrected. All compounds have been

characterized by NMR using 1D and 2D experiments at the exception of some intermediates that tend to degrade rapidly. New compounds were characterized by NMR, HRMS and melting point.

3.2 Procedures

General procedure for the enzymatic polymerization

An eppendorf tube containing a solution of monomer (0.1 M in DMSO, 0.5 µL) and recombinant CUS1 (0.4 µg/µL, 1.25 µL) in an ammonium acetate buffer (50 mM, pH 5, total volume: 50 µL) was incubated at 37 °C for 24 h. In the case of deutero-monomer competition experiments, the monomer solution was prepared by mixing a solution of deuterated monomer (0.1 M in DMSO, 10 µL) with a solution of non-deuterated monomer (0.1 M in DMSO, 0.5 µL). In the case of the carbamate inhibition, the carbamte solution (0.1 M in DMSO, 0.5 µL) was either, directly with the 2-MHG solution (direct competition) or incubated at 37 °C with CUS1 for 2 h prior to the addition of the 2-MHG solution (delayed competition). The samples were diluted in MeOH (150 µL) and the resulting solution (2 µL) was mixed with a solution of super DHB (2 µL) and analyzed by MALDI-TOF.

6-((tert-Butyldimethylsilyl)oxy)-N-methoxy-N-methylhexanamide (25)

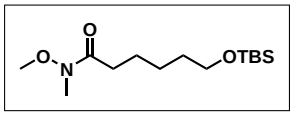

To a solution of *N*,*O*-dimethylhydroxylamine (2.13 g, 21.8 mmol) in anhydrous CH_2Cl_2 (44 mL) stirred at 0 °C under inert atmosphere, a solution of $AlMe_3$ in toluene (2 M, 11 mL, 22 mmol) was added over 30 min. The resulting solution was stirred at 0 °C for 1 h then a solution of ε-caprolactone (1.01 g, 8.25 mmol) in anhydrous CH_2Cl_2 (16 mL) was added dropwise. The resulting mixture was stirred at 0 °C for 30 min. The resulting mixture was poured into sat. aq. $NaHCO_3$ (50 mL) and extracted with CH_2Cl_2 (3 × 30 mL). The combined organic layers were washed with brine (50 mL), dried over Na_2SO_4 and concentrated *in vacuo*.

The crude mixture was dissolved in anhydrous CH_2Cl_2 (20 mL) under inert atmosphere and cooled down to 0 °C. 2,6-lutidine (1.13 g, 10.5 mmol) and TBSCl (1.35 g, 8.93 mmol) were added and the resulting mixture was allowed to warm at 20 °C and stirred overnight. The reaction mixture was washed with sat. aq. NH_4Cl (20 mL), sat. aq. $NaHCO_3$ (20 mL) and brine (20 mL), dried over $MgSO_4$ and the solvent was evaporated *in vacuo*. The crude was purified by DCVC (SiO_2, 28.3 cm^2, 0-14%, EtOAc :

heptane, 2% steps then 14-25% EtOAc : heptane, 1% steps, 100 mL fractions) affording **25** as a yellowish oil (2.22 g, 87%). $\mathbf{R_f}$ (EtOAc : heptane, 1 : 4) = 0.23; **^{1}H NMR** δ 3.67 (s, 3H), 3.60 (t, *J* = 6.5 Hz, 2H), 3.17 (s, 3H), 2.41 (t, *J* = 7.7 Hz, 2H), 1.64 (m, f2H), 1.59 – 1.49 (m, 2H), 1.44 – 1.31 (m, 2H), 0.88 (s, 9H), 0.04 (s, 6H); **^{13}C NMR** (101 MHz, Chloroform-d) δ 174.65, 63.53, 61.65, 33.10, 32.68, 32.35, 26.44 (3C), 26.13, 24.92, 18.83, -4.81 (2C); **HRMS** (MALDI+ FT-ICR, dithranol) m/z: calcd for $C_{14}H_{31}NO_3SiNa]^+$ 312.1965; found 312.1967.

7-((tert-Butyldimethylsilyl)oxy)heptan-2-one (20)

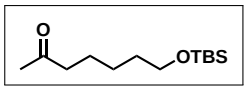

To a solution of Weinreb amide **25** (1.11 g, 3.84 mmol) in THF (40 mL) stirred at -78 °C under inert atmosphere, a solution of MeMgBr (2.5 M, 2.0 mL, 5.0 mmol). The reaction was stirred at -78 °C for 5 min. The reaction mixture was allowed to warm up to 0 °C then slowly to 20 °C and stirred overnight. The resulting mixture was poured into sat. aq. NH_4Cl (15 mL) and extracted with EtOAc (4 × 40 mL). The combined organic layer was washed with sat. aq. $NaHCO_3$ (60 mL) and brine (60 mL), dried over Na_2SO_4 and concentrated *in vacuo*. The crude was purified by DCVC (SiO_2, 78.5 cm^2, 0-5%, EtOAc : heptane, 1% steps then 5-8% EtOAc : heptane, 0.5% steps, 100 mL fractions) affording **20** as a transparent oil (0.756 g, 80%). $\mathbf{R_f}$ (EtOAc : heptane, 1 : 4) = 0.54; **^{1}H NMR** (400 MHz, Chloroform-d) δ 3.59 (t, J = 6.4 Hz, 3H), 2.42 (t, J = 7.5 Hz, 2H), 2.13 (s, 3H), 1.55 (m, 4H), 1.39 – 1.26 (m, 2H), 0.88 (s, 9H), 0.03 (s, 6H). **HRMS** (MALDI+ FT-ICR, dithranol) m/z: calcd for $[C_{13}H_{28}O_2SiH]^+$ 245.1931; found 245.1934.

9-(Benzyloxy)nonan-1-ol (28)

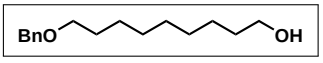

To a suspension of NaH (60 % in mineral oil, 1.51 g, 37.8 mmol) in anhydrous DMF (20 mL), stirred at 0 °C under inert atmosphere, a solution of 1,9-nonanediol (10.0 g, 62.4 mmol) in THF : DMF (25 mL : 20 mL) was added slowly over the course of 15 min. The solution was allowed to warm at 20 °C. After 2 h, BnBr (5.34 g, 31.2 mmol) was added dropwise and the resulting yellow solution was stirred overnight. Excess NaH was quenched by the slow addition of ice until bubbling ceased and the resulting mixture was extracted with Et_2O (3 × 100 mL). The combined organic layer was washed with brine (100 mL), dried over $MgSO_4$ and concentrated over silica *in vacuo*. The crude was purified by flash chromatography (SiO_2, EtOAC : heptane, 1 : 9 then EtOAC : heptane, 1 : 4) affording **28** as a yellowish oil (4.99 g, 64%); $\mathbf{R_f}$ (EtOAc : heptane, 1 : 4) = 0.18; **^{1}H NMR** (400 MHz, Chloroform-*d*) δ 7.36 – 7.27 (m, 5H), 4.50 (s, 2H), 3.63 (t, *J* = 6.6 Hz, 2H), 3.46 (t, *J* = 6.6

Hz, 2H), 1.65 – 1.52 (m, 4H), 1.39 – 1.27 (m, 10H); **^{13}C NMR** (101 MHz, Chloroform-*d*) δ 138.85, 128.48 (2C), 127.77 (2C), 127.61, 73.00, 70.65, 63.22, 32.93, 29.90, 29.67, 29.54, 29.50, 26.32, 25.85; **HRMS** (MALDI+ FT-ICR, dithranol) m/z: calcd for $[C_{16}H_{26}O_2Na]^+$ 273.1825; found 273.1827.

9-(Benzyloxy)nonanal (19)

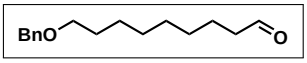

To a suspension of Dess-Martin periodane (6.45 g, 15.2 mmol) in anhydrous CH_2Cl_2 (40 mL) stirred at 0 °C under inert atmosphere, a solution of **28** (2.55, 10.2 mmol) in anhydrous CH_2Cl_2 (20 mL) was added dropwise and the resulting mixture was stirred for 3 h. The reaction was diluted with Et_2O (100 mL), sat. aq. $NaHCO_3$ (100 mL) containing $Na_2S_2O_3$ (25 g) was added and the reaction was stirred vigorously for 5 min. The aqueous layer was separated and extracted with Et_2O (100 mL). The combined organic layer was washed with sat. aq. $NaHCO_3$ (150 mL) and brine (150 mL), dried over $MgSO_4$ and concentrated *in vacuo* affording a yellowish oil. The crude product was used without further purification. $\mathbf{R_f}$ (EtOAc : heptane, 1 : 4) = 0.50; **^{1}H NMR** (400 MHz, Chloroform-*d*) δ 9.76 (t, *J* = 1.9 Hz, 1H), 7.39 – 7.27 (m, 5H), 4.50 (s, 2H), 3.46 (t, *J* = 6.6 Hz, 2H), 2.41 (td, *J* = 7.4, 1.9 Hz, 2H), 1.71 – 1.55 (m, 4H), 1.41 – 1.23 (m, 8H); **^{13}C NMR** (101 MHz, Chloroform-*d*) δ 203.07, 138.81, 128.48 (2C), 127.76 (2C), 127.62, 73.01, 70.58, 44.04, 29.87, 29.43, 29.38, 29.23, 26.27, 22.20.

7-((tert-Butyldimethylsilyl)oxy)-2-((trimethylsilyl)oxy)-hept-1-en-2-ol (26)

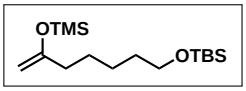

To a solution of LDA (1.54 M, 5.5 mL, 8.5 mmol) in THF (40 mL) stirred at -78 °C under inert atmosphere, a solution of **20** (1.63 g, 6.67 mmol) in THF (6 mL) was added dropwise. The resulting mixture was stirred at -78 °C for 5 min then TMSCl (1.3 mL, 1.1 g, 10.66 mmol) was slowly added. The reaction mixture was stirred for 90 min at -78 °C then allowed to warm to 20 °C. After 40 min, pentane was added (200 mL) and the resulting cloudy mixture was poured into sat. aq. $NaHCO_3$ (200 mL). The organic layer was dried over Na_2SO_4 and concentrated *in vacuo* affording **26** with minor impurities. The product was used without further purification. $\mathbf{R_f}$ (EtOAc : heptane, 1 : 9) = 0.90; **^{1}H NMR** (400 MHz, Benzene-d_6) δ 4.18 (d, *J* = 0.9 Hz, 1H), 4.16 – 4.12 (m, 1H), 3.53 (t, *J* = 6.3 Hz, 2H), 2.09 (t, *J* = 7.4 Hz, 2H), 1.54 (tdd, *J* = 12.7, 8.5, 6.8 Hz, 4H), 1.46 – 1.33 (m, 2H), 0.99 (s, 9H), 0.19 (s, 9H), 0.07 (s, 6H); **^{13}C NMR** (101 MHz, Benzene-d_6) δ 159.82, 89.93, 63.27, 37.07, 33.14, 27.13, 26.21 (3C), 25.78, 18.55, 0.23 (3C), -5.11 (2C).

16-(Benzyloxy)-1-((tert-butyldimethylsilyl)oxy)-8-hydroxyhexadecan-6-one (18)

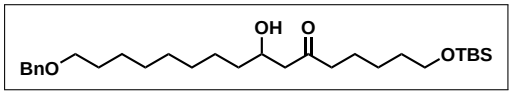

To a solution of **26** and **19**, prepared as previously mentioned, in anhydrous CH_2Cl_2 (30 mL) stirred at -78 °C under inert atmosphere, a solution of $TiCl_4$ in toluene (1 M, 9 mL, 9 mmol) was added dropwise. The solution was stirred at -78 °C for 45 min then sat. aq. $NaHCO_3$ (30 mL) was added at -78 °C. The resulting mixture was allowed to warm at 20 °C and the aqueous layer was extracted with CH_2Cl_2 (3 × 40 mL). The combined organic layer was dried over Na_2SO_4 and concentrated *in vacuo*. The crude mixture was purified by DCVC (SiO_2, 78.5 cm^2, 0-18%, EtOAc : heptane, 100 mL fractions) affording **18** as a transparent oil (969 mg, 30% over two steps). $\mathbf{R_f}$ (EtOAc : heptane, 1 : 4) = 0.27; **^{1}H NMR** (400 MHz, Chloroform-*d*) δ 7.38 – 7.24 (m, 5H), 4.49 (s, 1H), 4.07 – 3.95 (m, 1H), 3.59 (t, *J* = 6.6 Hz, 2H), 3.45 (t, *J* = 6.8 Hz, 2H), 2.62 – 2.37 (m, 4H), 1.68 – 1.19 (m, 20H), 0.88 (s, 12H), 0.04 (s, 8H). **^{13}C NMR** (101 MHz, Chloroform-*d*) δ 212.46, 138.77, 128.40 (2C), 127.68 (2C), 127.53, 72.92, 70.57, 67.70, 63.00, 49.08, 43.71, 36.55 (2C), 32.64, 29.83, 29.59, 29.58, 29.48, 26.25, 26.05 (3C), 25.52, 23.47, 18.43, -5.19 (2C); **HRMS** (ESI-TOF) m/z: calcd for $[C_{29}H_{52}O_4SiH]^+$ 493.3708; found 493.3713.

9-(Naphthalen-2-ylmethoxy)nonan-1-ol (43)

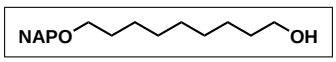

To a suspension of NaH (60 % in mineral oil, 2.60 g, 65.0 mmol) in anhydrous DMF (20 mL), stirred at 0 °C under inert atmosphere, a solution of 1,9-nonanediol (10.0 g, 62.4 mmol) in THF : DMF (25 mL : 20 mL) was added slowly over the course of 15 min. The solution was allowed to warm at 20 °C. After 2 h, NAPBr (6.90 g, 31.2 mmol) was added in three portions and the resulting yellow solution was stirred overnight. Excess NaH was quenched by the slow addition of ice until bubbling ceased and the resulting mixture was extracted with Et_2O (3 × 100 mL). The combined organic layer was washed with brine (100 mL), dried over $MgSO_4$ and concentrated over silica *in vacuo*. The crude was purified by flash chromatography (SiO_2, EtOAC : heptane, 1 : 4) affording **43** as a white solid (5.07 g, 54%); $\mathbf{R_f}$ (EtOAc : heptane, 1 : 4) = 0.20; **^{1}H NMR** 400 MHz, Chloroform-d) δ 7.86 – 7.81 (m, 3H), 7.78 (s, 1H), 7.51 – 7.42 (m, 3H), 4.67 (s, 2H), 3.63 (t, *J* = 6.6 Hz, 2H), 3.51 (t, *J* = 6.6 Hz, 2H), 1.69 – 1.51 (m, 4H), 1.43 – 1.25 (m, 10H); **^{13}C NMR** (101 MHz, Chloroform-*d*) δ 136.35, 133.44, 133.08, 128.24, 127.99, 127.82, 126.41, 126.16, 125.91, 125.88, 73.10, 70.66, 63.21, 32.93, 29.93, 29.68, 29.54, 29.50, 26.33, 25.85; **HRMS** (MALDI+ FT-ICR, dithranol) m/z: calcd for $[C_{20}H_{28}O_2Na]^+$ 323.1982; found 323.1983.

9-(Naphthalen-2-ylmethoxy)nonanal (39)

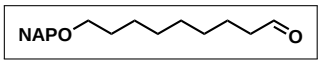

To a suspension of Dess-Martin periodane (15.34 g, 37.22 mmol) in anhydrous CH_2Cl_2 (75 mL) stirred at 0 °C under inert atmosphere, a solution of **43** (7.97 g, 27.8 mmol) in anhydrous CH_2Cl_2 (25 mL) was added dropwise and the resulting mixture was stirred for 3 h. The reaction was diluted with Et_2O (150 mL), sat. aq. $NaHCO_3$ (150 mL) containing $Na_2S_2O_3$ (37.5 g) was added and the reaction was stirred vigorously for 5 min. The aqueous layer was separated and extracted with Et_2O (150 mL). The combined organic layer was washed with sat. aq. $NaHCO_3$ (150 mL) and brine (150 mL), dried over Na_2SO_4 and concentrated *in vacuo* affording a yellowish oil. The crude product was used without further purification. $\mathbf{R_f}$ (EtOAc : heptane, 1 : 4) = 0.50; **^{1}H NMR** (400 MHz, Chloroform-*d*) δ 9.75 (t, *J* = 1.9 Hz, 1H), 7.87 – 7.80 (m, 3H), 7.78 (s, 1H), 7.51 – 7.42 (m, 3H), 4.67 (s, 2H), 3.50 (t, *J* = 6.6 Hz, 2H), 2.40 (td, *J* = 7.4, 1.9 Hz, 2H), 1.75 – 1.52 (m, 4H), 1.45 – 1.22 (m, 8H); **^{13}C NMR** (101 MHz, Chloroform-*d*) δ 203.06, 136.31, 133.43, 133.07, 128.24, 127.98, 127.82, 126.41, 126.16, 125.90, 125.89, 73.11, 70.58, 44.03, 29.89, 29.42, 29.37, 29.23, 26.27, 22.18.

tert-Butyl(hept-6-yn-1-yloxy)dimethylsilane (40)

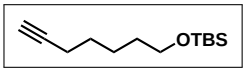

To a solution of 6-heptyn-1-ol (5.00 g, 44.6 mmol) and imidazole (3.93 g, 57.7) in anhydrous DMF (15 mL) stirred under inert atmosphere, TBSCl (8.10 g, 53.7 mmol) was added. The reaction was stirred at 20 °C overnight then poured into sat. aq. NH_4Cl (80 mL) and extracted (3 × 100 mL). The combined organic layers were washed with brine (100 mL), dried over Na_2SO_4 and concentrated *in vacuo*. The crude mixture was purified by flash chromatography (SiO_2, EtOAc : heptane, 1 : 19) affording compound **40** as a transparent oil (9.51 g, 95%), $\mathbf{R_f}$ (EtOAc : hept 1 : 9) = 0.74; **^{1}H NMR** (400 MHz, Chloroform-*d*) δ 3.61 (t, *J* = 6.3 Hz, 2H), 2.19 (td, *J* = 7.0, 2.6 Hz, 2H), 1.93 (t, *J* = 2.7 Hz, 1H), 1.61 – 1.39 (m, 6H), 0.89 (s, 9H), 0.05 (s, 6H); **^{13}C NMR** (101 MHz, Chloroform-*d*) δ 84.74, 68.30, 63.18, 32.46, 28.46, 26.12, 25.17, 18.56, 18.51, -5.12 (2C); HRMS (MALDI+ FT-ICR, dithranol) m/z: calcd for $[C_{13}H_{26}OSiH]^+$ 227.1826; found 227.1828.

1-((tert-Butyldimethylsilyl)oxy)-16-(naphthalen-2-ylmethoxy)hexadec-6-yn-8-ol (38)

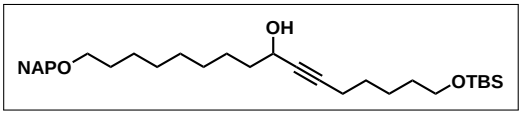

To a solution of alkyne **40** (7.87 g, 34.7 mmol) in anhydrous THF (40 mL) stirred at -78 °C under inert atmosphere, a solution of *n*-BuLi in hexane (2.3 M, 13 mL, 30 mmol). The resulting mixture was allowed to warm at 0 °C then a solution of crude aldehyde **39** in THF (35 mL) was added dropwise. The resulting mixture was allowed to warm at 20 °C and stirred overnight. The reaction mixture was poured into sat. aq. NH_4Cl (150 mL) and extracted with CH_2Cl_2 (3 × 150 mL). The combined organic layer was washed with brine (200 mL), dried over Na_2SO_4 and concentrated *in vacuo*. The crude mixture was purified by flash chromatography (SiO_2, EtOAc : heptane, 1 : 9) affording compound **38** as a yellow oil (8.96 g, 64% over two steps). $\mathbf{R_f}$ (EtOAc : heptane 1 : 9) = 0.14; **^{1}H NMR** (400 MHz, Chloroform-*d*) δ 7.89 – 7.80 (m, 3H), 7.78 (s, 1H), 7.52 – 7.43 (m, 3H), 4.67 (s, 2H), 4.33 (br. s, 1H), 3.60 (t, *J* = 6.4 Hz, 2H), 3.50 (t, *J* = 6.6 Hz, 2H), 2.21 (td, *J* = 7.0, 2.0 Hz, 2H), 1.76 – 1.24 (m, 20H), 0.89 (s, 9H), 0.04 (s, 6H); **^{13}C NMR** (101 MHz, Chloroform-*d*) δ 136.36, 133.45, 133.08, 128.25, 128.00, 127.83, 126.41, 126.17, 125.91, 125.89, 85.51, 81.57, 73.11, 70.67, 63.22, 62.91, 38.36, 32.48, 29.95, 29.66, 29.56, 29.39, 28.63, 26.34, 26.13 (3C), 25.36, 25.28, 18.84, 18.52, -5.11(2C). **HRMS** (MALDI+ FT-ICR, dithranol) m/z: calcd for $[C_{33}H_{52}O_3SiNa]^+$ 547.3578; found 547.3576.

1,8-Bis((tert-butyldimethylsilyl)oxy)-16-(naphthalen-2-ylmethoxy)hexadec-6-yne (44)

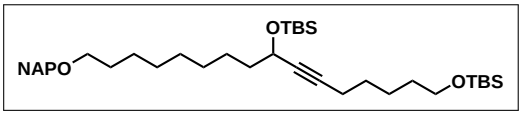

To a solution of **38** (8.82 g, 16.8 mmol) and imidazole (1.71 g, 25.1) in anhydrous DMF (34 mL) stirred under inert atmosphere, TBSCl (3.06 g, 20.3 mmol) was added. The reaction was stirred at 20 °C overnight then concentrated *in vacuo* and dissolved in EtOAc (100 mL). The resulting solution was poured into sat. aq. NH_4Cl (100 mL) and extracted (3 × 100 mL). The combined organic layers were washed with brine (100 mL), dried over Na_2SO_4 and concentrated *in vacuo*. The crude mixture was purified by flash chromatography (SiO_2, EtOAc : heptane, 3%) affording compound **40** as a transparent oil (9.51 g, 95%). $\mathbf{R_f}$ (EtOAc : heptane, 1 : 19) = 0.33; **^{1}H NMR** (400 MHz, Chloroform-*d*) δ 7.83 (mj, 3H), 7.78 (s, 1H), 7.50 – 7.43 (m, 3H), 4.67 (s, 2H), 4.30 (tt, *J* = 6.6, 2.0 Hz, 1H), 3.60 (t, *J* = 6.5 Hz, 2H), 3.50 (t, *J* = 6.7 Hz, 2H), 2.19 (td, *J* = 7.0, 2.0 Hz, 2H), 1.71 – 1.19 (m, 20H), 0.90 (s, 9H), 0.89 (s, 9H), 0.11 (s, 3H), 0.09 (s, 3H), 0.04 (s, 6H); **^{13}C NMR** (101 MHz, Chloroform-*d*) δ 136.37,

133.45, 133.08, 128.24, 128.00, 127.82, 126.40, 126.16, 125.91, 125.88, 84.35, 82.27, 73.11, 70.71, 63.37, 63.30, 39.19, 32.54, 29.96, 29.70, 29.60, 29.39, 28.70, 26.36, 26.14 (3C), 26.03 (3C), 25.51, 25.28, 18.87, 18.52, 18.46, -4.27, -4.79, -5.11 (2C); **HRMS** (MALDI+ FT-ICR, dithranol) m/z: calcd for $[C_{39}H_{66}O_3Si_2H]^+$ 639.4623; found 639.4622.

9,16-Bis((tert-butyldimethylsilyl)oxy)hexadec-10-yn-1-ol (45)

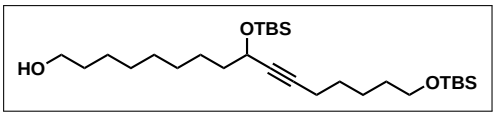

To a solution of **44** (5.38 g, 8.42 mmol) in CH_2Cl_2 (122 mL), 2,3-*d*ichloro-5,6-*d*icyano-1,4-benzoquinone (2.85 g, 12.6 mmol) and water (12 mL) was added. The resulting dark mixture was stirred overnight then poured into sat. aq. $NaHCO_3$ (130 mL). The aqueous layer was extracted with CH_2Cl_2 (3 × 130 mL). The combined organic layers were washed with sat. aq. $NaHCO_3$ (130 mL), dried over Na_2SO_4 and concentrated *in vacuo*. The crude mixture was purified by flash chromatography (SiO_2, EtOAc : heptane, 1 : 9) affording compound **45** as a yellow oil (2.23 g, 53%). $\mathbf{R_f}$ (EtOAc : heptane, 1 : 9) = 0.15; **^{1}H NMR** (400 MHz, Chloroform-*d*) δ 4.31 (tt, *J* = 6.6, 2.0 Hz, 1H), 3.69 – 3.56 (m, 4H), 2.19 (td, *J* = 7.0, 2.0 Hz, 2H), 1.68 – 1.22 (m, 20H), 0.90 (s, 9H), 0.89 (s, 9H), 0.11 (s, 3H), 0.09 (s, 3H), 0.04 (s, 6H). **^{13}C NMR** (101 MHz, Chloroform-*d*) δ 84.37, 82.25, 63.36, 63.30, 63.23, 39.16, 32.96, 32.53, 29.67, 29.50, 29.35, 28.70, 26.14 (3C), 26.02 (3C), 25.87, 25.46, 25.27, 18.86, 18.52, 18.45, -4.28, -4.80, -5.11 (2C); **HRMS** (MALDI+ FT-ICR, dithranol) m/z: calcd for $[C_{28}H_{58}O_3Si_2Na]^+$ 521.3817; found 521.3846.

9,16-Bis((tert-butyldimethylsilyl)oxy)hexadec-10-ynal (88)

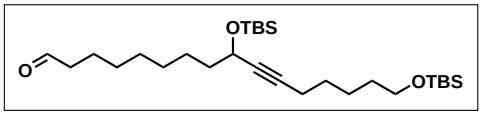

To a suspension of Dess-Martin periodane (1.06 g, 2.50 mmol) in anhydrous CH_2Cl_2 (10 mL) stirred at 0 °C under inert atmosphere, a solution of **43** (0.883 g, 1.77 mmol) in anhydrous CH_2Cl_2 (5 mL) was added dropwise and the resulting mixture was stirred for 2 h. The reaction was diluted with Et_2O (30 mL), sat. aq. $NaHCO_3$ (30 mL) containing $Na_2S_2O_3$ (9 g) was added and the reaction was stirred vigorously for 5 min. The aqueous layer was separated and extracted with Et_2O (30 mL). The combined organic layer was washed with sat. aq. $NaHCO_3$ (30 mL) and brine (30 mL), dried over Na_2SO_4 and concentrated *in vacuo* affording a yellowish oil. The crude product was used without further purification. $\mathbf{R_f}$ (EtOAc : heptane, 1 : 9) = 0.45; **^{1}H NMR** (400 MHz, Chloroform-*d*) δ 9.76 (t, *J* = 1.9 Hz, 1H), 4.30 (tt, *J* = 6.6, 2.0 Hz, 1H), 3.60 (t, *J* = 6.5 Hz, 2H), 2.41 (td, *J* = 7.3, 1.9 Hz, 2H), 2.19 (td, *J* = 7.0, 2.0 Hz, 2H), 1.70 – 1.26 (m, 18H), 0.90 (s, 9H), 0.89 (s, 9H), 0.11 (s, 3H), 0.09 (s, 3H), 0.04

(s, 6H); **^{13}C NMR** (101 MHz, Chloroform-*d*) δ 203.05, 84.42, 82.19, 66.01, 63.32, 63.29, 44.06, 39.12, 32.53, 29.44, 29.25, 29.22, 28.70, 26.13 (3C), 26.02 (3C), 25.40, 25.28, 22.22, 18.86, 18.45, 15.43, -4.27, -4.80, -5.11 (2C).

9,16-Bis((tert-butyldimethylsilyl)oxy)hexadec-10-ynoic acid (89)

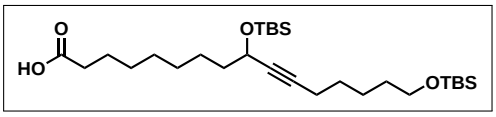

To a solution of crude aldehyde **88** and 2-methyl-2-butene (3.8 mL, 2.5 g, 36 mmol) in *t*-BuOH (87 mL), a solution of $NaHPO_4$ (1.70 g, 14.2 mmol) and $NaClO_2$ (220 mg, 2.43 mmol) in H_2O (15 mL) was added. The reaction was sheltered from light and stirred at 20 °C overnight. The resulting mixture was poured into an aq. NaH_2PO_4 (0.66 M, 90 mL) and extracted with CH_2Cl_2 (3 × 70 mL). The combined organic layer was washed with brine (70 mL), dried over Na_2SO_4 and concentrated *in vacuo* affording a yellow crude. The crude product was used without further purification. **^{1}H NMR** (400 MHz, Chloroform-*d*) δ 4.30 (tt, *J* = 6.6, 2.0 Hz, 1H), 3.68 – 3.55 (m, 2H), 2.34 (t, *J* = 7.5 Hz, 2H), 2.19 (td, *J* = 6.9, 2.0 Hz, 2H), 1.75 – 1.19 (m, 18H), 0.90 (s, 9H), 0.89 (s, 9H), 0.11 (s, 3H), 0.09 (s, 3H), 0.05 (s, 6H); **^{13}C NMR** (101 MHz, Chloroform-*d*) δ 178.61, 84.41, 82.20, 63.34, 63.33, 39.12, 33.94, 32.50, 29.32, 29.22, 29.13, 28.69, 26.13 (3C), 26.02 (3C), 25.39, 25.25, 24.83, 18.85, 18.53, 18.45, -4.28, -4.80, -5.11 (2C).

2-Phenyl-1,3-*d*ioxan-5-yl 9,16-bis((tert-butyldimethylsilyl)oxy)hexadec-10-ynoate (36)

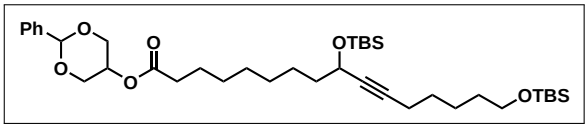

To a solution of crude carboxylic acid **89** in CH_2Cl_2 (25 mL), 1,3-*O*-benzylideneglycerol (416 mg, 2.31 mmol), DMAP (351 mg, 2.87 mmol) and EDC · HCl (494 mg, 2.57 mmol) were added. The resulting mixture was stirred overnight then concentrated over silica. The crude mixture was purified by solid deposit flash chromatography (EtOAc : heptane, 1 : 9) affording compound **36** as a transparent oil (912 mg, 76% over three steps). $\mathbf{R_f}$ (EtOAc : heptane, 1 : 4) = 0.47 **^{1}H NMR** (400 MHz, Chloroform-*d*) δ 7.54 – 7.48 (m, 2H), 7.41 – 7.32 (m, 3H), 5.56 (s, 1H), 4.72 (m, 1H), 4.34 – 4.24 (m, 3H), 4.17 (dd, *J* = 12.9, 1.7 Hz, 2H), 3.60 (t, *J* = 6.5 Hz, 2H), 2.43 (t, *J* = 7.6 Hz, 2H), 2.19 (td, *J* = 7.0, 2.0 Hz, 2H), 1.79 – 1.13 (m, 18H), 0.90 (s, 9H), 0.89 (s, 9H), 0.11 (s, 3H), 0.09 (s, 3H), 0.04 (s, 6H); **^{13}C NMR** (101 MHz, Chloroform-*d*) δ 173.98, 137.97, 129.21, 128.44 (2C), 126.17 (2C), 101.38, 84.37, 82.22, 69.29 (2C), 65.84, 63.33, 63.29, 39.14, 34.54, 32.52, 29.40, 29.27, 29.24, 28.69, 26.13

(3C), 26.02 (3C), 25.47, 25.28, 25.07, 18.86, 18.51, 18.44, -4.28, -4.80, -5.12 (2C); **HRMS** (ESI-TOF) m/z: calcd for $[C_{38}H_{66}O_6Si_2Na]^+$ 697.4290; found 697.4299.

2-Phenyl-1,3-*d*ioxan-5-yl 9,16-*d*ihydroxyhexadec-10-ynoate (46)

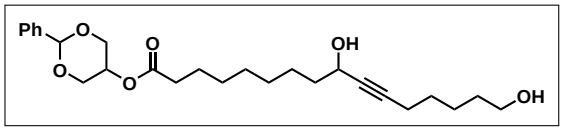

To a solution of **36** (1.05 g, 1.56 mmol) in acetonitrile (135 mL) stirred at 0 °C, aq. HF (20%, 5 mL) was slowly added. The resulting mixture was stirred at 0 °C for 7 h then TMSOMe (28 mL) was added. The resulting mixture was stirred at 0 °C for 30 min then poured into sat. aq. NH_4Cl (200 mL) and extracted with CH_2Cl_2 (3 × 200 mL). The combined organic layer was dried over Na_2SO_4 and concentrated *in vacuo*. The crude mixture was purified by flash chromatography (SiO_2, EtOAc : heptane, 1 : 1) affording compound **46** as a white solid (558 mg, 80%). $\mathbf{R_f}$ (EtOAc : heptane, 6 : 4) = 0.29; **^{1}H NMR** (400 MHz, Chloroform-*d*) δ 7.54 – 7.48 (m, 2H), 7.40 – 7.32 (m, 3H), 5.56 (s, 1H), 4.71 (mz, 1H), 4.37 – 4.24 (m, 3H), 4.17 (dd, *J* = 13.0, 1.7 Hz, 2H), 3.63 (t, *J* = 6.4 Hz, 2H), 2.43 (t, *J* = 7.5 Hz, 2H), 2.22 (td, *J* = 6.8, 2.0 Hz, 2H), 1.80 – 1.25 (m, 18H); **^{13}C NMR** (101 MHz, Chloroform-*d*) δ 174.00, 137.92, 129.22, 128.42 (2C), 126.15 (2C), 101.36, 85.25, 81.73, 69.25 (2C), 65.87, 62.84, 62.78, 38.23, 34.48, 32.27, 29.27, 29.16, 29.07, 28.44, 25.22, 25.05, 25.00, 18.76; **HRMS** (MALDI+ FT-ICR, dithranol) m/z: calcd for $[C_{26}H_{38}O_6Na]^+$ 469.2560; found 469.2559.

2-Phenyl-1,3-*d*ioxan-5-yl
9-((tert-butyldimethylsilyl)oxy)-16-hydroxyhexadec-10-ynoate (48)

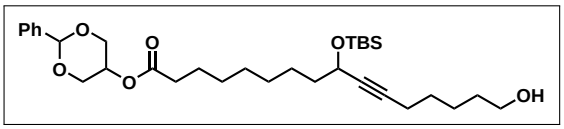

^{1}H NMR (400 MHz, Chloroform-*d*) δ 7.55 – 7.47 (m, 2H), 7.43 – 7.30 (m, 3H), 5.56 (s, 1H), 4.72 (p, *J* = 1.7 Hz, 1H), 4.35 – 4.24 (m, 3H), 4.17 (dd, *J* = 12.9, 1.7 Hz, 2H), 3.63 (t, *J* = 6.5 Hz, 2H), 2.44 (t, *J* = 7.6 Hz, 2H), 2.20 (td, *J* = 6.8, 2.0 Hz, 2H), 1.73 – 1.22 (m, 18H), 0.90 (s, 9H), 0.11 (s, 3H), 0.09 (s, 3H); **^{13}C NMR** (101 MHz, Chloroform-*d*) δ 173.88, 137.82, 129.08 (2C), 128.30 (2C), 126.03, 101.25, 84.07, 82.22, 69.15 (2C), 65.71, 63.21, 62.84, 38.97, 34.39, 32.27, 29.23, 29.09, 29.05, 28.43, 25.87 (3C), 25.28, 24.95, 24.91, 18.67, 18.31, -4.45, -4.94; **HRMS** (ESI-TOF) m/z: calcd for $[C_{32}H_{52}O_6SiNa]^+$ 583.3425; found 583.3434.

2-Phenyl-1,3-*d*ioxan-5-yl
9-((tert-butyldimethylsilyl)oxy)-16-hydroxyhexadecanoate (49)

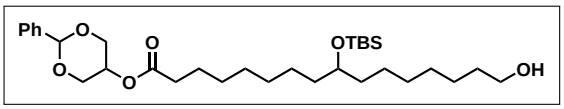

To a solution of **48** (386 mg, 0.688 mmol) in anhydrous THF stirred under inert atmosphere, was added lindlar catalyst (5%, 148 mg, 0.0695 mmol). H_2 gas was bubbled through the solution for 5 min then the reaction was stirred overnight under H_2 atmosphere. The solution was filtered through a pad of celite and concentrated *in vacuo* affording **49** as a transparent oil (352 mg, 91%). $\mathbf{R_f}$ (EtOAc : heptane, 3 : 7) = 0.14; **^{1}H NMR** (400 MHz, Chloroform-*d*) δ 7.55 – 7.47 (m, 2H), 7.42 – 7.32 (m, 3H), 5.56 (s, 1H), 4.72 (p, *J* = 1.6 Hz, 1H), 4.29 (dd, *J* = 13.0, 1.6 Hz, 2H), 4.17 (dd, *J* = 12.8, 1.6 Hz, 2H), 3.63 (m, 3H), 2.44 (t, *J* = 7.6 Hz, 2H), 1.67 (p, *J* = 7.5 Hz, 2H), 1.56 (p, *J* = 6.8 Hz, 2H), 1.51 – 1.19 (m, 20H), 0.88 (s, 9H), 0.03 (s, 6H); **^{13}C NMR** (101 MHz, Chloroform-*d*) δ 173.87, 137.82, 129.08 (2C), 128.30 (2C), 126.03, 101.25, 72.32, 69.15 (2C), 65.70, 63.06, 37.10, 37.08, 34.41, 32.79, 29.81, 29.68, 29.43, 29.31, 29.11, 25.95 (3C), 25.70, 25.29, 25.23, 24.93, 18.17, -4.39 (2C); **HRMS** (ESI-TOF) m/z: calcd for $[C_{32}H_{56}O_6SiNa]^+$ 587.3738; found 587.3746.

2-Phenyl-1,3-*d*ioxan-5-yl 9-((tert-butyldimethylsilyl)oxy)-16-oxohexadecanoate (50)

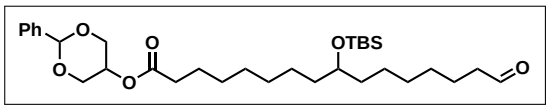

To a solution of **49** (194 mg, 0.343 mmol) in anhydrous CH_2Cl_2 (3.5 mL) stirred under inert atmosphere, Dess-Martin periodane (186 mg, 0.451 mmol) was added and the resulting mixture was stirred for 4 h. The reaction was diluted with Et_2O (15 mL), sat. aq. $NaHCO_3$ (15 mL) containing $Na_2S_2O_3$ (3.75 g) was added and the reaction was stirred vigorously for an extra 15 min. The aqueous layer was separated and extracted with Et_2O (15 mL). The combined organic layer was washed with sat. aq. $NaHCO_3$ (20 mL) and brine (20 mL), dried over Na_2SO_4 and concentrated *in vacuo* affording a transparent oil. The crude product was used without further purification. $\mathbf{R_f}$ (EtOAc : heptane, 3 : 7) = 0.36; **^{1}H NMR** (400 MHz, Chloroform-*d*) δ 9.76 (t, *J* = 1.9 Hz, 1H), 7.55 – 7.47 (m, 3H), 7.43 – 7.30 (m, 3H), 5.56 (s, 1H), 4.72 (p, *J* = 1.6 Hz, 1H), 4.29 (dd, *J* = 13.0, 1.6 Hz, 2H), 4.17 (dd, *J* = 13.0, 1.6 Hz, 2H), 3.60 (p, *J* = 5.4 Hz, 1H), 2.50 – 2.37 (m, 4H), 1.73 – 1.18 (m, 22H), 0.88 (s, 9H), 0.03 (s, 6H).

2-Phenyl-1,3-*d*ioxan-5-yl
9-((tert-butyldimethylsilyl)oxy)-16-hydroxyhexadecanoate-16-*d* (51)

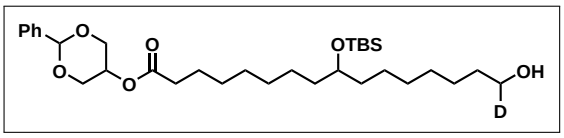

To a solution of **50** in EtOH (5 mL), $NaBD_4$ was added. The reatction was stirred for 20 min then the poured into sat. aq. NH_4Cl (20 mL) and extracted with CH_2Cl_2 (3 × 20 mL). The combined organic layer was dried over Na_2SO_4 and concentrated *in vacuo* affording a yellowish oil. The crude mixture was purified by flash chromatography (SiO_2, EtOAc : heptane, 3 : 7) affording **51** as a transparent oil (158 mg, 81%). $\mathbf{R_f}$ (EtOAc : heptane, 7 : 3) = 0.59; **^{1}H NMR** (400 MHz, Chloroform-*d*) δ 7.55 – 7.47 (m, 2H), 7.43 – 7.30 (m, 3H), 5.56 (s, 1H), 4.72 (p, *J* = 1.6 Hz, 1H), 4.29 (dd, *J* = 13.0, 1.6 Hz, 2H), 4.17 (dd, *J* = 13.0, 1.6 Hz, 2H), 3.67 – 3.54 (m, 2H), 2.44 (t, *J* = 7.6 Hz, 2H), 1.67 (p, *J* = 7.6 Hz, 2H), 1.56 (q, *J* = 6.9 Hz, 2H), 1.46 – 1.19 (m, 20H), 0.88 (s, 9H), 0.03 (s, 6H); **^{13}C NMR** (101 MHz, Chloroform-*d*) δ 174.02, 137.98, 129.23, 128.45 (2C), 126.18 (2C), 101.40, 72.46, 69.30 (2C), 65.85, 62.84 (t, *J* = 21.4 Hz), 37.25, 37.23, 34.56, 32.84, 29.96, 29.83, 29.58, 29.46, 29.26, 26.10 (3C), 25.83, 25.44, 25.38, 25.08, 18.32, -4.24 (2C); **HRMS** (ESI-TOF) m/z: calcd for $[C_{32}H_{55}DO_6SiNa]^+$ 588.3801; found 588.3808.

2-Phenyl-1,3-*d*ioxan-5-yl 9,16-*d*ihydroxyhexadecanoate-16-*d* (52)

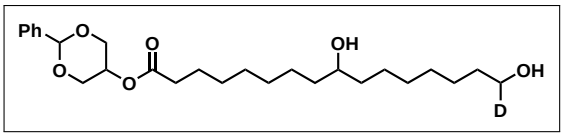

To a solution of **51** (158 mg, 0.279 mmol) in acetonitrile (25 mL) stirred at 0 °C, aq. HF (20%, 1.25 mL) was slowly added. The resulting mixture was stirred at 0 °C for 7 h then TMSOMe (5 mL) was added. The resulting mixture was stirred at 0 °C for 30 min then poured into sat. aq. NH_4Cl (40 mL) and extracted with CH_2Cl_2 (3 × 40 mL). The combined organic layer was dried over Na_2SO_4 and concentrated *in vacuo*. The crude mixture was purified by flash chromatography (SiO_2, EtOAc : heptane, 1 : 1) affording compound **53** as a white solid (95 mg, 76%). $\mathbf{R_f}$ (EtOAc : heptane, 7 : 3) = 0.28; **^{1}H NMR** (400 MHz, Chloroform-*d*) δ 7.57 – 7.46 (m, 2H), 7.42 – 7.31 (m, 3H), 5.56 (s, 1H), 4.72 m, 1H), 4.28 (d, J = 12.9 Hz, 2H), 4.17 (d, J = 12.9, 2H), 3.59 (m, 2H), 2.44 (t, J = 7.4 Hz, 2H), 1.67 (p, J = 7.4 Hz, 2H), 1.55 (q, J = 6.8 Hz, 2H), 1.49 – 1.20 (m, 20H); **^{13}C NMR** (101 MHz, Chloroform-*d*) δ 173.99, 137.95, 129.22, 128.43, 126.17, 101.39, 72.04, 69.27, 65.86, 62.79 (t, *J* = 21.7 Hz), 37.57 (2C), 34.52, 32.81, 29.77, 29.57, 29.52, 29.33, 29.13, 25.79, 25.70, 25.67, 25.03; **HRMS** (ESI-TOF) m/z: calcd for $[C_{26}H_{41}DO_6Na]^+$ 474.2936; found 474.2945.

2-Phenyl-1,3-*d*ioxan-5-yl 9,16-*d*ihydroxyhexadecanoate (53)

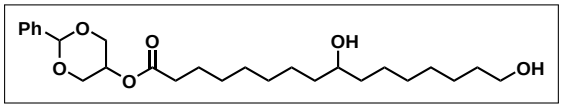

To a solution of **36** (154 mg, 0.273 mmol) in acetonitrile (25 mL) stirred at 0 °C, aq. HF (20%, 1.25 mL) was slowly added. The resulting mixture was stirred at 0 °C for 7 h then TMSOMe (5 mL) was added. The resulting mixture was stirred at 0 °C for 30 min then poured into sat. aq. NH_4Cl (40 mL) and extracted with CH_2Cl_2 (3 × 40 mL). The combined organic layer was dried over Na_2SO_4 and concentrated *in vacuo*. The crude mixture was purified by flash chromatography (SiO_2, EtOAc : heptane, 1 : 1) affording compound **53** as a white solid (118 mg, 96%). $\mathbf{R_f}$ (EtOAc : heptane, 7 : 3) = 0.28; **^{1}H NMR** (400 MHz, Chloroform-*d*) δ 7.54 – 7.46 (m, 2H), 7.42 – 7.31 (m, 3H), 5.56 (s, 1H), 4.72 (p, *J* = 1.7 Hz, 1H), 4.28 (dd, *J* = 13.0, 1.7 Hz, 2H), 4.17 (dd, *J* = 13.0, 1.7 Hz, 2H), 3.63 (t, *J* = 6.6 Hz, 2H), 3.60 – 3.51 (m, 1H), 2.43 (t, *J* = 7.5 Hz, 2H), 1.67 (p, *J* = 7.5 Hz, 2H), 1.55 (p, *J* = 6.9 Hz, 2H), 1.50 – 1.21 (m, 20H); **^{13}C NMR** (101 MHz, Chloroform-*d*) δ 173.99, 137.95, 129.22, 128.43 (2C), 126.17 (2C), 101.38, 72.03, 69.27 (2C), 65.85, 63.14, 37.55 (2C), 34.51, 32.89, 29.76, 29.57, 29.51, 29.33, 29.12, 25.81, 25.69, 25.66, 25.02; **HRMS** (ESI-TOF) m/z: calcd for $[C_{26}H_{42}O_6H]^+$ 451.3054; found 451.3061.

1,3-*d*ihydroxypropan-2-yl 9,16-*d*ihydroxyhexadecanoate (14)

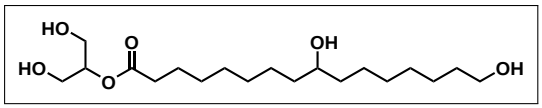

To a solution of **53** (109 mg, 0.241 mmol) in anhydrous THF (11 mL) stirred under inert atmosphere, $Pd(OH)_2/C$ (20%, 35 mg, 0.050 mmol) was added. H_2 gas was bubbled through the solution for 5 min then the reaction was stirred at 20 °C overnight under H_2 atmosphere. The solution was filtered through a pad of celite and concentrated *in vacuo*. The crude solid was recrystallized from EtOAC and heptane, affording **14** as a white solid (61 mg, 69%). $\mathbf{R_f}$ (EtOAc : heptane, 4 : 1) = 0.10; **^{1}H NMR** (400 MHz, Methanol-d_4) δ 4.91 (m, 1H), 3.74 – 3.60 (m, 4H), 3.55 (t, *J* = 6.7 Hz, 2H), 3.51 (m, 1H), 2.38 (t, *J* = 7.3 Hz, 2H), 1.64 (p, *J* = 7.3 Hz, 2H), 1.54 (p, *J* = 6.7 Hz, 2H), 1.49 – 1.24 (m, 20H); **^{13}C NMR** 13C NMR (101 MHz, Methanol-d_4) δ (101 MHz, Methanol-d_4) δ 175.31, 76.52, 72.41, 62.99, 61.70 (2C), 38.42, 38.40, 35.14, 33.66, 30.84, 30.67, 30.60, 30.40, 30.14, 26.92, 26.76, 26.74, 25.97; **HRMS** (ESI-TOF) m/z: calcd for $[C_{19}H_{38}O_6H]^+$ 385.2561; found 385.2562.

1,3-*d*ihydroxypropan-2-yl 9,16-*d*ihydroxyhexadecanoate-16-*d* (54)

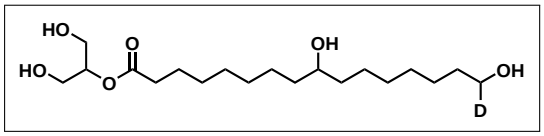

To a solution of **52** (85 mg, 0.19 mmol) in anhydrous THF (9 mL) stirred under inert atmosphere, $Pd(OH)_2/C$ (20%, 27 mg, 0.038 mmol) was added. H_2 gas was bubbled through the solution for 5 min then the reaction was stirred overnight under H_2 atmosphere. The solution was filtered through a pad of celite and concentrated *in vacuo*. The crude solid was recrystallized from EtOAC and heptane, affording **54** as a white solid (40 mg, 59%). $\mathbf{R_f}$ (EtOAc : heptane, 4 : 1) = 0.10; **^{1}H NMR** (400 MHz, Methanol-d_4) δ 4.95 – 4.86 (m, 1H), 3.74 – 3.60 (m, 4H), 3.59 – 3.46 (m, 2H), 2.38 (t, J = 7.4 Hz, 2H), 1.64 (p, J = 6.5 Hz, 3H), 1.53 (q, J = 6.7 Hz, 2H), 1.49 – 1.24 (m, 20H); **^{13}C NMR** (101 MHz, Methanol-d_4) δ 175.33, 76.54, 72.42, 62.63 (t, J = 21.5 Hz), 61.71 (2C), 38.43, 38.41, 35.15, 33.56, 30.84, 30.67, 30.61, 30.41, 30.15, 26.90, 26.77, 26.75, 25.98; **HRMS** (ESI-TOF) m/z: calcd for $[C_{19}H_{37}DO_6H]^+$ 364.2804; found 364.2802.

8-(Benzyloxy)octan-1-ol (7)

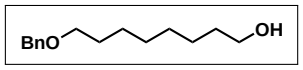

To a suspension of NaH (60 % in mineral oil, 4.18 g, 104 mmol) in anhydrous DMF (37 mL), stirred at 0 °C under inert atmosphere, a solution of 1,8-octanediol (15.01 g, 102.6 mmol) in THF : DMF (37 mL : 30 mL) was added slowly over the course of 15 min. The solution was allowed to warm at 20 °C. After 2 h, BnBr (9.35 g, 54.7 mmol) was added dropwise and the resulting yellow solution was stirred overnight. Excess NaH was quenched by the slow addition of ice until bubbling ceased and the resulting mixture was extracted with Et_2O (3 × 100 mL). The combined organic layer was washed with brine (100 mL), dried over $MgSO_4$ and concentrated over silica *in vacuo*. The crude was purified by flash chromatography (SiO_2, EtOAC : heptane, 1 : 4) affording **28** as a transparent oil (9.21 g, 71%); $\mathbf{R_f}$ (EtOAc : heptane, 1 : 4) = 0.19; **^{1}H NMR** (400 MHz, Chloroform-*d*) δ 9.76 (t, J = 1.9 Hz, 1H), 7.38 – 7.27 (m, 5H), 4.50 (s, 2H), 3.46 (t, J = 6.6 Hz, 3H), 2.41 (td, J = 7.3, 1.8 Hz, 2H), 1.68 – 1.55 (m, 4H), 1.43 – 1.27 (m, 6H); **^{13}C NMR** (101 MHz, Chloroform-*d*) δ 203.01, 138.79, 128.48, 127.76, 127.62, 73.02, 70.50, 44.02, 29.82, 29.31, 29.23, 26.14, 22.15; **HRMS** (ESI-TOF) m/z: calcd for $[C_{15}H_{24}OH]^+$ 237.1849; found 237.1853.

8-(Benzyloxy)octanal (61)

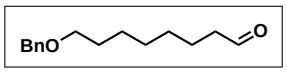

To a suspension of Dess-Martin periodane (20.25 g, 49,13 mmol) in anhydrous CH_2Cl_2 (10 mL) stirred at 0 °C under inert atmosphere, a solution of **7** (8,69 g, 36.8 mmol) in anhydrous CH_2Cl_2 (75 mL) was

added dropwise and the resulting mixture was stirred at 20 °C for 5 h. The reaction was diluted with Et_2O (150 mL), sat. aq. $NaHCO_3$ (150 mL) containing $Na_2S_2O_3$ (37 g) was added and the reaction was stirred vigorously for 5 min. The aqueous layer was separated and extracted with Et_2O (150 mL). The combined organic layer was washed with sat. aq. $NaHCO_3$ (150 mL) and brine (150 mL), dried over Na_2SO_4 and concentrated *in vacuo* affording a yellowish oil. The crude product was used without further purification. $\mathbf{R_f}$ (EtOAc : heptane, 1 : 4) = 0.43; **^{1}H NMR** (400 MHz, Chloroform-*d*) δ 9.76 (t, *J* = 1.9 Hz, 1H), 7.38 – 7.27 (m, 5H), 4.50 (s, 2H), 3.46 (t, *J* = 6.6 Hz, 3H), 2.41 (td, *J* = 7.3, 1.8 Hz, 2H), 1.68 – 1.55 (m, 4H), 1.43 – 1.27 (m, 6H); **^{13}C NMR** (101 MHz, Chloroform-*d*) δ 203.01, 138.79, 128.48, 127.76, 127.62, 73.02, 70.50, 44.02, 29.82, 29.31, 29.23, 26.14, 22.15.

tert-Butyl(hex-5-yn-1-yloxy)dimethylsilane (62)

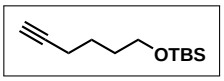

To a solution of 5-hexyn-1-ol (5.00 g, 51.0 mmol) and imidazole (4,52 g, 57.7) in anhydrous DMF (15 mL) stirred under inert atmosphere, TBSCl (8.10 g, 66.3 mmol) was added. The reaction was stirred at 20 °C overnight then poured into sat. aq. NH_4Cl (80 mL) and extracted (3 × 100 mL). The combined organic layers were washed with brine (100 mL), dried over Na_2SO_4 and concentrated *in vacuo*. The crude mixture was purified by flash chromatography (SiO_2, EtOAc : heptane, 1 : 19) affording compound **40** as a transparent oil (10.3 g, 95%). The compound analyses were in accordance with data from the literature.[169] $\mathbf{R_f}$ (EtOAc : hept 1 : 19) = 0.77; **^{1}H NMR** (400 MHz, Chloroform-*d*) δ 3.63 (t, J = 5.8 Hz, 2H), 2.22 (dt, J = 6.7, 3.0 Hz, 2H), 1.94 (t, J = 3.0 Hz, 1H), 1.71 – 1.49 (m, 4H), 0.89 (s, 9H), 0.05 (s, 6H); **^{13}C NMR** (101 MHz, Chloroform-*d*) δ 84.68, 68.39, 62.74, 31.96, 26.11, 25.11, 18.49, 18.37, -5.15 (2C).

14-(Benzyloxy)-1-((tert-butyldimethylsilyl)oxy)tetradec-5-yn-7-ol (65)

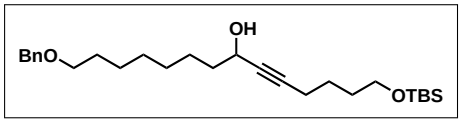

To a solution of alkyne **62** (9.81 g, 46.2 mmol) in anhydrous THF (40 mL) stirred at -78 °C under inert atmosphere, a solution of *n*-BuLi in hexane (2.3 M, 18 mL, 41 mmol). The resulting mixture was allowed to warm at 0 °C then a solution of crude aldehyde **61** in THF (35 mL) was added dropwise. The resulting mixture was allowed to warm at 20 °C and stirred overnight. The reaction mixture was poured into sat. aq. NH_4Cl (150 mL) and extracted with CH_2Cl_2 (3 × 150 mL). The combined organic layer was washed with brine (200 mL), dried over Na_2SO_4 and concentrated *in vacuo*. The crude mixture was purified by flash chromatography (SiO_2, EtOAc : heptane, 1 : 9) affording compound **38** as a yellow oil (8.96 g, 64% over two steps). $\mathbf{R_f}$

(EtOAc : heptane 1 : 4) = 0.33; **^{1}H NMR** (400 MHz, Chloroform-*d*) δ 7.41 – 7.28 (m, 5H), 4.50 (s, 2H), 4.33 (tt, *J* = 6.6, 2.0 Hz, 1H), 3.62 (t, *J* = 5.9 Hz, 2H), 3.46 (t, *J* = 6.6 Hz, 2H), 2.23 (td, *J* = 6.8, 2.0 Hz, 2H), 1.83 – 1.22 (m, 16H), 0.89 (s, 9H), 0.05 (s, 6H) **^{13}C NMR** (101 MHz, Chloroform-*d*) δ 138.84, 128.49 (2C), 127.76 (2C), 127.61, 85.46, 81.65, 73.01, 70.62, 62.88, 62.80, 38.33, 32.08, 29.90, 29.54, 29.39, 26.28, 26.11 (3C), 25.32, 25.29, 18.65, 18.50, -5.13 (2C); **HRMS** (ESI-TOF) m/z: calcd for [C27H46O3SiNa]+ 469.3108; found 469.3106.

14-(Benzyloxy)-1,7-bis((tert-butyldimethylsilyl)oxy)tetradec-5-yne (60)

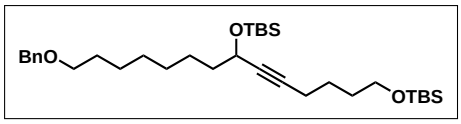

To a solution of **65** (4.09 g, 9.16 mmol) and imidazole (0.935 g, 13,7 mmol) in anhydrous DMF (20 mL) stirred under inert atmosphere, TBSCl (1,79 g, 11,9 mmol) was added. The reaction was stirred at 20 °C overnight then poured into sat. aq. NH_4Cl (250 mL) and extracted (3 × 250 mL). The combined organic layers were washed with brine (250 mL), dried over Na_2SO_4 and concentrated *in vacuo*. The crude mixture was purified by flash chromatography (SiO_2, EtOAc : heptane, 1 : 19) affording compound **40** as a transparent oil (4.38 g, 85%). **R_f** (EtOAc : heptane, 1 : 19) = 0.40; **^{1}H NMR** (400 MHz, Chloroform-*d*) δ 7.37 – 7.27 (m, 5H), 4.50 (s, 2H), 4.30 (tt, *J* = 6.5, 2.0 Hz, 1H), 3.61 (t, *J* = 6.1 Hz, 2H), 3.46 (t, *J* = 6.7 Hz, 2H), 2.21 (td, *J* = 6.9, 2.0 Hz, 2H), 1.69 – 1.25 (m, 16H), 0.90 (s, 9H), 0.89 (s, 9H), 0.11 (s, 3H), 0.09 (s, 3H), 0.04 (s, 6H); **^{13}C NMR** (101 MHz, Chloroform-*d*) δ 138.86, 128.48 (2C), 127.76 (2C), 127.60, 84.31, 82.35, 73.00, 70.66, 63.35, 62.81, 39.17, 32.12, 29.91, 29.58, 29.40, 26.30, 26.11 (3C), 26.02 (3C), 25.47, 25.33, 18.67, 18.49, 18.45, -4.27, -4.79, -5.14 (2C); **HRMS** (MALDI+ FT-ICR, dithranol) m/z: calcd for $[C_{33}H_{60}Si_2O_3Na]^+$ 583.3973; found 583.3967.

8,14-Bis((tert-butyldimethylsilyl)oxy)tetradecan-1-ol (59)

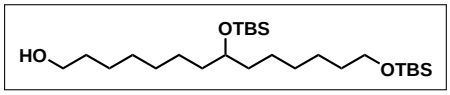

To a solution of **60** (5.02 g, 8.95 mmol) in EtOAc (90 mL) stirred under inert atmosphere, Pd/C (10%, 0.959 g, 0.900 mmol) was added. H_2 gas was bubbled through the solution for 5 min then the reaction was stirred at 20 °C overnight under H_2 atmosphere. The solution was filtered through a pad of celite and concentrated *in vacuo*. The crude mixture was purified by flash chromatography (SiO_2, EtOAc : heptane, 1 : 9) affording compound **59** as a transparent oil (3.32 g, 78%). **R_f** (EtOAc : heptane, 1 : 9) = 0.14; **^{1}H NMR** (400 MHz, Chloroform-*d*) δ 3.70 – 3.55 (m, 5H), 1.67 – 1.17 (m, 22H), 0.89 (s, 9H), 0.88 (s, 9H), 0.05 (s, 6H), 0.03 (s, 6H); **^{13}C NMR** 72.48, 63.47, 63.24, 37.24 (2C), 33.01, 32.95, 29.97, 29.82, 29.58, 26.15 (3C), 26.10 (3C), 25.98,

25.86, 25.48, 25.40, 18.54, 18.32, -4.25 (2C), -5.09 (2C); **HRMS** (ESI-TOF) m/z: calcd for $[C_{26}H_{58}O_3Si_2H]^+$ 475.3997; found 475.3990.

2-(8,14-Bis((tert-butyldimethylsilyl)oxy)tetradecyl)isoindoline-1,3-*d*ione (67)

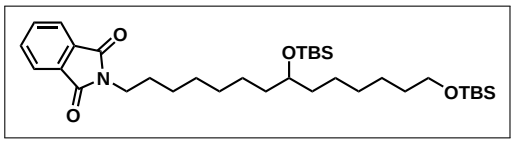

To a solution of **59** (113 mg, 0.237 mmol) and Et_3N (36 µL, 26 mg, 0.258 mmol) in anhydrous CH_2Cl_2 (2 mL) stirred under inert atmosphere, MsCl (21 µL, 31 mg, 0.27 mmol) was added. The mixture was stirred at 20 °C for 2 h and concentrated *in vacuo*. The crude mixture was used without further purification.

To a solution of crude mesylate in anhydrous DMF (4 mL) stirred under inert atmosphere, potassium phtalimide (160 mg, 0.866 mmol). The reaction was stirred at 20 °C overnight, then dissolved in CH_2Cl_2 (15 mL) and washed with H_2O (2 × 10 mL) and brine (10 mL). The organic layer was dried over Na_2SO_4 and concentrated *in vacuo*. The crude mixture was purified by flash chromatography affording compound **67** as a (53 mg, 37%). **^{1}H NMR** (400 MHz, Chloroform-*d*) δ 7.88 – 7.79 (m, 2H), 7.75 – 7.65 (m, 2H), 3.67 (t, *J* = 7.3 Hz, 2H), 3.63 – 3.55 (m, 3H), 1.67 (p, *J* = 6.1, 5.1 Hz, 2H), 1.49 (p, *J* = 7.1 Hz, 2H), 1.44 – 1.18 (m, 18H), 0.89 (s, 9H), 0.87 (s, 9H), 0.04 (s, 6H), 0.02 (s, 3H), 0.01 (s, 3H); **^{13}C NMR** (101 MHz, Chloroform-*d*) δ 168.59 (2C), 133.95 (2C), 132.33 (2C), 123.28 (2C), 72.46, 63.45, 38.22, 37.25, 37.23, 33.00, 29.88, 29.81, 29.39, 28.76, 27.01, 26.14 (3C), 26.09 (3C), 25.97, 25.47, 25.42, 18.52, 18.30, -4.26 (2C), -5.10 (2C).

8,14-Bis((tert-butyldimethylsilyl)oxy)tetradecyl 4-methylbenzenesulfonate (68)

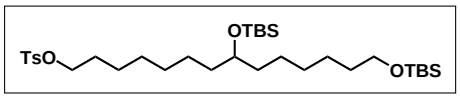

To a solution of **59** (503 mg, 1.06 mmol) in anhydrous pyridine (5 mL) stirred under inert atmosphere, TsCl (309 mg, 1,62 mmol) was slowly added. The reaction mixture was stirred at 20 °C for 1 h, if starting material was still present, more tosyl chloride (0.5 eq.) was added and the reaction was stirred for an extra 1 h. The reaction was poured into H_2O (25 mL) and extracted with Et_2O (3 × 25 mL). The combined organic layer was washed with aq. $CuSO_4$ (40 mM, 25 mL), H_2O (25 mL) and sat. aq. $NaHCO_3$ (25 mL). The organic layer was dried over Na_2SO_4 and concentrated *in vacuo*. The yellow crude mixture was purified by flash chromatography (SiO_2, EtOAc : heptane, 1 : 19) affording compound ?? as a transparent oil (385 mg, 58%). $\mathbf{R_f}$ (EtOAc : heptane, 1 : 4) = 0.57; **^{1}H NMR** 1H NMR (400 MHz, Chloroform-*d*) δ 7.79 (d, *J* = 8.1, 2H), 7.34 (d, *J* = 8.1 Hz, 2H), 4.01 (t, *J* = 6.5 Hz, 2H), 3.65 – 3.54 (m, 3H), 2.45 (s, 3H),

1.62 (m, 2H), 1.55 – 1.45 (m, 2H), 1.42 – 1.16 (m, 18H), 0.89 (s, 9H), 0.87 (s, 9H), 0.04 (s, 6H), 0.03 (s, 3H), 0.02 (s, 3H); **^{13}C NMR** (101 MHz, Chloroform-*d*) δ 144.73, 133.42, 129.93 (2C), 128.03 (2C), 72.43, 70.83, 63.46, 37.25, 37.20, 33.01, 29.83, 29.79, 29.14, 28.97, 26.14 (3C), 26.09 (3C), 25.99, 25.48 (2C), 25.33, 21.79, 18.54, 18.31, -4.24 (2C), -5.09 (2C).

8,14-Bis((tert-butyldimethylsilyl)oxy)tetradecan-1-azide (69)

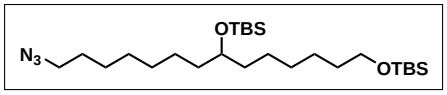

To a solution of **68** (390 mg, 0,587 mmol) in anhydrous DMF (2.5 mL) stirred under inert atmosphere, NaN_3 (113 mg, 1.74 mmol) was added. The solution was stirred at 20 °C overnight, poured into H_2O and extracted with Et_2O (3 × 20 mL). The combined organic layer was dried over Na_2SO_4 and concentrated *in vacuo*. The crude mixture was purified by flash chromatography (SiO_2, EtOAc : heptane, 1 : 19) affording **69** as a trtansparent oil (278 mg, 95%). $\mathbf{R_f}$ (EtOAc : heptane, 1 : 4) = 0.78; **^{1}H NMR** (400 MHz, Chloroform-*d*) δ 3.66 – 3.56 (m, 3H), 3.25 (t, *J* = 7.0 Hz, 2H), 1.59 (dt, *J* = 8.2, 6.8 Hz, 2H), 1.55 – 1.20 (m, 20H), 0.89 (s, 9H), 0.88 (s, 9H), 0.05 (s, 6H), 0.03 (s, 6H); **^{13}C NMR** (101 MHz, Chloroform-*d*) δ 72.46, 63.46, 51.64, 37.25, 37.21, 33.01, 29.86, 29.83, 29.32, 28.98, 26.84, 26.15 (3C), 26.10 (3C), 25.99, 25.49, 25.36, 18.54, 18.32, -4.23, -4.25, -5.09 (2C); **HRMS** (MALDI+ FT-ICR, dithranol) m/z: calcd for $[C_{26}H_{57}N_3O_2Si_2Na]^+$ 522.3882; found 522.3883.

8,14-Bis((tert-butyldimethylsilyl)oxy)tetradecan-1-amine (58)

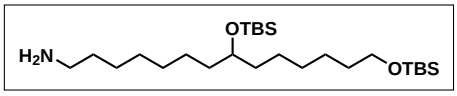

To a solution of **69** (1.09 g, 2.19 mmol) in EtOAc (45 mL) stirred at 0 °C under inert atmosphere, Pd/C (10%, 239 mg, 0,225 mmol) was added. H_2 gas was bubbled through the solution for 10 min then the reaction was stirred at 0 °C overnight under H_2 atmosphere. The solution was filtered through a pad of celite and concentrated *in vacuo*. The crude mixture was purified by flash chromatography (SiO_2, MeOH : EtOAc : Et_3N, 20 : 79 : 1) affording compound **58** as a transparent oil (708 mg, 69%). $\mathbf{R_f}$ (MeOH : EtOAc : NH_4OH, 19 : 80 : 1) = 0.12; **^{1}H NMR** (400 MHz, Chloroform-*d*) δ 3.60 (td, *J* = 6.6, 6.1, 4.2 Hz, 3H), 2.70 (t, *J* = 7.1 Hz, 2H), 2.09 (s, 2H), 1.59 – 1.23 (m, 22H), 0.89 (s, 9H), 0.88 (s, 9H), 0.04 (s, 6H), 0.03 (s, 6H); **^{13}C NMR** (101 MHz, Chloroform-*d*) δ 72.49, 63.47, 42.08, 37.26 (2C), 33.02 (2C), 29.99, 29.83, 29.62, 26.99, 26.15 (3C), 26.10 (3C), 25.99, 25.49, 25.44, 18.54, 18.32, -4.24 (2C), -5.09 (2C); **HRMS** (ESI-TOF) m/z: calcd for $[C_{26}H_{59}NO_2Si_2H]^+$ 474.4157; found 474.4168.

2-Phenyl-1,3-*d*ioxan-5-yl 1H-imidazole-1-carboxylate (75)

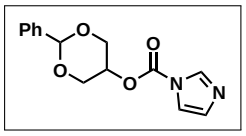

To a solution of 1,3-*O*-benzylideneglycerol (658 mg, 3.65 mmol) in anhydrous CH_2Cl_2 (1.5 mL) stirred under inert atmosphere, CDI (1,18 g, 7,26 mmol) was added. The reaction was stirred for 3 h then then concentrated *in vacuo*. The crude mixture was purified by flash chromatography (SiO_2, EtOAc : heptane, 2 : 3) affording compound **75** as a transparent oil (889 mg, 89%). $\mathbf{R_f}$ (EtOAc : heptane, 1 : 1) = 0,57; **^{1}H NMR** (400 MHz, Chloroform-*d*) δ 8.26 (t, *J* = 1.0 Hz, 1H), 7.55 – 7.47 (m, 3H), 7.45 – 7.34 (m, 3H), 7.09 (dd, *J* = 1.7, 0.8 Hz, 1H), 5.62 (s, 1H), 4.92 (p, *J* = 1.8 Hz, 1H), 4.46 (dd, *J* = 13.4, 1.6 Hz, 2H), 4.27 (dd, *J* = 13.4, 1.6 Hz, 2H); **^{13}C NMR** (101 MHz, Chloroform-*d*) δ 148.61, 137.53, 137.42, 130.93, 129.48, 128.54 (2C), 126.11 (2C), 117.35, 101.58, 70.18, 68.53 (2C).

2-Phenyl-1,3-*d*ioxan-5-yl (8,14-*d*ihydroxytetradecyl)carbamate (57)

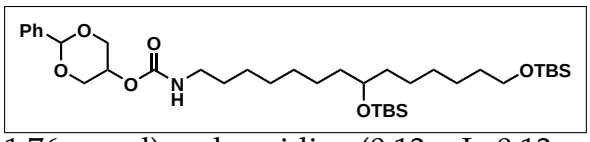

To a solution of **58** (647 mg, 1.37 mmol) in anhydrous DMF (10 mL) stirred under inert atmosphere, a solution of **75** (482 mg, 1.76 mmol) and pyridine (0.13 mL, 0.13 g, 1,68 mmol) in anhydrous DMF (10 mL) was added dropwise. The resulting mixture was stirred at 20 °C overnight then concentrated *in vacuo*. The crude mixture was purified by flash chromatography (SiO_2, EtOAc : heptane, 1 : 4) affording compound **57** as a white solid (834 mg, 90%). $\mathbf{R_f}$ (EtOAc : heptane, 1 : 4) 0,23; **^{1}H NMR** (400 MHz, Chloroform-*d*) δ 7.53 – 7.48 (m, 2H), 7.41 – 7.31 (m, 3H), 5.56 (s, 1H), 4.95 (t, *J* = 6.0 Hz, 1H), 4.66 (p, *J* = 1.7 Hz, 1H), 4.31 (dd, *J* = 13.0, 1.5 Hz, 2H), 4.17 (dd, *J* = 12.9, 1.7 Hz, 2H), 3.60 (td, *J* = 6.7, 6.1, 3.7 Hz, 3H), 3.22 – 3.09 (m, 2H), 1.56 – 1.44 (m, 4H), 1.44 – 1.20 (m, 18H), 0.89 (s, 9H), 0.88 (s, 9H), 0.05 (s, 6H), 0.03 (s, 6H); **^{13}C NMR** (101 MHz, Chloroform-*d*) δ 156.03, 137.96, 129.11, 128.39 (2C), 126.07 (2C), 101.19, 72.46, 69.73 (2C), 66.13, 63.45, 41.20, 37.24 (2C), 33.00, 29.99, 29.93, 29.82, 29.50, 29.45, 26.14 (3C), 26.09 (3C), 25.98, 25.47, 25.43, 18.53, 18.30, -4.25 (2C), -5.10 (2C). **HRMS** (ESI-TOF) m/z: calcd for $[C_{37}H_{69}NO_6Si_2H]^+$ 680.4736; found 680.4745.

2-Phenyl-1,3-*d*ioxan-5-yl (8,14-*d*ihydroxytetradecyl)carbamate (76)

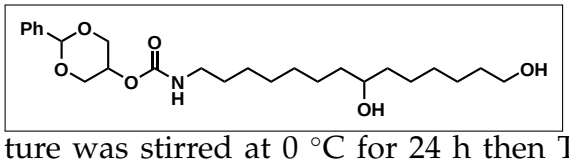

To a solution of **57** (276 mg, 0.406 mmol) in THF (42 mL) stirred at 0 °C, aq. HF (20%, 1.9 mL) was slowly added. The resulting mixture was stirred at 0 °C for 24 h then TMSOMe was added (7.2 mL). The resulting mixture was stirred at 0 °C for 20 min then poured into sat. aq. NH_4Cl (55 mL) and extracted with CH_2Cl_2 (3 × 30 mL). The combined organic layer was dried over Na_2SO_4

and concentrated *in vacuo*.

The crude mixture was redissolved in acetonitrile (40 mL) and stirred at 0 °C, aq. HF (20%, 1.7 mL) was added and the reaction was stirred at 0 °C for 4 h. TMSOMe (6.5 mL) and the resulting mixture was stirred at 0 °C for 20 min then poured into sat. aq. NH_4Cl (50 mL) and extracted with CH_2Cl_2 (3 × 50 mL). The combined organic layer was dried over Na_2SO_4 and concentrated *in vacuo*. The crude mixture was purified by flash chromatography (SiO_2, EtOAc : heptane, 3 : 7) affording compound **76** as a white solid (156 mg, 85%). $\mathbf{R_f}$ (EtOAc : heptane, 1 : 4) 0,15; **^{1}H NMR ^{13}C NMR HRMS** (ESI-TOF) m/z: calcd for $[C_{37}H_{69}NO_6Si_2Na]^+$ 474.2826; found 474.2831.

1,3-*di*hydroxypropan-2-yl (7,14-*di*hydroxytetradecyl)carbamate (56)

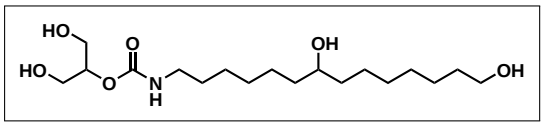

To a solution of **76** (117 mg, 0.259 mmol) in anhydrous THF (13 mL) stirred under inert atmosphere, $Pd(OH)_{2/}C$ (20%, 59 mg, 0.084 mmol) was added. H_2 gas was bubbled through the solution for 5 min then the reaction was stirred at 20 °C overnight under H_2 atmosphere. The solution was filtered through a pad of celite and concentrated *in vacuo*. The crude solid was recrystallized from EtOAC and heptane, affording **56** as a white solid (63 mg, 67%). $\mathbf{R_f}$ (EtOAc) = 0.05; **^{1}H NMR** (400 MHz, Methanol-d_4) δ 4.71 (p, *J* = 5.2 Hz, 1H), 3.69 (dt, *J* = 9.7, 5.0 Hz, 4H), 3.60 – 3.47 (m, 3H), 3.11 (t, *J* = 7.0 Hz, 2H), 1.60 – 1.27 (m, 22H); **^{13}C NMR** 76.93, 72.41, 62.99, 62.00 (2C), 41.81, 38.42, 38.39, 33.63, 30.90, 30.78, 30.68, 30.44, 27.83, 26.96, 26.81, 26.75; **HRMS** (ESI-TOF) m/z: calcd for $[C_{18}H_{37}NO_6Na]^+$ 386.2513; found 386.2517.

10,16-Bis((tert-butyldimethylsilyl)oxy)hexadecanoic acid (81)

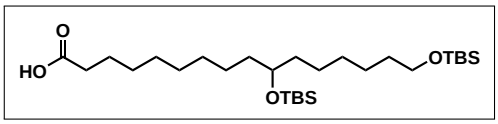

Method A: To a suspension of Dess-Martin periodane (1.77 g, 4.17 mmol) in anhydrous CH_2Cl_2 (20 mL) stirred at 0 °C under inert atmosphere, a solution of **10** (1.51 g, 3.00 mmol) in anhydrous CH_2Cl_2 (20 mL) was added dropwise and the resulting mixture was stirred for 2 h. The reaction was diluted with Et_2O (100 mL), sat. aq. $NaHCO_3$ (100 mL) containing $Na_2S_2O_3$ (25 g) was added and the reaction was stirred vigorously for 5 min. The aqueous layer was separated and extracted with Et_2O (100 mL). The combined organic layer was washed with sat. aq. $NaHCO_3$ (100 mL) and brine (100 mL), dried over $MgSO_4$ and concentrated *in vacuo* affording a

transparent oil. The crude product was used without further purification.

To a solution of crude aldehyde and 2-methyl-2-butene (6.4 mL, 4.2 g, 60 mmol) in *t*-BuOH (150 mL), a solution of $NaHPO_4$ (2.88 g, 24,0 mmol) and $NaClO_2$ (353 mg, 3.90 mmol) in H_2O (36.4 mL) was addded. The reaction was sheltered from light and stirred at 20 °C overnight. The resulting mixture was poured into an aq. NaH_2PO_4 (0.66 M, 150 mL) and extracted with CH_2Cl_2 (3 × 100 mL). The combined organic layer was washed with brine (100 mL), dried over $MgSO_4$ and concentrated *in vacuo* affording a yellow crude. The crude product was used without further purification.

Method B: To a solution of **10** (506 mg, 1,01 mmol) in CH_2Cl_2 (4 mL) and H_2O (2 mL) was added PIDA (834 mg, 2.58 mmol) and TEMPO (34 mg, 0.20 mmol). The resulting mixture was stirred vigorously for 6 h, poured into aq. $Na_2S_2O_3$ (10%, 10 mL) and extracted with EtOAc (3 × 20 mL). The combined organic phases were dried with $MgSO_4$, filtered and concentrated affording **81** as an orange-brown oil. The crude product was used without further purification.

(R)-2,3-Bis(benzyloxy)propyl 10,16-bis((tert-butyldimethylsilyl)oxy)hexadecanoate (82)

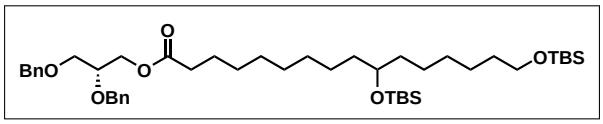

To a solution of crude acid **81** (Method A; 514 mg, 0.994 mmol) in CH_2Cl_2 (10 mL) was added (S)-(-)-2,3-*d*ibenzyloxy-1-propanol (360 mg, 1.32 mmol), DMAP (206 mg, 1.69 mmol) and EDC – HCl (285 mg, 1.49 mmol). The reaction was stirred overnight then concentrated over silica. The crude mixture was purified by solid deposit flash chromatography (SiO_2, EtOAc : heptane, 1 : 19) affording **82** as a colorless oil (530 mg, 69% over three steps). $\mathbf{R_f}$ (EtOAc : heptane, 1 : 19) = 0.13; **^{1}H NMR** (400 MHz, Chloroform-*d*) δ 7.37 – 7.26 (m, 10H), 4.67 (s, 2H), 4.54 (s, 2H), 4.31 (dd, *J* = 11.6, 4.2 Hz, 1H), 4.17 (dd, *J* = 11.6, 5.6 Hz, 1H), 3.81 (qd, *J* = 5.6, 4.2 Hz, 1H), 3.64 – 3.55 (m, 5H), 2.28 (t, *J* = 7.4 Hz, 2H), 1.58 (p, *J* = 7.4 Hz, 2H), 1.51 (p, *J* = 6.8 Hz, 2H), 1.45 – 1.36 (m, 4H), 1.36 – 1.21 (m, 16H), 0.90 (s, 9H), 0.88 (s, 9H), 0.05 (s, 6H), 0.03 (s, 6H); **^{13}C NMR** (101 MHz, Chloroform-*d*) δ 173.8, 138.4, 138.2, 128.5 (2C), 128.5 (2C), 127.9 (2C), 127.8 (2C), 127.8 (2C), 76.0, 73.6, 72.5, 72.3, 69.8, 63.8, 63.5, 37.3, 37.3, 34.4, 33.0, 30.0, 29.8, 29.7, 29.4, 29.3, 26.2 (3C), 26.1 (3C), 26.0, 25.5 (2C), 25.1, 18.5, 18.3, -4.2 (2C), -5.1 (2C); **HRMS** (MALDI+ FT-ICR, dithranol) m/z: calcd for $[C_{45}H_{78}O_6Si_2Na]^+$ 793.5229; found 793.5245.

2-(Benzyloxy)ethyl 10,16-bis((tert-butyldimethylsilyl)oxy)hexadecanoate (83)

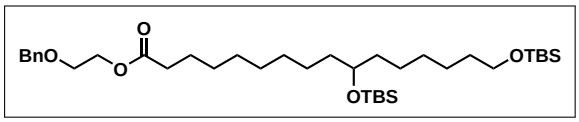

To a solution of crude acid **81** (Method A; 514 mg, 0.994 mmol) in CH_2Cl_2 (10 mL) was added 2-benzyloxyethanol (201 mg, 1.32 mmol), DMAP (209 mg, 1.71 mmol) and EDC−HCl (290 mg, 1.51 mmol). The reaction was stirred overnight then concentrated over silica. The crude mixture was purified by solid deposit flash chromatography (SiO_2, EtOAc : heptane, 1 : 19) affording **83** as a colorless oil (519 mg, 80% over three steps). $\mathbf{R_f}$ (EtOAc : heptane, 1 : 19) = 0.12; **^{1}H NMR** (400 MHz, Chloroform-*d*) δ 7.38 – 7.27 (m, 5H), 4.57 (s, 2H), 4.25 (t, *J* = 4.7 Hz, 2H), 3.67 (t, *J* = 4.7 Hz, 2H), 3.63 – 3.56 (m, 3H), 2.33 (t, *J* = 7.5 Hz, 2H), 1.61 (p, *J* = 7.5 Hz, 2H), 1.51 (p, *J* = 7.0 Hz, 2H), 1.44 – 1.35 (m, 4H), 1.35 – 1.21 (m, 16H), 0.89 (s, 9H), 0.88 (s, 9H), 0.05 (s, 6H), 0.03 (s, 6H); **^{13}C NMR** (101 MHz, Chloroform-*d*) δ 174.0, 138.0, 128.6 (2C), 127.9, 127.9 (2C), 73.3, 72.5, 68.1, 63.5, 63.5, 37.3, 37.3, 34.4, 33.0, 30.0, 29.8, 29.6, 29.4, 29.3, 26.1 (3C), 26.1 (3C), 26.0, 25.5 (2C), 25.1, 18.5, 18.3, -4.2 (2C), -5.1 (2C); **HRMS** (MALDI+ FT-ICR, dithranol) m/z: calcd for $[C_{37}H_{70}O_5Si_2Na]^+$ 673.4654; found 673.4669.

2-Propanol 10,16-bis((tert-butyldimethylsilyl)oxy)hexadecanoate (84)

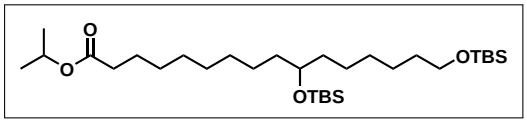

To a solution of crude acid **81** (Method A; 514 mg, 0.994 mmol) in CH_2Cl_2 (10 mL) was added 2-propanol (80 mg, 1.3 mmol), DMAP (212 mg, 1.74 mmol) and EDC−HCl (285 mg, 1.49 mmol). The reaction was stirred overnight then concentrated over silica. The crude mixture was purified by solid deposit flash chromatography (SiO_2, EtOAc : heptane, 3 : 97) affording **84** as a colorless oil (400 mg, 72% over three steps). m.p. = 46 - 47 °C; $\mathbf{R_f}$ (EtOAc : heptane, 3 : 97) = 0.14; **^{1}H NMR** (400 MHz, Chloroform-*d*) δ 5.00 (hept, *J* = 6.3 Hz, 1H), 3.65 – 3.55 (m, 3H), 2.25 (t, *J* = 7.4 Hz, 2H), 1.59 (p, *J* = 7.4 Hz, 2H), 1.51 (p, *J* = 6.7 Hz, 2H), 1.45 – 1.35 (m, 4H), 1.35 – 1.23 (m, 16H), 1.22 (d, *J* = 6.3 Hz, 6H), 0.89 (s, 9H), 0.88 (s, 9H), 0.04 (s, 6H), 0.03 (s, 6H); **^{13}C NMR** (101 MHz, Chloroform-*d*) δ 173.6, 72.5, 67.5, 63.5, 37.3, 37.3, 34.9, 33.0, 30.0, 29.8, 29.6, 29.4, 29.3, 26.1 (3C), 26.1 (3C), 26.0, 25.5, 25.5, 25.2, 22.0 (2C), 18.5, 18.3, -4.3 (2C), -5.1 (2C); **HRMS** (MALDI+ FT-ICR, dithranol) m/z: calcd for $[C_{31}H_{66}O_4Si_2Na]^+$ 581.4392; found 581.4405.

1,3-*d*imethoxypropan-2-yl 10,16-*d*ihydroxyhexadecanoate (85)

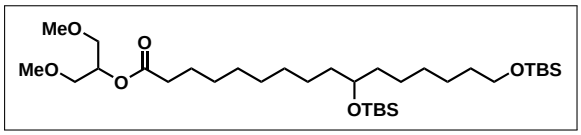

To a solution of crude acid **81** (Method B; 514 mg, 0.994 mmol) in CH_2Cl_2 (10 mL) was added 1,3-*d*imethoxy-2-propanol (159 mg, 1.32 mmol), DMAP (206 mg, 1.69 mmol) and EDC – HCl (287 mg, 1.50 mmol). The reaction was stirred overnight then concentrated over silica. The crude mixture was purified by solid deposit flash chromatography (SiO_2, EtOAc : heptane, 3 : 97) affording **85** as a colorless oil (357 mg, 58% over two steps). m.p. = 52 - 53 °C; $\mathbf{R_f}$ (EtOAc : heptane, 1 : 19) = 0.10; **^{1}H NMR** (400 MHz, Chloroform-*d*) δ 5.14 (p, *J* = 5.1 Hz, 1H), 3.62 – 3.57 (m, 3H), 3.53 (d, *J* = 5.1 Hz, 4H), 3.36 (s, 6H), 2.34 (t, *J* = 7.4 Hz, 2H), 1.63 (p, *J* = 7.4 Hz, 2H), 1.50 (p, *J* = 6.6 Hz, 2H), 1.44 – 1.34 (m, 4H), 1.35 – 1.17 (m, 16H), 0.89 (s, 9H), 0.88 (s, 9H), 0.04 (s, 6H), 0.03 (s, 6H); **^{13}C NMR** (101 MHz, Chloroform-*d*) δ 173.5, 72.5, 71.4 (2C), 71.1, 63.5, 59.4 (2C), 37.3, 37.3, 34.6, 33.0, 30.0, 29.8, 29.7, 29.4, 29.2, 26.1 (3C), 26.1 (3C), 26.0, 25.5 (2C), 25.1, 18.5, 18.3, -4.3 (2C), -5.1 (2C); **HRMS** (MALDI+ FT-ICR, dithranol) m/z: calcd for $[C_{33}H_{70}O_6Si_2Na]^+$ 641.4603; found 641.4617.

(R)-2,3-*d*ibenzyloxypropan-1-yl 10,16-*d*ihydroxyhexadecanoate (86)

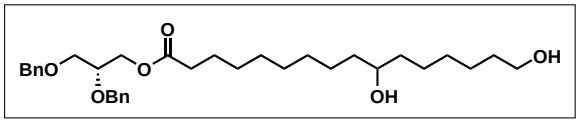

To a solution of **82** (341 mg, 0.442 mmol) in MeCN (48 mL) at 0 °C, aq. HF (20%, 2 mL,) was slowly added. The resulting mixture was stirred at 0 °C for 7 h then TMSOMe (7.7 mL) was added. The resulting mixture was stirred at 0 °C for 20 min then poured into sat. aq. NH_4Cl (50 mL) and extracted with CH_2Cl_2 (3 × 50 mL). The combined organic layer was dried over Na_2SO_4 and concentrated *in vacuo*. The crude mixture was purified by flash chromatography (SiO_2, EtOAc : heptane, 1 : 1) affording compound **86** as a white solid (224 mg, 75%). m.p. = 34 - 35 °C; $\mathbf{R_f}$ (EtOAc : heptane, 1 : 1) = 0.15; **^{1}H NMR** (400 MHz, Chloroform-*d*) δ 7.39 – 7.25 (m, 10H), 4.67 (s, 2H), 4.54 (s, 2H), 4.30 (dd, *J* = 11.7, 4.2 Hz, 1H), 4.17 (dd, *J* = 11.7, 5.6 Hz, 1H), 3.81 (qd, *J* = 5.6, 4.2 Hz, 1H), 3.64 (t, *J* = 6.6 Hz, 2H), 3.61 – 3.54 (m, 3H), 2.28 (t, *J* = 7.5 Hz, 2H), 1.64 – 1.51 (m, 4H), 1.49 – 1.24 (m, 20H); **^{13}C NMR** (101 MHz, Chloroform-*d*) δ 173.8, 138.4, 138.2, 128.5 (2C), 128.5 (2C), 127.9 (2C), 127.8 (2C), 127.8 (2C), 76.0, 73.6, 72.3, 72.1, 69.8, 63.8, 63.1, 37.6, 37.5, 34.4, 32.8, 29.8, 29.6, 29.5, 29.3, 29.3, 25.9, 25.7 (2C), 25.0; **HRMS** (MALDI+ FT-ICR, dithranol) m/z: calcd for $[C_{33}H_{50}O_6Na]^+$ 565.3500; found 565.3513.

(R)-2,3-*d*ihydroxypropan-1-yl 10,16-*d*ihydroxyhexadecanoate (77)

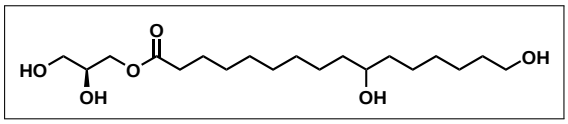

To a solution of **86** (166 mg, 0.306 mmol) in anhydrous THF (15 mL) stirred under inert atmosphere, $Pd(OH)_2/C$ (20%, 24 mg, 0.034 mmol) was added. H_2 gas was bubbled through the solution for 8 min then the reaction was stirred at 20 °C overnight under H_2 atmosphere. The solution was filtered through a pad of celite and concentrated *in vacuo*. The crude solid was recrystallized from EtOAC and heptane, affording **77** as a white solid (89 mg, 80%). m.p. = 65 - 66 °C; $\mathbf{R_f}$ (EtOAc : heptane, 7 : 3) = 0.01; **^{1}H NMR** (400 MHz, Methanol-d_4) δ 4.05 (dd, *J* = 11.1, 5.1 Hz, 1H), 4.02 – 3.96 (m, 2H), 3.75 – 3.64 (m, 2H), 3.51 – 3.36 (m, 5H), 3.29 (td, *J* = 5.2, 1.3 Hz, 1H), 3.26 (dd, *J* = 5.3, 1.3 Hz, 1H), 2.28 (t, *J* = 7.2 Hz, 2H), 1.59 (p, *J* = 7.2 Hz, 2H), 1.52 – 1.41 (m, 4H), 1.43 – 1.23 (m, 18H); **^{13}C NMR** (101 MHz, Methanol-d_4) δ 173.5, 71.4, 71.0, 66.4, 64.4, 62.6, 38.9 (2C), 34.7, 34.2, 30.8 (2C), 30.6, 30.3, 30.1, 27.1, 26.9, 26.8, 25.9; **HRMS** (MALDI+ FT-ICR, dithranol) m/z: calcd for $[C_{19}H_{38}O_6Na]^+$ 385.2561; found 385.2571.

2-(Benzyloxy)ethyl 10,16-*d*ihydroxyhexadecanoate (87)

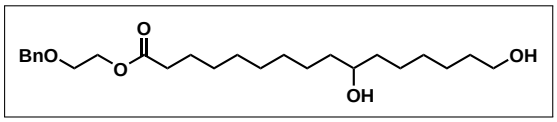

To a solution of ?? (353 mg, 0.542 mmol) in MeCN (58 mL) at 0 °C, aq. HF (20%, 2 mL) was slowly added. The resulting mixture was stirred at 0 °C for 7 h then TMSOMe (9.5 mL) was added. The resulting mixture was stirred at 0 °C for 20 min then poured into sat. aq. NH_4Cl (60 mL) and extracted with CH_2Cl_2 (3 × 60 mL). The combined organic layer was dried over Na_2SO_4 and concentrated *in vacuo*. The crude mixture was purified by flash chromatography (SiO_2, EtOAc : heptane, 1 : 1) affording compound **87** as a white solid (202 mg, 88%). $\mathbf{R_f}$ (EtOAc : heptane, 1 : 1) = 0.11; m.p. = 64 - 65 °C; **^{1}H NMR** (400 MHz, Chloroform-*d*) δ 7.38 – 7.27 (m, 5H), 4.57 (s, 2H), 4.25 (t, *J* = 4.7 Hz, 2H), 3.67 (t, *J* = 4.7 Hz, 2H), 3.63 (t, *J* = 6.6 Hz, 2H), 3.61 – 3.54 (m, 1H), 2.33 (t, *J* = 7.5 Hz, 2H), 1.68 – 1.52 (m, 4H), 1.47 – 1.24 (m, 20H); **^{13}C NMR** (101 MHz, Chloroform-*d*) δ 174.0, 138.0, 128.6 (2C), 127.9, 127.9 (2C), 73.3, 72.1, 68.1, 63.5, 63.1, 37.6, 37.5, 34.4, 32.8, 29.7, 29.6, 29.5, 29.3, 29.2, 25.9, 25.7 (2C), 25.0; **HRMS** (MALDI+ FT-ICR, dithranol) m/z: calcd for $[C_{25}H_{42}O_5Na]^+$ 445.2924; found 445.2935.

2-Hydroxyethyl 10,16-*d*ihydroxyhexadecanoate (78)

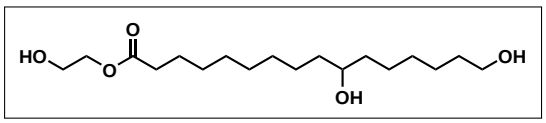

To a solution of **87** (147 mg, 0.348 mmol) in anhydrous THF (15 mL) stirred under inert atmosphere, $Pd(OH)_2/C$ (20%, 27 mg, 0.038

mmol) was added. H_2 gas was bubbled through the solution for 8 min then the reaction was stirred at 20 °C overnight under H_2 atmosphere. The solution was filtered through a pad of celite and concentrated *in vacuo*. The crude solid was recrystallized from EtOAC and heptane, affording **78** as a white solid (92 mg, 78%). m.p. = 62 - 64 °C; $\mathbf{R_f}$ (EtOAc : heptane, 7 : 3) = 0.07; **^{1}H NMR** (400 MHz, Chloroform-*d*) δ 4.25 – 4.17 (m, 2H), 3.86 – 3.79 (m, 2H), 3.64 (t, *J* = 6.6 Hz, 2H), 3.63 – 3.53 (m, 1H), 2.35 (t, *J* = 7.5 Hz, 2H), 1.72 – 1.51 (m, 4H), 1.50 – 1.24 (m, 20H); **^{13}C NMR** (101 MHz, Chloroform-*d*) δ 174.4, 72.1, 66.1, 63.1, 61.5, 37.6, 37.5, 34.3, 32.8, 29.7, 29.6, 29.5, 29.2, 29.2, 25.9, 25.7, 25.7, 25.0; **HRMS** (MALDI+ FT-ICR, dithranol) m/z: calcd for $[C_{18}H_{36}O_5Na]^+$ 355.2455; found 355.2464.

2-Propanol 10,16-*d*ihydroxyhexadecanoate (79)

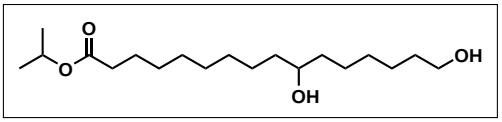

To a solution of ?? (196 mg, 0.351 mmol) in MeCN (37 mL) at 0 °C, aq. HF (20%, 1.5 mL) was slowly added. The resulting mixture was stirred at 0 °C for 7 h then TMSOMe (6.1 mL) was added. The resulting mixture was stirred at 0 °C for 20 min then poured into sat. aq. NH_4Cl (40 mL) and extracted with CH_2Cl_2 (3 × 40 mL). The combined organic layer was dried over Na_2SO_4 and concentrated *in vacuo*. The crude mixture was purified by flash chromatography (SiO_2, EtOAc : heptane, 1 : 1) affording compound **79** as a white solid (113 mg, 95%). $\mathbf{R_f}$ (EtOAc : heptane, 1 : 1) = 0.11; **^{1}H NMR** (400 MHz, Chloroform-*d*) δ 5.00 (hept, *J* = 6.3 Hz, 1H), 3.64 (t, *J* = 6.6 Hz, 2H), 3.61 – 3.53 (m, 1H), 2.25 (t, *J* = 7.5 Hz, 2H), 1.65 – 1.52 (m, 4H), 1.45 – 1.25 (m, 20H), 1.22 (d, *J* = 6.3 Hz, 6H); **^{13}C NMR** (101 MHz, Chloroform-*d*) δ 173.6, 72.1, 67.5, 63.1, 37.6, 37.5, 34.9, 32.8, 29.7, 29.6, 29.5, 29.3, 29.2, 25.9, 25.7 (2C), 25.2, 22.0 (2C); **HRMS** (MALDI+ FT-ICR, dithranol) m/z: calcd for $[C_{19}H_{38}O_4Na]^+$ 353.2662; found 353.2671.

1,3-*d*imethoxypropan-2-yl 10,16-*d*ihydroxyhexadecanoate (80)

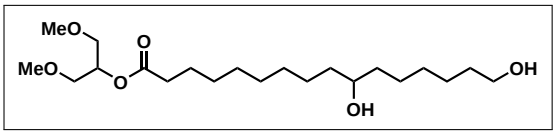

To a solution of **85** (192 mg, 0.310 mmol) in MeCN (35 mL) at 0 °C, aq. HF (20%, 1.5 mL) was slowly added. The resulting mixture was stirred at 0 °C for 5 h then TMSOMe (5.6 mL) was added. The resulting mixture was stirred at 0 °C for 20 min then poured into sat. aq. NH_4Cl (45 mL) and extracted with CH_2Cl_2 (3 × 45 mL). The combined organic layer was dried over Na_2SO_4 and concentrated *in vacuo*. The crude mixture was purified by flash chromatography (SiO_2, EtOAc : heptane, 1 : 1) affording compound **53** as a white solid (113 mg, 95%).

R_f (EtOAc : heptane, 1 : 1) = 0.11; **^{1}H NMR** (400 MHz, Chloroform-*d*) δ 5.14 (p, *J* = 5.0 Hz, 1H), 3.64 (t, *J* = 6.6 Hz, 2H), 3.60 – 3.55 (m, 1H), 3.53 (d, *J* = 5.0 Hz, 4H), 3.36 (s, 6H), 2.34 (t, *J* = 7.5 Hz, 2H), 1.68 – 1.51 (m, 4H), 1.47 – 1.26 (m, 20H); **^{13}C NMR** (101 MHz, Chloroform-*d*) δ 173.5, 72.1, 71.4 (2C), 71.0, 63.1, 59.4 (2C), 37.6, 37.5, 34.5, 32.8, 29.7, 29.6, 29.5, 29.3, 29.2, 25.9, 25.7 (2C), 25.1; **HRMS** (MALDI+ FT-ICR, dithranol) m/z: calcd for $[C_{21}H_{42}O_6Na]^+$ 413.2874; found 413.2884.

Chapter 4

Towards the Discovery of Suberin Synthases and a Better Understanding of CUS1 Mechanism - A Biological Approach

The following chapter is the result of a four month external stay performed at Cornell University under the supervision of Professor Jocelyn K. C. Rose. During this time period, I have had the chance to work with Ph.D. student Nicholas Segerson on two different ongoing projects.

4.1 Investigation of *Arabidopsis thaliana* GDSL-mutant lines

4.1.1 Objectives

Owing to the many similarities between the chemical composition of suberin and cutin, a common belief is that those two polymers may have arisen from similar origins. In 2012, the group of Jocelyn K. C. Rose discovered the first cutin synthase, CUS1, a member of the GDSL esterase/lipase superfamily. Suberin and cutin have been shown to share many biosynthetic families of enzymes. In this context, GDSL lipases have been the focus of attention as potential candidates for suberin synthases (SUS). The objective of this project is to investigate several Arabidopsis GDSL lipases and their potential ties to suberin biosynthesis.

4.1.2 Results and discussions

4.1.2.1 Previous work

This section will describe the work that have been performed by other members of the group prior to my arrival.

This study started by the selection of putative SUS enzymes using the ePlant visualizing tool.[170,171] The selection process relied on different criteria. For reasons that were

previously mentioned, we focused our attention on GDSL lipases/esterases. More specifically, due to the required expression of genes involved in suberin monomer biosynthesis, we selected GDSL encoding genes that are co-expressed with suberin monomer biosynthetic genes such as *GPAT5*. Furthermore, the selection was limited to genes known to be expressed in the root endodermis, the site of suberin deposition. This selection allowed us to pull four different GDSL-encoding genes, which will be conveniently named *GDSL1* to *GDSL4* for the rest of this study. The co-expression analysis as well as the expression pattern of those four genes can be found on Figure 4.1.

To delineate the function of the selected *GDSL* genes, RNAi-silenced Arabidopsis transgenic lines were generated for each of those genes. In order to prepare these mutants, a vector containing an artificial microRNA (amiRNA) cassette was transformed into *Agrobacterium tumefaciens* for each GDSL-encoding genes. Agrobacterium is a bacterium which is able to infect plants and inject a sequence of DNA, called transfer DNA (T-DNA), contained into a tumor inducing plasmid (Ti plasmid) into the plants genetic material. In the case of RNAi silencing, Ti plamids are designed to insert T-DNA encoding for interfering RNA which promotes the destruction of messenger RNA and in turns decreases the expression of a selected targeted gene. Additionally, promotion of the RNAi expression is done through the use of the Cauliflower mosaic virus 35S promoter (P35S promoter), a very strong constitutive promoters which induces a high level of expression of the RNAi gene. To facilitate the selection process, the T-DNA insert also presents the *bar* gene which encodes for phosphinothricin acetyltransferase and provides resistance to the herbicide glufosinate-ammonium.[172,173] Mutants can be obtained by infecting a flowering plant with the transgenic Agrobacterium. Due to the random nature of the T-DNA insertion, the seeds obtained by this plants should contain T-DNA inserted randomly into their genome and can be grown and selected for further analysis. Furthermore, the *GDSL1* RNAi mutation was also applied to a known GDSL4 Arabidopsis null mutant. The double mutants, named *GDSL1/4b* were generated to assess for the potential redundancy of those two *GDSL* genes.

To obtain statistically relevant data on a group of individuals, the obtention of homozygotes mutant is necessary as their offspring, which are used for various experiments, are guaranteed to be homozygotes mutants themselves. At the time of my arrival, the second generation (T_2) of *GDSL1*, *GDSL3*, *GDSL4* were growing in soil in growth chamber. On the other hand, the *GDSL2*-line first generation (T_1) were being planted and grown in growth chamber.

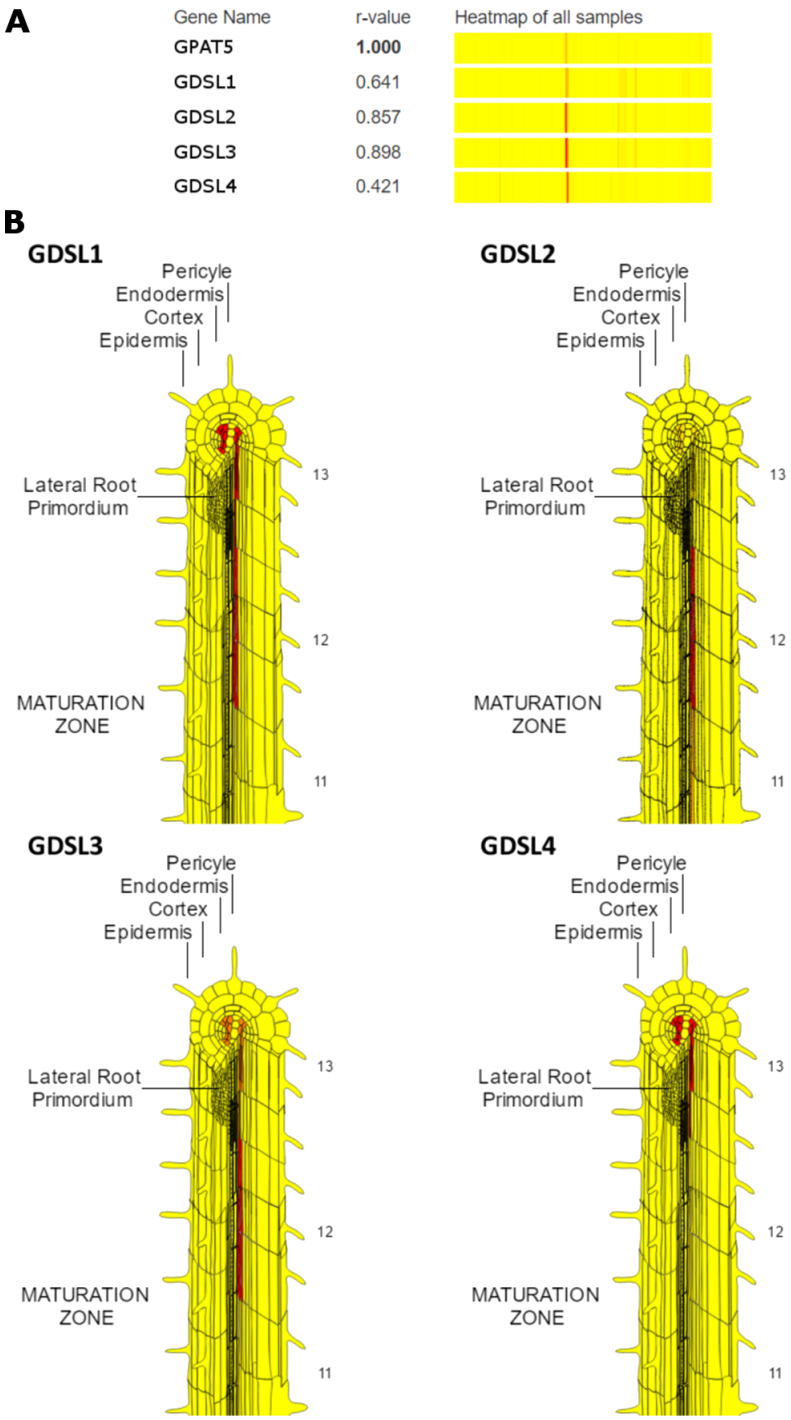

Figure 4.1: Co-expression analysis of GPAT5 with the four selected GDSL lipases. A, Expression heatmap of the genes encoding for GPAT5 and all four GDSL genes in Arabidopsis root; red bars represents expression areas; r-value represents the correlation coefficient between the corresponding gene expression and the GPAT5 related gene. B, Expression pattern of all four GDSL genes in arabidopsis; Red area represents the areas of high expression. (Data and figures obtained via the ePlant visualizing tool[170,171])

4.1.2.2 Genotyping and selection of the GDSL-mutants

To differentiate mutant plants from the wild type ones, plants were frequently sprinkled with a solution of glufosinate-ammonium (10 mg/mL). In order to confirm the mutation, full DNA extracts of each plants were amplified by polymerase chain reaction (PCR) using a set of primer specific for each corresponding GDSL-RNAi insert, and the PCR product was analyzed by DNA gel electrophoresis. Positive plants were grown in growth chamber and their seeds were collected for further treatment. *GDSL2* seeds were planted in soil to grow a second generation of plants. The seeds from each *GDSL1*, *GDSL3*, *GDSL4* and *GDSL1/4b* plants were sterilized and planted (around 30 seeds per plants) on 1/4x MS growth media containing glufosinate-ammonium (10 mg/mL) and incubated in growth chamber for 9 to 12 days. The use of glufosinate-ammonium as a selection agent allows for a fast screen for homozygotes. Plates where all seeds did not grow were discarded as this was an evidence that the parent plant was not a homozygote mutant. Conversely, plates where all the plants grew normally, as depicted in Figure 4.2, were used for further treatment. It is important to note that the reasoning behind using this method instead of a proper genotyping of each parent plants for homozygotes was driven by time constraints. Contrastingly, wild type plants were grown on growth media without the presence of glufosinate-ammonium. A list of the selected mutant lines can be found on Table 4.1

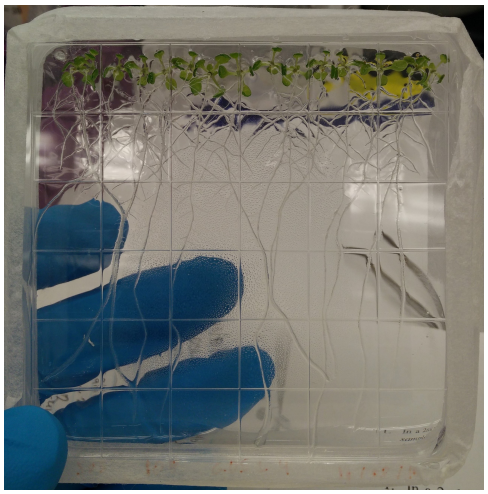

Figure 4.2: Example of a plate of Arabidopsis after 9 to 12 days of incubation in growth chamber.

Table 4.1: Given name for all the selected mutants for each mutant types

GDSL1	*GDSL3*	*GDSL4*	*GDSL1/4b*
GDSL1-2	*GDSL3-3D*	*GDSL4-10B*	*GDSL1/4b-23A*
GDSL1-3	*GDSL3-3*	*GDSL4-2*	*GDSL1/4b-1*
GDSL1-5	*GDSL3-5*		*GDSL1/4b-5*

4.1.2.3 *GDSL* expression of the homozygote-mutants

To assess the effectiveness of the mutant inserts, a comparative studies between the level expression of each *GDSL* genes for each mutants and Arabidopsis wild type is necessary. In this context, total RNA extraction using the Trizol™ reagent was performed on a group of roots for each mutants as well as for three different wild type culture. The RNA extracts was then converted into complementary DNA (cDNA) using the SuperScript™ II reverse transcriptase. The obtained cDNA was then diluted to 100 ng/µL. Quantitative PCR (qPCR) was performed using the cDNA solutions. qPCR is a standard method that allows for the quantification of specific single strand DNA in a sample. The amount of cDNA present for each *GDSL* genes in our cDNA samples is directly related to the amount of messenger RNA present during the RNA extraction. Hence, the quantity of a *GDSL*-related cDNA in a sample correlates directly to the expression level of this particular gene. To account for small variation in initial cDNA concentration, the expression of a gene is normalized by the expression of an ubiquitous reference gene such as *UBQ10*, *PP2A*, *TIP41*.[174–176] Finally, the normalized expression of a gene in a mutant is compared to the expression of the same gene in wild type plant.

In our case, the amplification was performed using primers specific for each different GDSL genes. The expression of each individual gene was normalized to the expression of *PP2A* and *TIP41* gene. The relative expression of *GDSL1* to *4* was measured for all the mutants, as depicted in Figure 4.3 to Figure 4.6, to assure that each insert only affects the expression of the targeted *GDSL* gene.

As seen on Figure 4.3, the expression of *GDSL1* for *GDSL1* single mutants was found to be reliably diminished. Similar results were observed for the *GDSL4* expression of *GDSl1/4b* double mutants. Unfortunately, the rest of the data did not allow us to get conclusive results. A high disparity within technical replicates as well as within referenced wild types render those data unusable for the most part. Additionally, *GDSL4* expression seems to be reduced for all *GDSL1/4b* mutants though this gene should not be expressed for these mutants. These results are most likely due to an

issue in the technique used to prepare the qPCR analysis. However, time constraints did not allow us to optimize the qPCR setup.

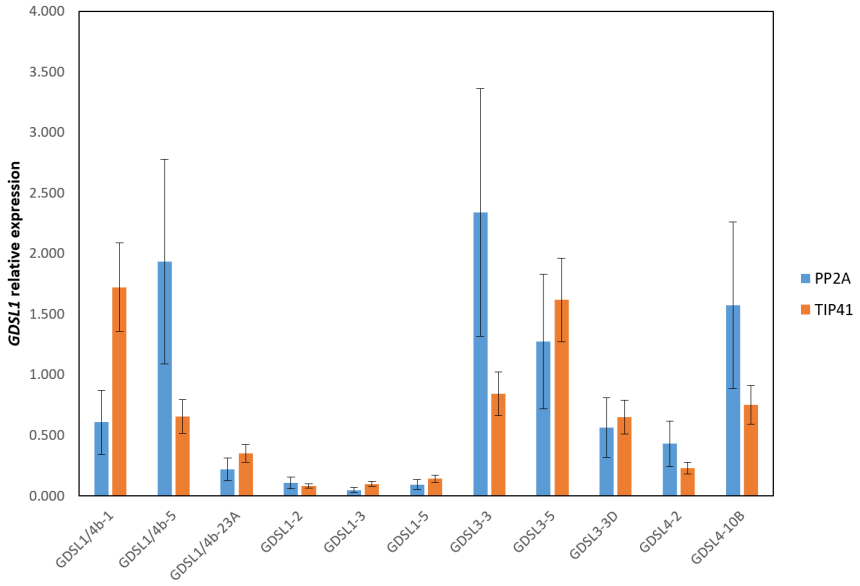

Figure 4.3: Relative expression of *GDSL1* for each mutants as compared to wild type plants (n=3) measured using *PP2A* and *TIP41* as reference genes. Average of 4 technical replicates per sample.

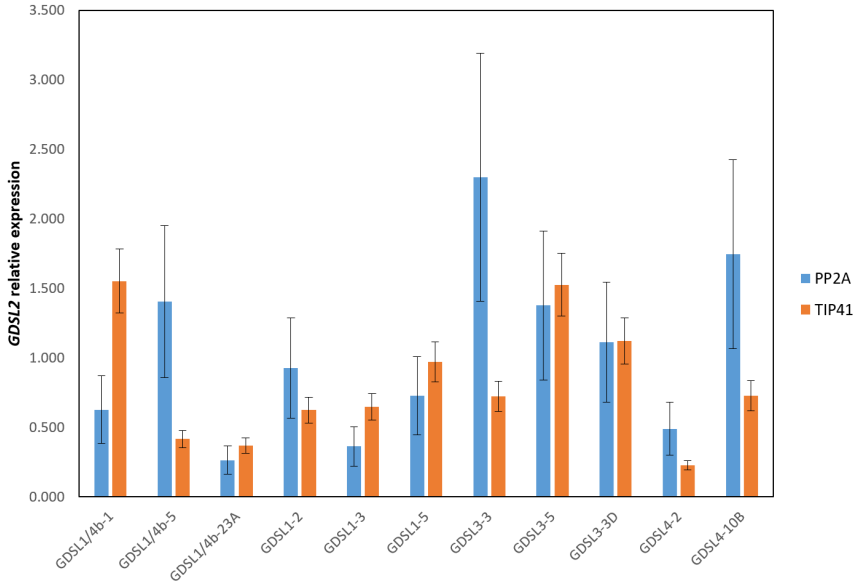

Figure 4.4: Relative expression of *GDSL2* for each mutants as compared to wild type plants (n=3) measured using *PP2A* and *TIP41* as reference genes. Average of 4 technical replicates per sample.

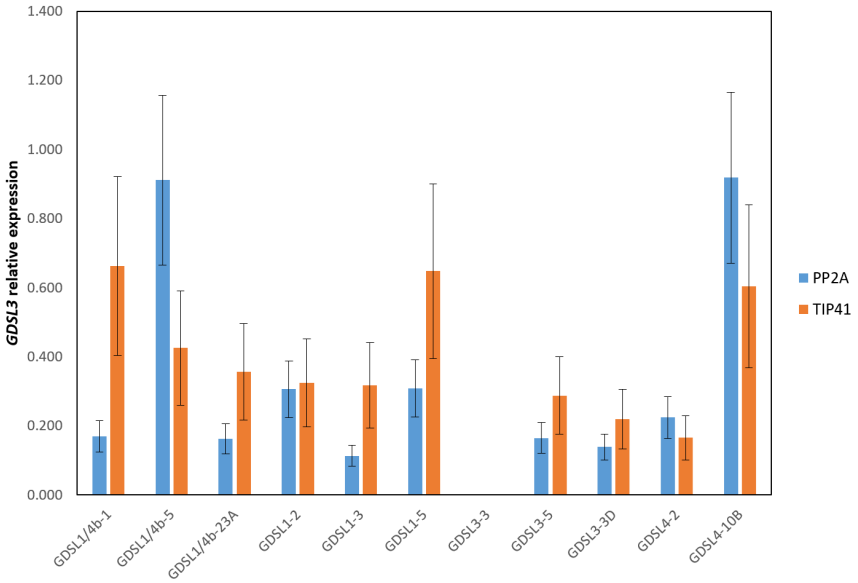

Figure 4.5: Relative expression of *GDSL3* for each mutants as compared to wild type plants (n=3) measured using *PP2A* and *TIP41* as reference genes. Average of 4 technical replicates per sample; Missing data are due to failed amplification.

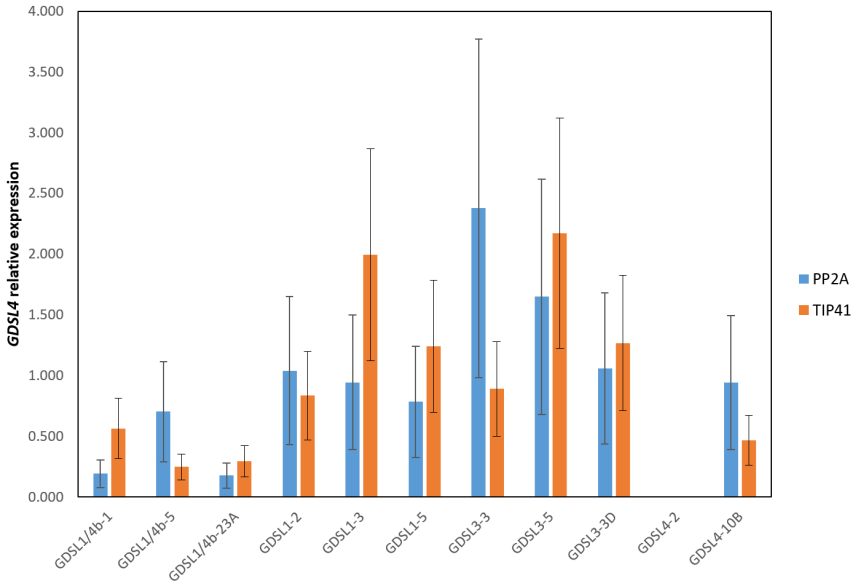

Figure 4.6: Relative expression of *GDSL4* for each mutants as compared to wild type plants (n=3) measured using *PP2A* and *TIP41* as reference genes. Average of 4 technical replicates per sample; Missing data are due to failed amplification.

Due to the inconclusive qPCR analysis along with the lack of time, semi quantitative PCR followed by DNA gel electrophoresis was used. *UBQ10* was used as a reference gene. The results for the expression of *GDSL1* is depicted in Figure 4.7. According to this analysis, the expression of *GDSL1* is significantly decreased for all *GDSL1* single mutants as well as for *GDSL1/4b-23A*. Contrastingly, the intensity for *GDSL1/4b-1* seems to be only slightly decreased and is not considered statistically relevant. Unfortunately, the results for *GDSL1/4b-5* are still not conclusive as the intensity of the reference gene varies for the mutant sample compared to the wild type sample.

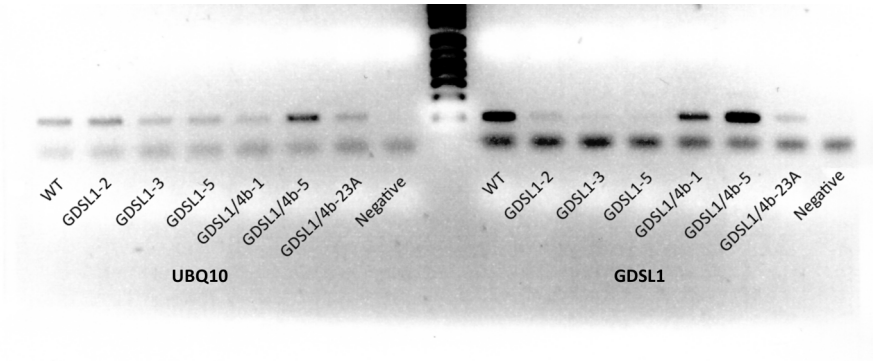

Figure 4.7: Semi-quantitative PCR analysis for *GDSL1* expression. WT, wild type.

The results obtained for *GDSL3* mutants, shown on Figure 4.8, indicates that *GDSL3-5* and *GDSL3-3D* seems to be knock-down. However, the intensity of *GDSL3* PCR products is low, even in the wild type samples, despite a higher number of PCR cycles, hinting that *GDSL3* may be poorly expressed compared to other *GDSL* genes. Alternatively, poor interaction between the pair of primer used for the amplification and the *GDSL3* cDNA fragment might be responsible for the low intensity of the PCR products.

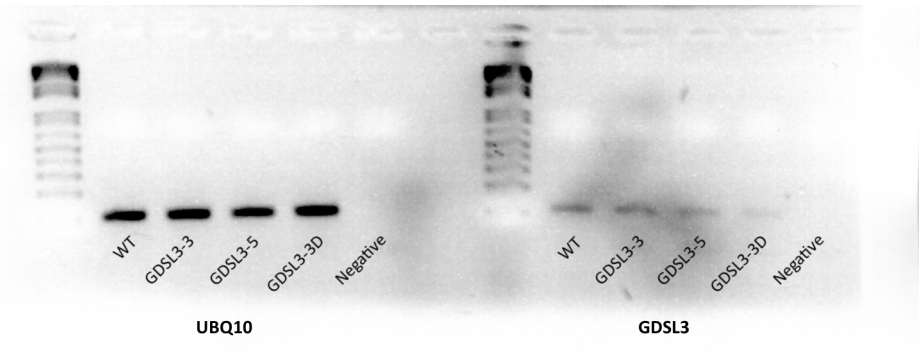

Figure 4.8: Semi-quantitative PCR analysis for *GDSL1* expression. WT, wild type.

Finally, semi-quantitative analysis of *GDSL4* expression clearly demonstrates that none of the *GDSL1/4b* double-mutants expresses *GDSL4*. This result is in accordance with the null-mutation nature of the original mutants. Similarly, *GDSL4-2* seems to express *GDSL4* to a lower extent. Conversely, the *GDSL4* expression seems to be unaltered in *GDSL1* single mutants as well as for *GDSL4-10B*.

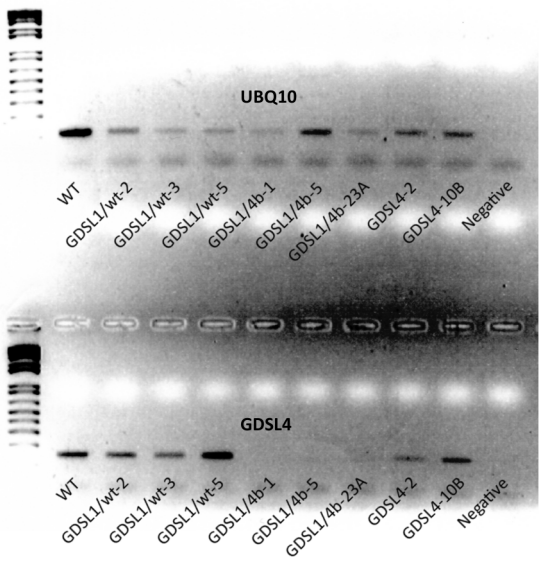

Figure 4.9: Semi-quantitative PCR analysis for *GDSL4* expression. WT, wild type.

4.1.2.4 Phenotyping of the homozygote-mutants

To assess for the effect of *GDSL*-related mutations on suberin deposition, we investigated for suberin related phenotypes. As a starting point, we focused our attention on the deposition of suberin in Arabidopsis roots. In particular, root samples were subjected to Oil Red O staining, a lipophilic stain that accumulates where suberin is deposited. Light microscopic analysis of the stained roots allowed us to see that for the *GDSL1/4b-23A* mutant, the deposition of suberin, typically observed as a thin intense red layer around at the root endodermis, seems to be altered compared to the wild type plant as depicted in Figure 4.10 at the exception of areas where lateral root are developing. However, this result still needs to be confirmed on a larger sample size. Furthermore, this result was not observed with any other mutant. Taking into account that *GDSl4b/23A* is both, a *GDSL4* knockout and a *GDSL1* knockdown mutant, this observation might indicate that redundancy exists between GDSL4 and GDSL1.

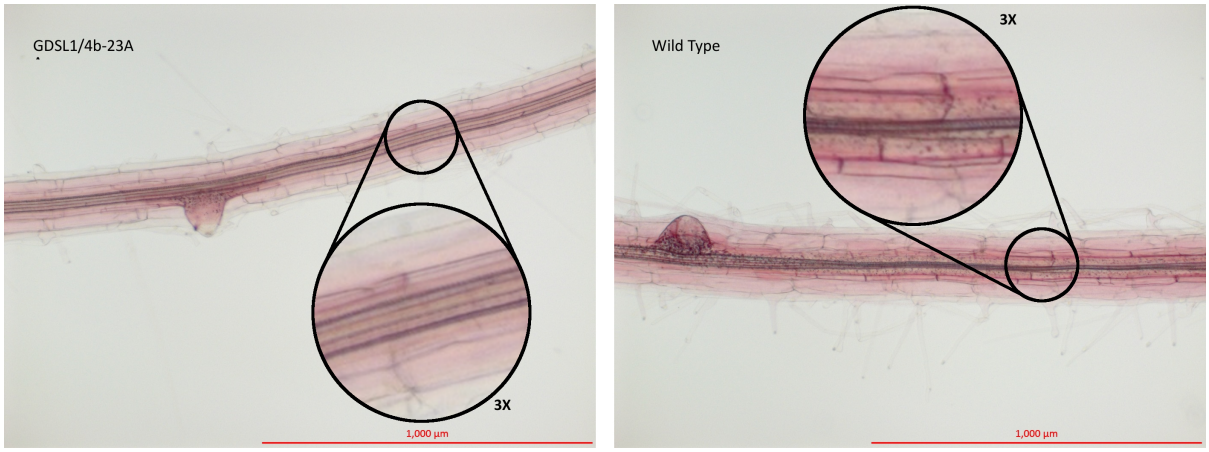

Figure 4.10: Oil Red O staining of Arabidopsis root after 12 days of growth. Both picture were taken at the same distance from the root tip.

Additionally, the distance between the tip of the root and the place at which suberin deposition begins was also recorded for one of each type of mutants and is recorded on Figure 4.11. The observed results indicate that even if suberin is still deposited for those mutants, it seems to be deposited at a later stage for most of the mutants.

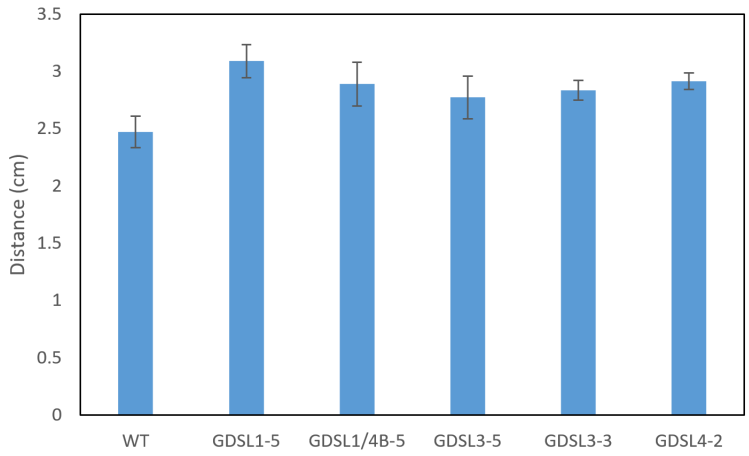

Figure 4.11: Measurement of the distance of deposition of suberin from the root tip for Arabidopsis plants after 12 days of growth. Each data represent the average of 7 samples (except for *GDSL1/4B-5* which represent the average of 3 samples).

Both of these results seems to indicate that the selected *GDSL* genes might be involved in some way in suberin biosynthesis. However, it seems that redundancy exists between the different genes. In this context, *GDSL* double and triple mutants have been prepared by crossing mutants flower together. However, due to time constraints, these mutants could not be grown and studied in time.

4.1.3 Perspectives and conclusions

This study provided some promising results towards the discovery of suberin synthase. Four different GDSL esterase/lipase, conveniently named GDSL1, *GDSL2*, *GDSL3* and *GDSL4*, have been selected due to their co-expression with GPAT5 within Arabidopsis root endodermis. Arabidopsis plants were successfully mutated to produce various lines of RNAi-silenced mutants for each of the genes encoding for the selected GDSL enzymes. Homozygotes for each mutant lines were obtained for further experiments. The selected *GDSL* genes seems to be involved in suberin biosynthesis as mutation of each genes seems to affect the speed of deposition of suberin. Furthermore, the *GDSL1-GDSL4* double mutation seems to drastically decreases suberin deposition in most of the root endodermis at the exception of areas of lateral root growth.

However, more convincing evidence and stronger statistical analysis is required to draw any kind of conclusion. Since my departure from Cornell University, this project has been handed in to a new student. At the time of writing, double and triple mutants are still under investigation.

4.2 Production and expression of CUS1 mutants through site-directed mutagenesis

4.2.1 Objectives

As discussed in section 1.3.4.3, the tertiary structure of CUS1 and the interaction between CUS1 and its substrates are still a mystery. As stated previously, X-Ray diffraction (XRD) of a CUS1-ligand complex would provide us with these data. Alternatively, one can build a homology model, based on the known three-dimensional structure of enzymes possessing similar primary structure domains. The main limitation of homology models are that they often rely on unproven assumptions, however, they can serve as the basis for some biochemical structure analysis such as site-directed mutagenesis (SDM). SDM is a molecular biology technique that relies on the formation of mutated DNA to produce a modified version of a known protein where one or several amino acids would be exchanged for another amino acid. A change in activity between the mutant protein and the original protein would indicate that the modified amino acid might play an important role in either the protein tertiary structure or in the interaction between the enzyme and its substrates.

Candida rugosa lipase was shown to possess a hydrophobic tunnel that allows for the stabilization of its substrate through Van der Waals interactions.[177] In this context, it was hypothesized that CUS1 might interact with its substrate through a similar mechanism. Specifically, homology model of CUS1, developed using the computational protein structure modeling software, PHYRE2,[178,179] suggested the presence of hydrophobic residues in the vicinity of the predicted catalytic site of the enzyme that might contribute to the CUS1 mode of action. For the remainder of this study, these residues will be referred to as I1 to I4.

The goal of this study is to produce different CUS1 mutants through SDM in order to delineate the importance of the four identified amino acid in the polymerase activity of CUS1.

4.2.2 Results and discussions

4.2.2.1 The megaprimer method

The site-directed mutagenesis was first attempted using the megaprimer method. This method relies on the use of a mutagenic primer, a primer that contains the desired variation that would encode for a different amino acid at the targeted position. This primer is used in a first PCR amplification, using the desired gene as a template, to create a corresponding megaprimer. This megaprimers can then be used for a second round of PCR to complete the replication of the full sequence and introducing the desired mutation. The product of this last PCR will contain a mixture of parent and mutated DNA sequence.

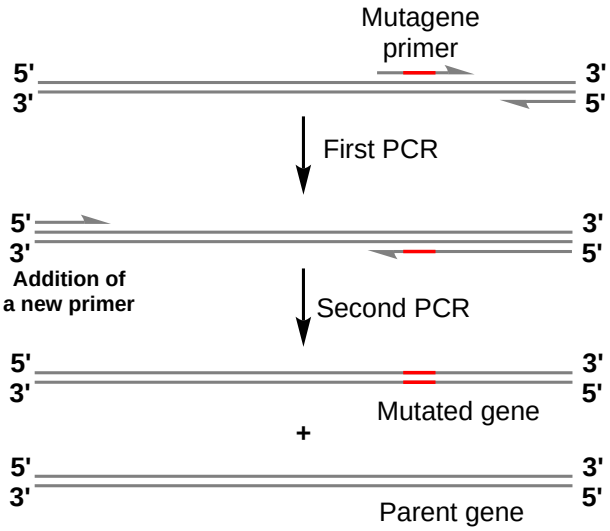

Scheme 4.1: Schematic representation of the megaprimer process. Half-arrow, primers and direction of replication; red area, mutated region.

In this specific case, a Ti plasmid containing a T-DNA insert encoding for a P35S promoted recombinant CUS1 along with ampicillin resistance was used as a template. The mutagenic primers were designed by Ph.D. student Nicholas Segerson to exchange the target isoleucines into tyrosines.

After the second round of PCR, the PCR product was purified, associated to a TOPO vector and transfected to a strain of *E. Coli*. The modified *E. Coli* were incubated on Lysogeny broth (LB) containing ampicillin as a selective agent. Single colonies of *E. Coli* were then selected and analyzed by PCR to confirm the presence of the CUS1 insert. The positive colonies were grown on LB and the TOPO-insert plasmids were extracted from the grown colonies. Samples of the obtained plasmids were mixed

with CUS1 related primer and send for sequencing. Unfortunately, sequencing of the TOPO-insert plasmid was unsuccessful. Furthermore, the next step in the process, consisting of a digestion of the plasmid in order to recover the insert followed by the can be attached to the expression vector, pEAQ-HT, in order to form a functional Ti plasmid, failed despite the use of different compatible digestive enzymes. These two results indicates that something went wrong with the whole process. Repeating the process a second time using Phusion®, a high-fidelity DNA polymerase, did not afford any better results and the SDM using this method was discontinued in favor of the QuickChange® method.

4.2.2.2 The QuickChange® method

Conversely to the megaprimer method, the QuickChange®method allows for the mutagenesis of a fully functional plasmid directly. This method, depicted in Scheme 4.2 relies on the use of a set of corresponding mutagenic primer and a functional bacterial Ti plasmid as a templates. PCR amplification using these primers allows for the formation of mutated plasmids. Further treatment of the PCR mixture with DpnI, a restriction enzyme that induce the degradation of methylated DNA of bacterial origin, allows for the degradation of the parent plasmid leaving only the mutated plasmid intact.

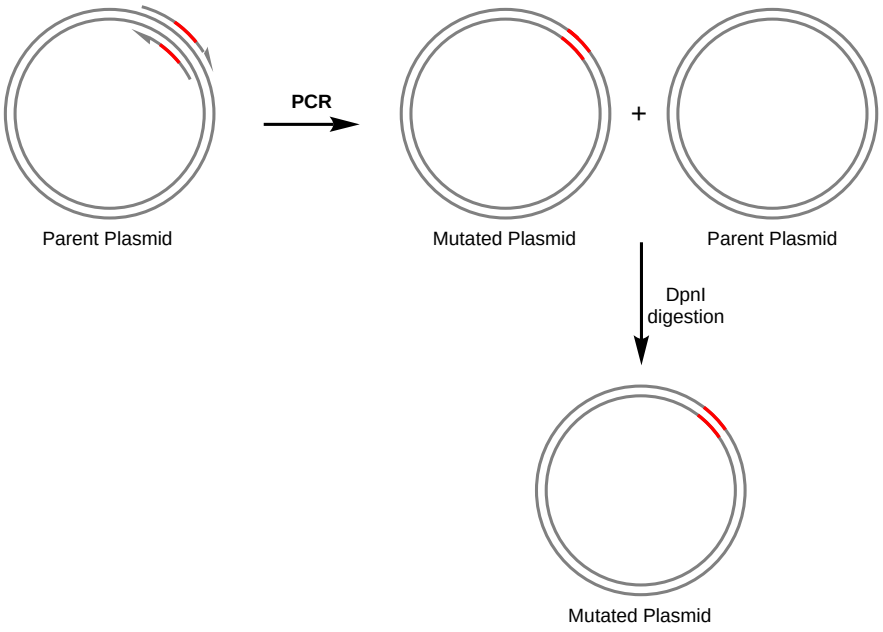

Scheme 4.2: Schematic representation of the megaprimer process. Half-arrow, primers and direction of replication; red area, mutated region.

To broaden the field of this study, 2 different type of mutations were planned for each isoleucine of interest. Firstly, the replacement of isoleucine for the polar amino acids tyrosine and asparagine was envisaged. The goal of those two mutations is to disrupt the formation of the hydrophobic tunnel and hamper the interactions between the enzymes and its substrates. Additionally, to assess for the impact of conformational changes caused by the mutagenesis, mutation of isoleucines into non-polar alanine was also considered. A set of forward and reverse mutagenic primers were designed for each target mutation. Unfortunately, the primers required for the tyrosines mutagenesis were not received on time and the preparation of the different tyrosine mutants could not be completed within the time of this study.

One of the advantage of this technique is that it allows for the preparation of a fully functional plasmids. Furthermore, the pEAQ-HT vector carries the Neomycin phosphotransferase III *nptIII* gene, which provides resistance to an antibiotic called kanamycin A. Hence, *E. Coli* can be directly transformed with the digestion product, dispersed on a LB filled petri dish containing kanamycin A as a selection agent. A selection of colonies were tested by PCR to assess for the presence of the insert and the positive colonies were grown in LB overnight. The plasmids of the bacteria culture were extracted using the E.Z.N.A® kit and a sample of each plasmid was sent for sequencing. Unfortunately, despite several attempts, no colonies containing a plasmid encoding for CUS1-I3A mutant were produced as observed on the sequencing data. The rest of the solution of plasmid was used to transform a suspension of *Agrobacterium tumefaciens* (GV3101) by electroporation. The modified Agrobacterium were dispersed on a LB filled petri dish containing kanamycin A and incubated at 28 °C for 2 days. Single colonies were selected for each mutants and tested by PCR to confirm the presence of the insert. Positive colonies were incubated in a LB solution containing kanamycin A at 28 °C for 2 days and diluted to a standard concentration as measured by the optical density of the solution at 600 nm. The obtained solution was used to infiltrate 4 weeks old *Nicotiana benthamiana* plants. The infiltrated plants were incubated in a growth chamber for 4 days then the leaves were cut and frozen.

To prove the expression of the CUS1 mutants by the infiltrated plants, total protein extraction was performed on approximately 500 mg of frozen tissue. The extracts were subjected to western blot analysis. The results of this analysis are shown on Figure 4.12. According to the total extraction data, every infiltrated plants, at the exception of the CUS1-I1A and CUS1-I1N mutants infiltrated plants, contains a recombinant protein possessing a similar size than the reference CUS1. This suggests that

the desired proteins are likely expressed. However, the mutants band were found to be way less intense than the one obtained from a CUS1 total protein extract, indicating that the mutant infiltration was less efficient than for the reference protein.

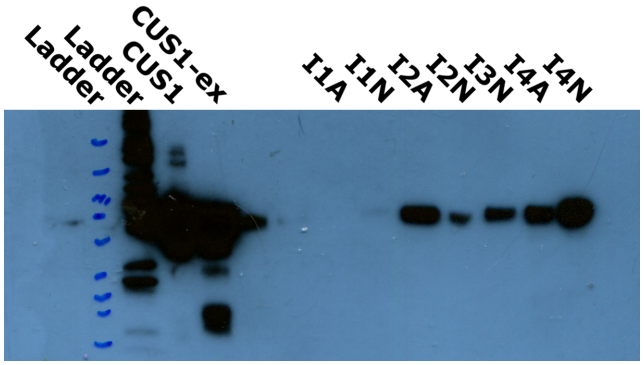

Figure 4.12: Western blot analysis of the total extraction of each infiltrated plants. CUS1-ex, Total protein extract of a CUS1 infiltrated plant.

Due to a lack of time, purification of the produced proteins could not be performed. Therefore, the exact nature of the produced proteins could not be confirmed and enzymatic polymerization assays could not be studied.

4.2.3 Perspectives and conclusions

Our first attempt at producing mutagenated plasmids using the megaprimer method unfortunately failed at the vector transfer step for unknown reasons. However, switching to the QuickChange® method, which does not require a vector transfer, proved to be more effective. Due to a lack of time, only seven of the twelve mutated plasmids were successfully produced. *Agrobacterium tumefaciens* was modified to obtain several modified colonies for each of the insert of interest. Tobacco plant were infiltrated with the modified *Agrobacterium* and five of the seven infiltrated plants were proven to express a recombinant protein of the desired size.

The mutants are currently still under investigation. One of the purified asparagine mutant presents a loss of activity while another one possesses a decreased activity. Additionally, the mutants possessing a loss of function promotes the hydrolysis of the glycerol esters. However, it is unclear to this point if this loss of activity arises from the disruption of the hydrophobic tunnel or from conformational changes and further investigation is required.

4.3 Experimental

Plants and Mutation *Arabidopsis thaliana* Columbia (Col-0) plants were used as WT in this study. RNAi-lines were prepared by treating flowering plants with a solution of *Agrobacterium tumefaciens* previously transfected with the desired RNAi insert and collecting the seeds of the treated plants. *Arabidopsis thaliana* plants were grown in a growth chamber (photoperiod, 16 h : 8 h, light : dark; 50% RH). *Nicotiana benthamiana* plants were grown in a growth chamber (photoperiod, 14 h : 10 h, light : dark; 50% RH)

Arabidopsis DNA extraction and PCR analysis

Edward solution: Tris-HCl (200 mM; pH 7.5), NaCl (250 mM), EDTA (25 mM) and SDS (0.5%).
TE buffer: Tris-HCl (10 mM; pH 8.0) and EDTA (1 mM).
Extraction buffer: Edward buffer : TE Buffer (1 : 9).
TAE buffer: Tris (40 mM), acetic acid (20 mM) EDTA (1 mM).

Arabidopsis leaves (3-5 mg) were submerged in Extraction Buffer (200 µL) and crushed with a plastic rod. The resulting mixture was used directly as a PCR sample. The PCR mixture were prepared as follow: Gotaq® buffer (5 µL), dNTP solution (10 mM; 0.5 µL), forward primer (100 µM; 0.1 µL), reverse primer (100 µM; 0.1 µL), Gotaq® enzyme (5U/µL; 0.2 µL), distilled water (18.1 µL) DNA extract (1 µL). The cycling parameters were as follows: (1) 95 °C for 2 min; (2) 30 cycles of 95 °C for 30 s, 60 °C for 30 s, 72 °C for 30 s; (3) 72 °C for 7 min 30 s. The samples were separated by gel electrophoresis on a 1 % agarose in TAE buffer containing ethidium bromide (1 $mg.mL^{-1}$) and revealed by UV irradiation.

RNA extraction

Each RNA samples was a representation of 15-20 roots from plate-grown seedlings at the age of 12 d. TRIZOL reagent (1 mL) was added and the sample was incubated at 20 °C for 5 minutes. The samples were centrifuged at 10500 rpm for 10 min at 4 °C and the supernatant was taken up and mixed with chloroform (0.2 mL). The resulting solution was shaken up for 15 s by hand and incubated at 20 °C for 3 minutes. The samples were centrifuged at 10500 rpm for 15 minutes at 4 °C. The aq. layer was diluted with isopropyl alcohol (0.5 mL) and the resulting solution was incubated at 20 °C for 10 minutes then centrifuged at 10500 rpm for 10 min at 4 °C. The supernatant

was removed and the the RNA pellet was washed with 75% ethanol (2 x 1 mL). The RNA pellet was air dried for 10 minutes and dissolved in RNase-free DEPC-water (1 mL).

cDNA synthesis

RQ1 DNase 10x buffer: Tris-HCl (400 mM; pH 8.0), $MgSO_4$ (100 mM) and $CaCl_2$ (10 mM).
First-strand 5x buffer: Tris-HCl (250 mM; pH 8.3), KCl (375 mM) and $MgCl_2$ (15 mM).

RNA samples (1 - 4 µg) were mixed with RQ1 DNase 10x buffer (1 µL), RQ1 DNase (1000 $U.mL^{-1}$; 1 µL) and RNaseOut (5000 $U.mL^{-1}$; 0.25 µL) in RNase-free DEPC-water (total volume: 10 µL). The resulting mixture was incubated at 37 °C for 30 min then RQ1 DNase stop solution (1 µL) was added. The resulting mixture was incubated at 65 °C for 10 min then 3 µL were removed for analysis. The remaining solution was mixed with oligo dT (100 µM; 1 µL) and dNTP solution (10 mM; 1 µL), and incubated at 65 °C for 5 min. The sample were put on ice for 1 min then mixed with first-strand 5x buffer (4 µL), DTT (0.1 M; 2 µL) and RNaseOut (5000 $U.mL^{-1}$; 1 µL). The resulting mixture was incubated at 42 °C for 2 minutes then SuperScript™ II (200 $U.\mu L^{-1}$; 1 µL) amd the mixture was further incubated at 42 °C for 50 min then at 70 °C for 15 min. The samples were cooled on ice and RNase H (5$U.\mu L^{-1}$; 1 µL) was added and the samples were incubated at 37 °C for 20 min. Finally, the cDNA samples were diluted to a final concentration of approximately 100 $ng.\mu L^{-1}$ and stored at -20 °C.

qPCR analysis

For each set of primers, a master mix was prepared: qPCR Mix (SYBR™ green; 6 µL per sample), ROX fluorescent dye (2 µM; 0.25 µL per sample), primer mix (0.2 µM; 1 µL per sample) distilled water (4.25 µL per sample). qPCR samples were prepared by mixing 11.5 µL of master mix with 0.5 µL of cDNA sample on a multiwell plate. Each samples were prepared in 4 technical replicates and analyzed using a Life Technologies/ABI ViiA™7 Real-Time PCR system.
Each average Ct values were normalized to a reference gene and compared to the normalized value obtained with wild type plant. The relative expression shown represents the average of the relative expression of a gene in a mutants compared to three biological replicates of wild type plants.

semi quantitative PCR

sqPCR samples were prepared as follow: Gotaq® buffer (5 µL), dNTP solution (10 mM; 0.5 µL), primer mix (10 µM; 1 µL), Gotaq® enzyme (5U/µL; 0.2 µL), distilled water (17.3 µL) and cDNA sample (1 µL). The cycling parameters were as follows: (1) 95 °C for 2 min; (2) **X** cycles of 95 °C for 30 s, 60 °C for 30 s, 72 °C for 30 s; (3) 72 °C for 7 min 30 s; GDSL1 and GDSL4, **X** = 30; GDSL3, X = 36. The samples were separated by gel electrophoresis on a 2 % agarose in TAE buffer containing ethidium bromide (1 $mg.mL^{-1}$) and revealed by UV irradiation.

Agrobacterium tumefaciens modification

For each modified plasmid, a suspension of *Agrobacterium tumefaciens* (50 µL) was mixed with a solution of plasmid (500 - 1000 ng) and the transformation was performed by electroporation. The modified bacteria suspension was diluted in LB (1 mL) and incubated at 28 °C for 1 hour. The bacteria were centrifuged at 5000 rpm for 5 minutes and the supernatant was removed to leave 100 µL of bacterial suspension which was plated on LB containing kanamycin (1 $\mu L.mL^{-1}$). The petri dish were incubated at 28 °C for 2 days. Several colonies were transferred to a master plate and tested by PCR to confirm the presence of the CUS1 gene.

Nicotiana benthamiana infiltration

Infiltration buffer: MES (10 mM; pH 5.8), $MgCl_2$ (10 mM), acetosyringone (500 µM).

The modified *Agrobacterium* was transferred to LB (5 mL) containing kanamycin (5 µL) and rifampicin (2.5 µL) and incubated at 28 °C for 2 days. The colonies were transferred to LB (200 mL) containing kanamycin (200 µL) and rifampicin (100 µL). The colonies were transferred to two falcon tube (2 x 100 mL) and centrifuged at 4500 rpm for 15 min. The bacteria pellet was resuspended in freshly made infiltration buffer (50 mL per tube), place in the dark and shaken for 3 hours at 20 °C. The solution were centrifuged at 4500 rpm for 15 min. The pellet were resuspended in freshly made infiltration buffer and diluted to obtain a solution of optical density of around 1.2 at 600 nm. The solution was used to infiltrate 4 weeks old *Nicotiana benthamiana* plants by performing a small incision on the back of the plant and forcing the bacterial solution through the incision. The plants were left in growth chamber and the leaves were collected and frozen at 6 days post infiltration.

Total protein extraction

Laemmli buffer: Tris-HCl (120 mM; pH 7.0), SDS (14 mM), DTT (100 mM), bromophenol blue (30 µM).
TBST buffer: Tris (50 mM; pH 7.5), NaCl (150 mM) and Tween 20 (0.1%).

Frozen tissue (0.5 mg) were grinded in Laemmli buffer (0.5 mL). The resulting mixture was boiled for 15 min then cooled to 20 °C. The supernatant was taken up and separated by gel electrophoresis on Mini-PROTEAN® TGX™ precast gel. The gel was transferred to a nitrocellulose membrane and the membrane was blocked with milk (5%) in TBST for 1 h then washed with TBST (10 min). The membrane was submerged in milk (5%) in TBST containing a Anti-His(C-term) primary antibody (2 µL) for 1 hour. The membrane was washed with TBST (15 min; 3 times) then submerged in milk (5%) in TBST containing an Anti-mouse IgG secondary antibody (2 µL) for 1 hour. The membrane was washed with TBST (15 min; 3 times) then revealed using the Clarity™ Western ECL Substrate Kit and developed on a film (Exposition time: 11 minutes).

References

1. Wolf, S.; Hématy, K.; Höfte, H. Growth Control and Cell Wall Signaling in Plants. *Annual Review of Plant Biology* **2012**, *63*, 381–407.
2. Kinnaert, C.; Daugaard, M.; Nami, F.; Clausen, M. H. Chemical Synthesis of Oligosaccharides Related to the Cell Walls of Plants and Algae. *Chemical Reviews* **2017**, *117*, 11337–11405.
3. https : / / commons . wikimedia . org / wiki / File % 3APlant_cell_wall_diagram - en.svg (accessed 13/12/2017).
4. Scheller, H. V.; Ulvskov, P. Hemicelluloses. *Annual Review of Plant Biology* **2010**, *61*, 263–289.
5. Caffall, K. H.; Mohnen, D. The structure, function, and biosynthesis of plant cell wall pectic polysaccharides. *Carbohydrate Research* **2009**, *344*, 1879–1900.
6. Yeats, T. H.; Rose, J. K. C. The Formation and Function of Plant Cuticles. *Plant Physiology* **2013**, *163*, 5–20.
7. Lenton, T. M.; Dahl, T. W.; Daines, S. J.; Mills, B. J. W.; Ozaki, K.; Saltzman, M. R.; Porada, P. Earliest land plants created modern levels of atmospheric oxygen. *Proceedings of the National Academy of Sciences* **2016**, *113*, 9704–9709.
8. Espelie, K. E.; Davis, R. W.; Kolattukudy, P. E. Composition, ultrastructure and function of the cutin- and suberin-containing layers in the leaf, fruit peel, juice-sac and inner seed coat of grapefruit (Citrus paradisi Macfed.). *Planta* **1980**, *511*, 498–511.
9. Riederer, M. In *Biology of the Plant Cuticle*; Blackwell Publishing Ltd: Oxford, UK, 2007; Vol. 23, pp 1–10.
10. Dominguez, E.; Heredia-Guerrero, J. A.; Heredia, A. The biophysical design of plant cuticles: An overview. *New Phytologist* **2011**, *189*, 938–949.
11. Martin, L. B.; Rose, J. K. There's more than one way to skin a fruit: Formation and functions of fruit cuticles. *Journal of Experimental Botany* **2014**, *65*, 4639–4651.
12. Solovchenko, A.; Merzlyak, M. Optical properties and contribution of cuticle to UV protection in plants: experiments with apple fruit. *Photochemical & Photobiological Sciences* **2003**, *2*, 861.
13. Lolle, S. J.; Hsu, W.; Pruitt, R. E. Genetic analysis of organ fusion in Arabidopsis thaliana. *Genetics* **1998**, *149*, 607–619.
14. Krolikowski, K. A.; Victor, J. L.; Wagler, T. N.; Lolle, S. J.; Pruitt, R. E. Isolation and characterization of the Arabidopsis organ fusion gene HOTHEAD. *Plant Journal* **2003**, *35*, 501–511.

15. Yeats, T. H.; Howe, K. J.; Matas, A. J.; Buda, G. J.; Thannhauser, T. W.; Rose, J. K. Mining the surface proteome of tomato (Solanum lycopersicum) fruit for proteins associated with cuticle biogenesis. *Journal of Experimental Botany* **2010**, *61*, 3759–3771.

16. Takahashi, K.; Shimada, T.; Kondo, M.; Tamai, A.; Mori, M.; Nishimura, M.; Hara-Nishimura, I. Ectopic expression of an esterase, which is a candidate for the unidentified plant cutinase, causes cuticular defects in arabidopsis thaliana. *Plant and Cell Physiology* **2010**, *51*, 123–131.

17. Jeffree, C. E. The fine structure of the plant cuticle. *Annual Plant Reviews Volume 23: Biology of the Plant Cuticle* **2006**, 11–125.

18. Pollard, M.; Beisson, F.; Li, Y.; Ohlrogge, J. B. Building lipid barriers: biosynthesis of cutin and suberin. *Trends in Plant Science* **2008**, *13*, 236–246.

19. Baker, E. A.; Procopiou, J.; Hunt, G. M. The cuticles of Citrus species. Composition of leaf and fruit waxes. *Journal of the Science of Food and Agriculture* **1975**, *26*, 1093–1101.

20. Jetter, R.; Kunst, L.; Samuels, A. L. Composition of Plant Cuticular Waxes. *Annual Plant Reviews* **2007**, *23*, 145–181.

21. Girard, A.-L.; Mounet, F.; Lemaire-Chamley, M.; Gaillard, C.; Elmorjani, K.; Vivancos, J.; Runavot, J.-L.; Quemener, B.; Petit, J.; Germain, V.; Rothan, C.; Marion, D.; Bakan, B. Tomato GDSL1 Is Required for Cutin Deposition in the Fruit Cuticle. *The Plant Cell* **2012**, *24*, 3119–3134.

22. Gülz, P. G.; Scora, R. W.; Müller, E.; Marner, F. J. Epicuticular Leaf Waxes of Citrus halimii Stone. *Journal of Agricultural and Food Chemistry* **1987**, *35*, 716–720.

23. Sümmchen, P.; Markstädter, C.; Wienhaus, O. Composition of the epicuticular wax esters of Picea abies (L.) Karst. *Zeitschrift für Naturforschung C* **1995**, *50*, 11–14.

24. Hunt, G. M.; Baker, E. A. Phenolic constituents of tomato fruit cuticles. *Phytochemistry* **1980**, *19*, 1415–1419.

25. Vogg, G.; Fischer, S.; Leide, J.; Emmanuel, E.; Jetter, R.; Levy, A. A.; Riederer, M. Tomato fruit cuticular waxes and their effects on transpiration barrier properties: Functional characterization of a mutant deficient in a very-long-chain fatty acid β-ketoacyl-CoA synthase. *Journal of Experimental Botany* **2004**, *55*, 1401–1410.

26. Leide, J.; Hildebrandt, U.; Reussing, K.; Riederer, M.; Vogg, G. The Developmental Pattern of Tomato Fruit Wax Accumulation and Its Impact on Cuticular Transpiration Barrier Properties: Effects of a Deficiency in a beta-Ketoacyl-Coenzyme A Synthase (LeCER6). *Plant Physiology* **2007**, *144*, 1667–1679.
27. Riedel, M.; Eichner, A.; Jetter, R. Slippery surfaces of carnivorous plants: Composition of epicuticular wax crystals in Nepenthes alata Blanco pitchers. *Planta* **2003**, *218*, 87–97.
28. Barthlott, W.; Neinhuis, C. Purity of the sacred lotus, or escape from contamination in biological surfaces. *Planta* **1997**, *202*, 1–8.
29. Bargel, H.; Koch, K.; Cerman, Z.; Neinhuis, C. Structure-function relationships of the plant cuticle and cuticular waxes - A smart material? *Functional Plant Biology* **2006**, *33*, 893–910.
30. Zhang, M.; Feng, S.; Wang, L.; Zheng, Y. Lotus effect in wetting and self-cleaning. *Biotribology* **2016**, *5*, 31–43.
31. Fich, E. A.; Segerson, N. A.; Rose, J. K. The Plant Polyester Cutin: Biosynthesis, Structure, and Biological Roles. *Annual Review of Plant Biology* **2016**, *67*, 207–233.
32. Kallio, H.; Nieminen, R.; Tuomasjukka, S.; Hakala, M. Cutin composition of five finnish berries. *Journal of Agricultural and Food Chemistry* **2006**, *54*, 457–462.
33. Franke, R.; Briesen, I.; Wojciechowski, T.; Faust, A.; Yephremov, A.; Nawrath, C.; Schreiber, L. Apoplastic polyesters in Arabidopsis surface tissues - A typical suberin and a particular cutin. *Phytochemistry* **2005**, *66*, 2643–2658.
34. Li-Beisson, Y.; Pollard, M.; Sauveplane, V.; Pinot, F.; Ohlrogge, J.; Beisson, F. Nanoridges that characterize the surface morphology of flowers require the synthesis of cutin polyester. *Proceedings of the National Academy of Sciences* **2009**, *106*, 22008–22013.
35. Mazurek, S.; Garroum, I.; Daraspe, J.; De Bellis, D.; Olsson, V.; Mucciolo, A.; Butenko, M. A.; Humbel, B. M.; Nawrath, C. Connecting the Molecular Structure of Cutin to Ultrastructure and Physical Properties of the Cuticle in Petals of Arabidopsis. *Plant Physiology* **2017**, *173*, 1146–1163.
36. Hong, L.; Brown, J.; Segerson, N. A.; Rose, J. K.; Roeder, A. H. CUTIN SYNTHASE 2 Maintains Progressively Developing Cuticular Ridges in Arabidopsis Sepals. *Molecular Plant* **2017**, *10*, 560–574.
37. Graça, J.; Schreiber, L.; Rodrigues, J.; Pereira, H. Glycerol and glyceryl esters of ω-hydroxyacids in cutins. *Phytochemistry* **2002**, *61*, 205–215.

38. Saladie, M.; Matas, A. J.; Isaacson, T.; Jenks, M. A.; Goodwin, S. M.; Niklas, K. J.; Xiaolin, R.; Labavitch, J. M.; Shackel, K. A.; Fernie, A. R.; Lytovchenko, A.; O'Neill, M. A.; Watkins, C. B.; Rose, J. K. A Reevaluation of the Key Factors That Influence Tomato Fruit Softening and Integrity. *Plant Physiology* **2007**, *144*, 1012–1028.

39. Bonaventure, G.; Beisson, F.; Ohlrogge, J.; Pollard, M. Analysis of the aliphatic monomer composition of polyesters associated with Arabidopsis epidermis: Occurrence of octadeca-cis-6, cis-9-diene-1,18-dioate as the major component. *Plant Journal* **2004**, *40*, 920–930.

40. Beisson, F.; Li, Y.; Bonaventure, G.; Pollard, M.; Ohlrogge, J. B. The Acyltransferase GPAT5 Is Required for the Synthesis of Suberin in Seed Coat and Root of Arabidopsis. *the Plant Cell Online* **2007**, *19*, 351–368.

41. Suh, M. C. Cuticular Lipid Composition, Surface Structure, and Gene Expression in Arabidopsis Stem Epidermis. *Plant Physiology* **2005**, *139*, 1649–1665.

42. Li, Y.; Beisson, F.; Koo, A. J. K.; Molina, I.; Pollard, M.; Ohlrogge, J. Identification of acyltransferases required for cutin biosynthesis and production of cutin with suberin-like monomers. *Proceedings of the National Academy of Sciences* **2007**, *104*, 18339–18344.

43. Petit, J.; Bres, C.; Just, D.; Garcia, V.; Mauxion, J.-P.; Marion, D.; Bakan, B.; Joubes, J.; Domergue, F.; Rothan, C. Analyses of Tomato Fruit Brightness Mutants Uncover Both Cutin-Deficient and Cutin-Abundant Mutants and a New Hypomorphic Allele of GDSL Lipase. *Plant Physiology* **2014**, *164*, 888–906.

44. Yeats, T. H.; Martin, L. B. B.; Viart, H. M.-F.; Isaacson, T.; He, Y.; Zhao, L.; Matas, A. J.; Buda, G. J.; Domozych, D. S.; Clausen, M. H.; Rose, J. K. C. The identification of cutin synthase: formation of the plant polyester cutin. *Nature Chemical Biology* **2012**, *8*, 609–611.

45. Yang, W.; Pollard, M.; Li-Beisson, Y.; Ohlrogge, J. Quantitative analysis of glycerol in dicarboxylic acid-rich cutins provides insights into Arabidopsis cutin structure. *Phytochemistry* **2016**, *130*, 159–169.

46. Rani, S. H.; Krishna, T. H.; Saha, S.; Negi, A. S.; Rajasekharan, R. Defective in Cuticular Ridges (DCR) of Arabidopsis thaliana, a gene associated with surface cutin formation, encodes a soluble diacylglycerol acyltransferase. *Journal of Biological Chemistry* **2010**, *285*, 38337–38347.

47. Luque, P.; Bruque, S.; Heredia, A. Water permeability of isolated cuticular membranes: A structural analysis., 1995.

48. Heide-Jørgensen, H. S. Cuticle development and ultrastructure: evidence for a procuticle of high osmium affinity. *Planta* **1991**, *183*, 511–519.

49. Kolattukudy, P. E. Structure, Biosynthesis, and Biodegradation of Cutin and Suberin. *Annual Review of Plant Physiology* **1981**, *32*, 539–567.

50. Agulló, C.; Collar, C.; Seoane, E. Free and bound hydroxyl and carboxyl groups in the cutin of Quercus suber leaves. *Phytochemistry* **1984**, *23*, 2059–2060.

51. Fang, X.; Qiu, F.; Yan, B.; Wang, H.; Mort, A. J.; Stark, R. E. NMR studies of molecular structure in fruit cuticle polyesters. *Phytochemistry* **2001**, *57*, 1035–1042.

52. Tian, S.; Fang, X.; Wang, W.; Yu, B.; Cheng, X.; Qiu, F.; Mort, A. J.; Stark, R. E. Isolation and identification of oligomers from partial degradation of lime fruit cutin. *Journal of Agricultural and Food Chemistry* **2008**, *56*, 10318–10325.

53. Garbow, J. R.; Stark, R. E. Nuclear Magnetic Resonance Relaxation Studies of Plant Polyester Dynamics. 1. Cutin from Limes. *Macromolecules* **1990**, *23*, 2814–2819.

54. Isaacson, T.; Kosma, D. K.; Matas, A. J.; Buda, G. J.; He, Y.; Yu, B.; Pravitasari, A.; Batteas, J. D.; Stark, R. E.; Jenks, M. A.; Rose, J. K. Cutin deficiency in the tomato fruit cuticle consistently affects resistance to microbial infection and biomechanical properties, but not transpirational water loss. *Plant Journal* **2009**, *60*, 363–377.

55. Riederer, M.; Schreiber, L. Protecting against water loss: analysis of the barrier properties of plant cuticles. *Journal of Experimental Botany* **2001**, *52*, 2023–2032.

56. Schreiber, L.; Riederer, M.; Schorn, K. Mobilities of organic compounds in reconstituted cuticular wax of barley leaves: Effects of monodisperse alcohol ethoxylates on diffusion of pentachlorophenol and tetracosanoic acid. *Pesticide Science* **1996**, *48*, 117–124.

57. Wellesen, K.; Durst, F.; Pinot, F.; Benveniste, I.; Nettesheim, K.; Wisman, E.; Steiner-Lange, S.; Saedler, H.; Yephremov, A. Functional analysis of the LACERATA gene of Arabidopsis provides evidence for different roles of fatty acid ω-hydroxylation in development. *Proceedings of the National Academy of Sciences of the United States of America* **2001**, *98*, 9694–9699.

58. Kurdyukov, S. The Epidermis-Specific Extracellular BODYGUARD Controls Cuticle Development and Morphogenesis in Arabidopsis. *the Plant Cell Online* **2006**, *18*, 321–339.

59. Bird, D.; Beisson, F.; Brigham, A.; Shin, J.; Greer, S.; Jetter, R.; Kunst, L.; Wu, X.; Yephremov, A.; Samuels, L. Characterization of Arabidopsis ABCG11/WBC11, an ATP binding cassette (ABC) transporter that is required for cuticular lipid secretion. *Plant Journal* **2007**, *52*, 485–498.

60. Shi, J. X.; Malitsky, S.; de Oliveira, S.; Branigan, C.; Franke, R. B.; Schreiber, L.; Aharoni, A. SHINE transcription factors act redundantly to pattern the archetypal surface of arabidopsis flower organs. *PLoS Genetics* **2011**, *7*, DOI: 10.1371/journal.pgen.1001388.

61. Weng, H.; Molina, I.; Shockey, J.; Browse, J. Organ fusion and defective cuticle function in a lacs1 lacs2 double mutant of Arabidopsis. *Planta* **2010**, *231*, 1089–1100.

62. Sieber, P.; Schorderet, M.; Ryser, U.; Buchala, A.; Kolattukudy, P.; Métraux, J.-P.; Nawrath, C. Transgenic Arabidopsis Plants Expressing a Fungal Cutinase Show Alterations in the Structure and Properties of the Cuticle and Postgenital Organ Fusions. *The Plant Cell* **2000**, *12*, 721–737.

63. Smirnova, A.; Leide, J.; Riederer, M. Deficiency in a Very-Long-Chain Fatty Acid -Ketoacyl-Coenzyme A Synthase of Tomato Impairs Microgametogenesis and Causes Floral Organ Fusion. *Plant Physiology* **2013**, *161*, 196–209.

64. Tanaka, T.; Tanaka, H.; Machida, C.; Watanabe, M.; Machida, Y. A new method for rapid visualization of defects in leaf cuticle reveals five intrinsic patterns of surface defects in Arabidopsis. *Plant Journal* **2004**, *37*, 139–146.

65. Jakobson, L.; Lindgren, L. O.; Verdier, G.; Laanemets, K.; Brosché, M.; Beisson, F.; Kollist, H. BODYGUARD is required for the biosynthesis of cutin in Arabidopsis. *New Phytologist* **2016**, *211*, 614–626.

66. Kutschera, U.; Bergfeld, R.; Schopfer, P. Cooperation of epidermis and inner tissues in auxin-mediated growth of maize coleoptiles. *Planta* **1987**, *170*, 168–180.

67. Lara, I.; Belge, B.; Goulao, L. F. The fruit cuticle as a modulator of postharvest quality. *Postharvest Biology and Technology* **2014**, *87*, 103–112.

68. España, L.; Heredia-Guerrero, J. A.; Segado, P.; Benítez, J. J.; Heredia, A.; Domínguez, E. Biomechanical properties of the tomato (Solanum lycopersicum) fruit cuticle during development are modulated by changes in the relative amounts of its components. *New Phytologist* **2014**, *202*, 790–802.

69. Bargel, H.; Neinhuis, C. Tomato (Lycopersicon esculentum Mill.) fruit growth and ripening as related to the biomechanical properties of fruit skin and isolated cuticle. *Journal of Experimental Botany* **2005**, *56*, 1049–1060.

70. López-Casado, G.; Matas, A. J.; Domínguez, E.; Cuartero, J.; Heredia, A. Biomechanics of isolated tomato (Solanum lycopersicum L.) fruit cuticles: The role of the cutin matrix and polysaccharides. *Journal of Experimental Botany* **2007**, *58*, 3875–3883.

71. Petracek, P. D.; Bukovac, M. J. Rheological Properties of Enzymatically lsolated Tomato Fruit Cuticle. *Plant Physiology* **1995**, *109*, 675–679.

72. Bargel, H.; Neinhuis, C. Altered tomato (Lycopersicon esculentum Mill.) fruit cuticle biomechanics of a pleiotropic non ripening mutant. *Journal of Plant Growth Regulation* **2004**, *23*, 61–75.

73. Domnguez, E.; Espaa, L.; Lpez-Casado, G.; Cuartero, J.; Heredia, A. Biomechanics of isolated tomato (Solanum lycopersicum) fruit cuticles during ripening: The role of flavonoids. *Functional Plant Biology* **2009**, *36*, 613–620.

74. Takahashi, Y.; Tsubaki, S.; Sakamoto, M.; Watanabe, S.; Azuma, J. I. Growth-dependent chemical and mechanical properties of cuticular membranes from leaves of Sonneratia alba. *Plant, Cell and Environment* **2012**, *35*, 1201–1210.

75. Tsubaki, S.; Ozaki, Y.; Yonemori, K.; Azuma, J. I. Mechanical properties of fruit-cuticular membranes isolated from 27 cultivars of Diospyros kaki Thunb. *Food Chemistry* **2012**, *132*, 2135–2139.

76. Marga, F.; Pesacreta, T. C.; Hasenstein, K. H. Biochemical analysis of elastic and rigid cuticles of Cirsium horridulum. *Planta* **2001**, *213*, 841–848.

77. Heredia-Guerrero, J. A.; Heredia, A.; Domínguez, E.; Cingolani, R.; Bayer, I. S.; Athanassiou, A.; Benítez, J. J. Cutin from agro-waste as a raw material for the production of bioplastics. *Journal of Experimental Botany* **2017**, *68*, 5401–5410.

78. Chaudhari, S. A.; Singhal, R. S. Cutin from watermelon peels: A novel inducer for cutinase production and its physicochemical characterization. *International Journal of Biological Macromolecules* **2015**, *79*, 398–404.

79. Dickman, M. B.; Patil, S. S.; Kolattukudy, P. E. Purification, characterization and rôle in infection of an extracellular cutinolytic enzyme from Colletotrichum gloeosporioides Penz. on Carica papaya L. *Physiological Plant Pathology* **1982**, *20*, 333–347.

80. Tang, D.; Simonich, M. T.; Innes, R. W. Mutations in LACS2, a Long-Chain Acyl-Coenzyme A Synthetase, Enhance Susceptibility to Avirulent Pseudomonas syringae But Confer Resistance to Botrytis cinerea in Arabidopsis. *Plant Physiology* **2007**, *144*, 1093–1103.

81. Bessire, M.; Chassot, C.; Jacquat, A. C.; Humphry, M.; Borel, S.; Petétot, J. M.D. C.; Métraux, J. P.; Nawrath, C. A permeable cuticle in Arabidopsis leads to a strong resistance to Botrytis cinerea. *EMBO Journal* **2007**, *26*, 2158–2168.

82. Bessire, M.; Borel, S.; Fabre, G.; Carraça, L.; Efremova, N.; Yephremov, A.; Cao, Y.; Jetter, R.; Jacquat, A.-C.; Métraux, J.-P.; Nawrath, C. A Member of the PLEIOTROPIC DRUG RESISTANCE Family of ATP Binding Cassette Transporters Is Required for the Formation of a Functional Cuticle in Arabidopsis. *The Plant Cell* **2011**, *23*, 1958–1970.

83. Voisin, D.; Nawrath, C.; Kurdyukov, S.; Franke, R. B.; Reina-Pinto, J. J.; Efremova, N.; Will, I.; Schreiber, L.; Yephremov, A. Dissection of the complex phenotype in cuticular mutants of Arabidopsis reveals a role of SERRATE as a mediator. *PLoS Genetics* **2009**, *5*, DOI: 10.1371/journal.pgen.1000703.

84. Chassot, C.; Nawrath, C.; Métraux, J. P. Cuticular defects lead to full immunity to a major plant pathogen. *Plant Journal* **2007**, *49*, 972–980.

85. Schweizer, P.; Jeanguenat, A.; Msinger, E. Patrick Schweizer1.2, **1994**, *3*, 371–372.

86. Schweizer, P.; Felix, G.; Buchala, A.; Muller, C.; Metraux, J.-P. Perception of free cutin monomers by plant cells. *The Plant Journal* **1996**, *10*, 331–341.

87. Kauss, H.; Fauth, M.; Merten, A.; Jeblick, W. Cucumber Hypocotyls Respond to Cutin Monomers via Both an Inducible and a Constitutive H2O2-Generating System1. *Plant physiology* **1999**, *120*, 1175–1182.

88. Lü, S.; Song, T.; Kosma, D. K.; Parsons, E. P.; Rowland, O.; Jenks, M. A. Arabidopsis CER8 encodes LONG-CHAIN ACYL-COA SYNTHETASE 1 (LACS1) that has overlapping functions with LACS2 in plant wax and cutin synthesis. *Plant Journal* **2009**, *59*, 553–564.

89. Molina, I.; Ohlrogge, J. B.; Pollard, M. Deposition and localization of lipid polyester in developing seeds of Brassica napus and Arabidopsis thaliana. *Plant Journal* **2008**, *53*, 437–449.

90. Xiao, F.; Goodwin, S. M.; Xiao, Y.; Sun, Z.; Baker, D.; Tang, X.; Jenks, M. A.; Zhou, J. M. Arabidopsis CYP86A2 represses Pseudomonas syringae type III genes and is required for cuticle development. *EMBO Journal* **2004**, *23*, 2903–2913.

91. Duan, H.; Schuler, M. A. Differential Expression and Evolution of the Arabidopsis. *Plant Physiol* **2005**, *137*, 1067–1081.

92. Rupasinghe, S. G.; Duan, H.; Schuler, M. A. Molecular definitions of fatty acid hydroxylases in Arabidopsis thaliana. *Proteins: Structure, Function, and Bioinformatics* **2007**, *68*, 279–293.

93. Han, J.; Clement, J. M.; Li, J.; King, A.; Ng, S.; Jaworski, J. G. The cytochrome P450 CYP86A22 is a fatty acyl-CoA ω-hydroxylase essential for estolide synthesis in the stigma of Petunia hybrida. *Journal of Biological Chemistry* **2010**, *285*, 3986–3996.

94. Kurdyukov, S.; Faust, A.; Trenkamp, S.; Bär, S.; Franke, R.; Efremova, N.; Tietjen, K.; Schreiber, L.; Saedler, H.; Yephremov, A. Genetic and biochemical evidence for involvement of HOTHEAD in the biosynthesis of long-chain α-,ω-dicarboxylic fatty acids and formation of extracellular matrix. *Planta* **2006**, *224*, 315–329.

95. Sauveplane, V.; Kandel, S.; Kastner, P.-E.; Ehlting, J.; Compagnon, V.; Werck-Reichhart, D.; Pinot, F. Arabidopsis thaliana CYP77A4 is the first cytochrome P450 able to catalyze the epoxidation of free fatty acids in plants. *FEBS Journal* **2009**, *276*, 719–735.

96. Yang, W.; Pollard, M.; Li-Beisson, Y.; Beisson, F.; Feig, M.; Ohlrogge, J. A distinct type of glycerol-3-phosphate acyltransferase with sn-2 preference and phosphatase activity producing 2-monoacylglycerol. *Proceedings of the National Academy of Sciences* **2010**, *107*, 12040–12045.

97. Yang, W.; Simpson, J. P.; Li-Beisson, Y.; Beisson, F.; Pollard, M.; Ohlrogge, J. B. A Land-Plant-Specific Glycerol-3-Phosphate Acyltransferase Family in Arabidopsis: Substrate Specificity, sn-2 Preference, and Evolution. *Plant Physiology* **2012**, *160*, 638–652.

98. Domínguez, E.; Heredia-Guerrero, J. A.; Heredia, A. Plant cutin genesis: Unanswered questions., 2015.

99. Panikashvili, D.; Shi, J. X.; Schreiber, L.; Aharoni, A. The Arabidopsis ABCG13 transporter is required for flower cuticle secretion and patterning of the petal epidermis. *New Phytologist* **2011**, *190*, 113–124.

100. Yeats, T. H.; Rose, J. K. The biochemistry and biology of extracellular plant lipid-transfer proteins (LTPs). *Protein Sci* **2008**, *17*, 191–198.

101. Lee, S. B.; Go, Y. S.; Bae, H.-J.; Park, J. H.; Cho, S. H.; Cho, H. J.; Lee, D. S.; Park, O. K.; Hwang, I.; Suh, M. C. Disruption of Glycosylphosphatidylinositol-Anchored Lipid Transfer Protein Gene Altered Cuticular Lipid Composition, Increased Plastoglobules, and Enhanced Susceptibility to Infection by the Fungal Pathogen Alternaria brassicicola. *Plant Physiology* **2009**, *150*, 42–54.

102. DeBono, A.; Yeats, T. H.; Rose, J. K.; Bird, D.; Jetter, R.; Kunst, L.; Samuels, L. Arabidopsis LTPG Is a Glycosylphosphatidylinositol-Anchored Lipid Transfer Protein Required for Export of Lipids to the Plant Surface. *the Plant Cell Online* **2009**, *21*, 1230–1238.

103. Kim, H.; Lee, S. B.; Kim, H. J.; Min, M. K.; Hwang, I.; Suh, M. C. Characterization of glycosylphosphatidylinositol-anchored lipid transfer protein 2 (LTPG2) and overlapping function between LTPG/LTPG1 and LTPG2 in cuticular wax export or accumulation in arabidopsis thaliana. *Plant and Cell Physiology* **2012**, *53*, 1391–1403.

104. Croteau, R.; Kolattukudy, P. E. Biosynthesis of Hydroxyfatty Acid Polymers. Enzymatic Synthesis of Cutin from Monomer Acids by Cell-Free Preparations from the Epidermis of Vicia faba Leaves. *Biochemistry* **1974**, *13*, 3193–3202.

105. Panikashvili, D.; Shi, J. X.; Schreiber, L.; Aharoni, A. The Arabidopsis DCR Encoding a Soluble BAHD Acyltransferase Is Required for Cutin Polyester Formation and Seed Hydration Properties. *Plant Physiology* **2009**, *151*, 1773–1789.

106. Kannangara, R.; Branigan, C.; Liu, Y.; Penfield, T.; Rao, V.; Mouille, G.; Hofte, H.; Pauly, M.; Riechmann, J. L.; Broun, P. The Transcription Factor WIN1/SHN1 Regulates Cutin Biosynthesis in Arabidopsis thaliana. *the Plant Cell Online* **2007**, *19*, 1278–1294.

107. Mintz-Oron, S.; Mandel, T.; Rogachev, I.; Feldberg, L.; Lotan, O.; Yativ, M.; Wang, Z.; Jetter, R.; Venger, I.; Adato, A.; Aharoni, A. Gene Expression and Metabolism in Tomato Fruit Surface Tissues. *Plant Physiology* **2008**, *147*, 823–851.

108. Yeats, T. H.; Huang, W.; Chatterjee, S.; Viart, H. M.-F.; Clausen, M. H.; Stark, R. E.; Rose, J. K. Tomato Cutin Deficient 1 (CD1) and putative orthologs comprise an ancient family of cutin synthase-like (CUS) proteins that are conserved among land plants. *The Plant Journal* **2014**, *77*, 667–675.

109. Kolattukudy, P. E. COMPOSITION OF THE ALIPHATIC COMPONENTS OF ' SUBERIN ' FROM THE BUNDLE SHEATHS OF Z E A MA ¥ $ LEAVES * The aliphatic components of the polymeric lipid of the bundle sheaths of the leaves of Zea maya were analyzed by combined gas-liquid chromatography and. *Plant Science Letters* **1979**, *15*, 225–230.

110. Hattersley, P. W.; Browning, A. J. Occurrence of the suberized lamella in leaves of grasses of different photosynthetic types. I. In parenchymatous bundle sheaths and PCR ("Kranz") sheaths. *Protoplasma* **1981**, *109*, 371–401.

111. Wilson, C. A.; Peterson, C. A. Chemical Composition of the Epidermal, Hypodermal, Endodermal and Intervening Cortical Cell Walls of Various Plant Roots. *Annals of Botany* **1983**, *51*, 759–769.

112. Karahara, I.; Shibaoka, H. The Casparian strip in pea epicotyls: Effects of light on its development. *Planta* **1994**, *192*, 269–275.

113. Schreiber, L.; Hartmann, K.; Skrabs, M.; Zeier, J. Apoplastic barriers in roots: chemical composition of endodermal and hypodermal cell walls. *Journal of Experimental Botany* **1999**, *50*, 1267–1280.

114. Zeier, J.; Goll, A.; Yokoyama, M.; Karahara, I.; Schreiber, L. Structure and chemical composition of endodermal and rhizodermal/hypodermal walls of several species. *Plant, Cell and Environment* **1999**, *22*, 271–279.

115. Hartmann, K.; Peiter, E.; Koch, K.; Schubert, S.; Schreiber, L. Chemical composition and ultrastructure of broad bean (Vicia faba L.) nodule endodermis in comparison to the root endodermis. *Planta* **2002**, *215*, 14–25.

116. Schreiber, L. Transport barriers made of cutin, suberin and associated waxes. *Trends in Plant Science* **2010**, *15*, 546–553.

117. Van Doom, W. G.; Stead, A. D. Abscission of flowers and floral parts. *Journal of Experimental Botany* **1997**, *48*, 821–837.

118. Schreiber, L.; Franke, R.; Hartmann, K. Wax and suberin development of native and wound periderm of potato (Solanum tuberosum L.) and its relation to peridermal transpiration. *Planta* **2005**, *220*, 520–530.

119. Graça, J. Suberin: the biopolyester at the frontier of plants. *Frontiers in Chemistry* **2015**, *3*, 1–11.

120. Vishwanath, S. J.; Kosma, D. K.; Pulsifer, I. P.; Scandola, S.; Pascal, S.; Joubes, J.; Dittrich-Domergue, F.; Lessire, R.; Rowland, O.; Domergue, F. Suberin-Associated Fatty Alcohols in Arabidopsis: Distributions in Roots and Contributions to Seed Coat Barrier Properties. *Plant Physiology* **2013**, *163*, 1118–1132.

121. Serra, O.; Soler, M.; Hohn, C.; Franke, R.; Schreiber, L.; Prat, S.; Molinas, M.; Figueras, M. Silencing of StKCS6 in potato periderm leads to reduced chain lengths of suberin and wax compounds and increased peridermal transpiration. *Journal of Experimental Botany* **2009**, *60*, 697–707.

122. Graça, J.; Santos, S. Suberin: A biopolyester of plants' skin. *Macromolecular Bioscience* **2007**, *7*, 128–135.

123. Ranathunge, K.; Schreiber, L.; Franke, R. Suberin research in the genomics era-New interest for an old polymer. *Plant Science* **2011**, *180*, 339–413.

124. Lulai, E. C.; Corsini, D. L. Differential deposition of suberin phenolic and aliphatic domains and their roles in resistance to infection during potato tuber (Solanum tuberosum L.) wound-healing. *Physiological and Molecular Plant Pathology* **1998**, *53*, 209–222.

125. Teixeira, R. T.; Pereira, H. Suberized cell walls of cork from cork oak differ from other species. *Microscopy and Microanalysis* **2010**, *16*, 569–575.

126. Graça, J.; Pereira, H. Suberin structure in potato periderm: Glycerol, long-chain monomers, and glyceryl and feruloyl dimers. *Journal of Agricultural and Food Chemistry* **2000**, *48*, 5476–5483.

127. Graça, J.; Pereira, H. Methanolysis of bark suberins: analysis of glycerol and acid monomers. *Phytochemical Analysis* **2000**, *11*, 45–51.

128. Marques, A. V.; Pereira, H.; Meier, D.; Faix, O. Isolation and Characterization of a Guaiacyl Lignin from Saponified Cork of Quercus suber L. *Holzforschung* **1996**, *50*, 393–400.

129. Bernards, M. A.; Lopez, M. L.; Zajicek, J.; Lewis, N. G. Hydroxycinnamic acid-derived polymers constitute the polyaromatic domain of suberin., 1995.

130. Mattinen, M. L.; Filpponen, I.; Järvinen, R.; Li, B.; Kallio, H.; Lektinen, P.; Argyropoulos, D. Structure of the polyphenolic component of suberin isolated from potato (Solanum tuberosum war. Nikola). *Journal of Agricultural and Food Chemistry* **2009**, *57*, 9747–9753.

131. Bernards, M. A. Demystifying suberin. *Canadian Journal of Botany* **2002**, *80*, 227–240.

132. Schmutz, a.; Buchala, a. J.; Ryser, U. Changing the Dimensions of Suberin Lamellae of Green Cotton Fibers with a Specific Inhibitor of the Endoplasmic Reticulum-Associated Fatty Acid Elongases. *Plant physiology* **1996**, *110*, 403–411.

133. Graça, J.; Santos, S. Glycerol-derived ester oligomers from cork suberin. *Chemistry and Physics of Lipids* **2006**, *144*, 96–107.

134. Yan, B.; Stark, R. E. A WISE NMR approach to heterogeneous biopolymer mixtures: Dynamics and domains in wounded potato tissues. *Macromolecules* **1998**, *31*, 2600–2605.

135. Gil, A.; Lopes, M; Rocha, J; Pascoal Neto, C A 13C solid state nuclear magnetic resonance spectroscopic study of cork cell wall structure: the effect of suberin removal. *International Journal of Biological Macromolecules* **1997**, *20*, 293–305.

136. Vishwanath, S. J.; Delude, C.; Domergue, F.; Rowland, O. Suberin: biosynthesis, regulation, and polymer assembly of a protective extracellular barrier. *Plant Cell Reports* **2015**, *34*, 573–586.

137. Höfer, R.; Briesen, I.; Beck, M.; Pinot, F.; Schreiber, L.; Franke, R. The Arabidopsis cytochrome P450 CYP86A1 encodes a fatty acid ω-hydroxylase involved in suberin monomer biosynthesis. *Journal of Experimental Botany* **2008**, *59*, 2347–2360.

138. Compagnon, V.; Diehl, P.; Benveniste, I.; Meyer, D.; Schaller, H.; Schreiber, L.; Franke, R.; Pinot, F. CYP86B1 Is Required for Very Long Chain -Hydroxyacid and , -Dicarboxylic Acid Synthesis in Root and Seed Suberin Polyester. *Plant Physiology* **2009**, *150*, 1831–1843.

139. Molina, I.; Li-Beisson, Y.; Beisson, F.; Ohlrogge, J. B.; Pollard, M. Identification of an Arabidopsis Feruloyl-Coenzyme A Transferase Required for Suberin Synthesis. *Plant Physiology* **2009**, *151*, 1317–1328.

140. Li-Beisson, Y.; Shorrosh, B.; Beisson, F.; Andersson, M. X.; Arondel, V.; Bates, P. D. *et al.* Acyl-Lipid Metabolism. *The Arabidopsis Book* **2013**, *11*, e0161.

141. Domergue, F.; Vishwanath, S. J.; Joubes, J.; Ono, J.; Lee, J. A.; Bourdon, M.; Alhattab, R.; Lowe, C.; Pascal, S.; Lessire, R.; Rowland, O. Three Arabidopsis Fatty Acyl-Coenzyme A Reductases, FAR1, FAR4, and FAR5, Generate Primary Fatty Alcohols Associated with Suberin Deposition. *Plant Physiology* **2010**, *153*, 1539–1554.

142. Samuels, L.; Kunst, L.; Jetter, R. Sealing Plant Surfaces: Cuticular Wax Formation by Epidermal Cells. *Annual Review of Plant Biology* **2008**, *59*, 683–707.

143. Millar, A. a.; Kunst, L. Very-long-chain fatty acid biosynthesis is controlled through the expression and specificity of the condensing enzyme. *The Plant Journal* **1997**, *12*, 121–131.

144. Franke, R.; Höfer, R.; Briesen, I.; Emsermann, M.; Efremova, N.; Yephremov, A.; Schreiber, L. The DAISY gene from Arabidopsis encodes a fatty acid elongase condensing enzyme involved in the biosynthesis of aliphatic suberin in roots and the chalaza-micropyle region of seeds. *The Plant Journal* **2009**, *57*, 80–95.

145. Denic, V.; Weissman, J. S. A Molecular Caliper Mechanism for Determining Very Long-Chain Fatty Acid Length. *Cell* **2007**, *130*, 663–677.

146. Yadav, V.; Molina, I.; Ranathunge, K.; Castillo, I. Q.; Rothstein, S. J.; Reed, J. W. ABCG Transporters Are Required for Suberin and Pollen Wall Extracellular Barriers in Arabidopsis. *The Plant Cell* **2014**, *26*, 3569–3588.

147. Ahmed, A.; Crawford, T.; Gould, S.; Ha, Y. S.; Hollrah, M.; Noor-E-Ain, F.; Dickman, M. B.; Dussault, P. H. Synthesis of (R)- and (S)-10,16-dihydroxyhexadecanoic acid: Cutin stereochemistry and fungal activation. *Phytochemistry* **2003**, *63*, 47–52.

148. Matsuo, J. I.; Murakami, M. The Mukaiyama aldol reaction: 40years of continuous development. *Angewandte Chemie - International Edition* **2013**, *52*, 9109–9118.

149. McMurry, J. E.; Silvestri, M. G.; Fleming, M. P.; Hoz, T.; Grayston, M. W. Some Deoxygenation Reactions with Low-Valent Titanium (Titanium Trichloride/Lithium Tetrahydroaluminate). *Journal of Organic Chemistry* **1978**, *43*, 3249–3255.

150. Stoltz, B. M.; Kano, T.; Corey, E. J. Enantioselective Total Synthesis of Nicandrenones. *Journal of the American Chemical Society* **2000**, *122*, 9044–9045.

151. Guo, Y.; Tao, G. H.; Blumenfeld, A.; Shreeve, J. M. Impact of silyl enol ether stability on palladium-catalyzed arylations. *Organometallics* **2010**, *29*, 1818–1823.

152. Holloway, P.; Deas, A. Occurrence of positional isomers of dihydroxyhexadecanoic acid in plant cutins and suberins. *Phytochemistry* **1971**, *10*, 2781–2785.

153. Vasan, M.; Rauvolfova, J.; Wolfert, M. A.; Leoff, C.; Kannenberg, E. L.; Quinn, C. P.; Carlson, R. W.; Boons, G. J. Chemical synthesis and immunological properties of oligosaccharides derived from the vegetative cell wall of Bacillus anthracis. *ChemBioChem* **2008**, *9*, 1716–1720.

154. Edens, M.; Boerner, D.; Chase, C. R.; Nass, D.; Schiavelli, M. D. Mechanism of the Meyer-Schuster Rearrangement. *Journal of Organic Chemistry* **1977**, *42*, 3403–3408.

155. Sajiki, H.; Kurita, T.; Esaki, H.; Aoki, F.; Maegawa, T.; Hirota, K. Complete replacement of H2 by D2 via Pd/C-catalyzed H/D exchange reaction. *Organic Letters* **2004**, *6*, 3521–3523.

156. Kurita, T.; Aoki, F.; Mizumoto, T.; Maejima, T.; Esaki, H.; Maegawa, T.; Monguchi, Y.; Sajiki, H. Facile and convenient method of deuterium gas generation using a Pd/C-catalyzed H2-D2 exchange reaction and itsapplication to synthesis of deuterium-labeled compounds. *Chemistry - A European Journal* **2008**, *14*, 3371–3379.

157. Parker, M. W. Protein Structure from X-Ray Diffraction. *Journal of Biological Physics* **2003**, *29*, 341–362.

158. Wouters, J Cation-π (Na+-Trp) interactions in the crystal structure of tetragonal lysozyme. *Protein Science* **1998**, *7*, 2472–5.

159. Wlodawer, A.; Minor, W.; Dauter, Z.; Jaskolski, M. Protein crystallography for aspiring crystallographers or how to avoid pitfalls and traps in macromolecular structure determination. *FEBS Journal* **2013**, *280*, 5705–5736.

160. McPherson, A.; Gavira, J. A. Introduction to protein crystallization. *Acta Crystallographica Section F:Structural Biology Communications* **2014**, *70*, 2–20.

161. Ghosh, A. K.; Brindisi, M. Organic Carbamates in Drug Design and Medicinal Chemistry. *Journal of Medicinal Chemistry* **2015**, *58*, 2895–2940.

162. Baron, R.; Casterline, J.; Fitzhugh, O. Specificity of carbamate-induced esterase inhibition in mice. *Toxicology and Applied Pharmacology* **1964**, *6*, 402–410.

163. Mumby, S. M.; Hammock, B. D.; Sparks, T. C.; Ota, K. Synthesis and Bioassay of Carbamate Inhibitors of the Juvenile Hormone Hydrolyzing Esterases from the Housefly, Musca Domestica. *Journal of Agricultural and Food Chemistry* **1979**, *27*, 763–765.

164. Lange, M.; Pettersen, A. L.; Undheim, K. Synthesis of secondary amines by reductive dimerization of azides. *Tetrahedron* **1998**, *54*, 5745–5752.

165. An, I. H.; Seong, H. R.; Ahn, K. H. Reductive dimerization of azides to secondary amines under hydrogenation conditions. *Bulletin of the Korean Chemical Society* **2004**, *25*, 420–422.

166. Armarego, W. L.; Chai, C. L. L., *Purification of Laboratory Chemicals*, 7th Ed.; Butterworth-Heinemann, Ed.; Elsevier: 2009.

167. Still, W. C.; Kahn, M.; Mitra, A. Rapid Chromatographic Technique for Preparative Separations with Moderate Resolution. *Journal of Organic Chemistry* **1978**, *43*, 2923–2925.

168. Pedersen, D.; Rosenbohm, C. Dry Column Vacuum Chromatography. *Synthesis* **2001**, *2001*, 2431–2434.

169. Guay, B.; Deslongchamps, P. Cascade polycyclization: Exploration of a convergent route to access various tricyclic and tetracyclic products related to sterols. *Journal of Organic Chemistry* **2003**, *68*, 6140–6148.

170. http://bar.utoronto.ca/eplant/?ActiveSpecies=Arabidopsis%20thaliana&Genes=AT3G11430,AT2G23540,AT3G50400,AT1G74460,AT5G37690&ActiveGe\ne=AT3G11430&ActiveView=HeatMapView (accessed 15/01/2018).

171. Waese, J.; Fan, J.; Pasha, A.; Yu, H.; Fucile, G.; Shi, R.; Cumming, M.; Kelley, L. A.; Sternberg, M. J.; Krishnakumar, V.; Ferlanti, E.; Miller, J.; Town, C.; Stuerzlinger, W.; Provart, N. J. ePlant: Visualizing and Exploring Multiple Levels of Data for Hypothesis Generation in Plant Biology. *The Plant Cell* **2017**, *29*, 1806–1821.

172. Mengiste, T; Amedeo, P; Paszkowski, J High-efficieny transformation of Arabidopsis thaliana with a selectable marker gene regulated by the T-DNA 1' promoter. *The Plant Journal* **1997**, *12*, 945–948.

173. Zhang, Z.; Xing, A.; Staswick, P.; Clemente, T. E. The use of glufosinate as a selective agent in Agrobacterium-mediated transformation of soybean. *Plant Cell, Tissue and Organ Culture* **1999**, *56*, 37–46.

174. Czechowski, T. Genome-Wide Identification and Testing of Superior Reference Genes for Transcript Normalization in Arabidopsis. *Plant Physiology* **2005**, *139*, 5–17.

175. Hong, S. M.; Bahn, S. C.; Lyu, A.; Jung, H. S.; Ahn, J. H. Identification and testing of superior reference genes for a starting pool of transcript normalization in Arabidopsis. *Plant and Cell Physiology* **2010**, *51*, 1694–1706.

176. Lilly, S. T.; Drummond, R. S. M.; Pearson, M. N.; MacDiarmid, R. M. Identification and validation of reference genes for normalization of transcripts from virus-infected Arabidopsis thaliana. *Molecular plant-microbe interactions : MPMI* **2011**, *24*, 294–304.

177. Cygler, M; Schrag, J. D. Structure and conformational flexibility of Candida rugosa lipase. *Biochimica et biophysica acta* **1999**, *1441*, 205–14.

178. http://www.sbg.bio.ic.ac.uk/~phyre2/ (accessed 15/01/2018).

179. Kelley, L. A.; Mezulis, S.; Yates, C. M.; Wass, M. N.; Sternberg, M. J. E. The Phyre2 web portal for protein modeling, prediction and analysis. *Nature protocols* **2015**, *10*, 845–58.